10
I29A
535
COPY 1

UILU-ENG-87-2006

L ENGINEERING STUDIES

JRAL RESEARCH SERIES NO. 535

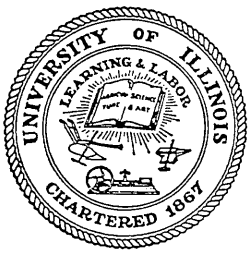

ISSN: 0069-4274

RELIABILITY EVALUATION OF STATIC AND SEISMIC STABILITY OF CUT SLOPES

By
HIROSHI HAYASHI
and
A. H-S. ANG

Technical Report of Research
Supported by the
NATIONAL SCIENCE FOUNDATION
(Under Grant ECE 85-11972)
and the
KAJIMA CORPORATION

UNIVERSITY OF ILLINOIS
at URBANA-CHAMPAIGN
JUNE 1987

50272-101

REPORT DOCUMENTATION PAGE	1. REPORT NO.	2.	3. Recipient's Accession No.

4. Title and Subtitle
RELIABILITY EVALUATION OF STATIC AND SEISMIC STABILITY OF CUT SLOPES

5. Report Date
JUNE 1987

6.

7. Author(s)
Hiroshi Hayashi and A. H-S. Ang

8. Performing Organization Rept. No.
SRS 535

9. Performing Organization Name and Address
Department of Civil Engineering
University of Illinois
208 N. Romine Street
Urbana, IL 61801

10. Project/Task/Work Unit No.

11. Contract(C) or Grant(G) No.
(C)
(G) NSF ECE 85-11972

12. Sponsoring Organization Name and Address
National Science Foundation
Washington, D. C.
and
Kajima Corporation
Tokyo, Japan

13. Type of Report & Period Covered
Technical Report

14.

15. Supplementary Notes

16. Abstract (Limit: 200 words)

A method is developed for evaluating the static stability of a cut slope formed by strain-softening soil such as highly overconsolidated clay considering progressive failure as the critical failure mode. The stress condition along a potential failure surface both prior to and after an excavation is investigated by finite-element elasto-plastic analysis; in this process, a potential failure surface is modeled as joint elements. Through the investigation, the redistribution of an unbalanced force caused by a local failure is determined. This stress redistribution is combined with the inherent variability of the shear strength of a soil, which is the main contributor to the uncertainties in the static stability evaluation of a cut slope, to determine the failure probability and the expected length of local failure along an assumed potential failure surface.

A method is also developed for evaluating the seismic stability of a cut slope consisting of the following: (1) the horizontal vibration of a sliding mass subjected to an earthquake loading is converted into an equivalent SDF system with a smooth hysteretic restoring force; (2) a failure criterion and a damage index for the converted SDF system is established; and (3) the safety based on the response statistics obtained through random vibration analysis is evaluated. The reliability against sliding failure conditional on the intensity and duration of an earthquake loading is obtained using the results from the random vibration analysis; the uncertainties associated with several parameters including the dynamic soil properties and the randomness in the frequency content of an earthquake loading are considered.

17. Document Analysis a. Descriptors

Reliability
Cut Slope

b. Identifiers/Open-Ended Terms

c. COSATI Field/Group

18. Availability Statement
UNLIMITED

19. Security Class (This Report)
UNCLASSIFIED

21. No. of Pages
126

20. Security Class (This Page)
UNCLASSIFIED

22. Price

ACKNOWLEDGMENTS

This report is based on the doctoral dissertation of Dr. H. Hayashi submitted in partial fulfillment for the Ph.D. degree at the University of Illinois at Urbana-Champaign. The research has been supported by Kajima Corporation and the National Science Foundation under Grant ECE 85-11972. These supports are gratefully acknowledged.

Thanks are due to Professors W. Tang, Y. K. Wen, A. J. Hendron, and E. J. Cording for many helpful discussions.

TABLE OF CONTENTS

Page

LIST OF TABLES

LIST OF FIGURES

Page

CHAPTER 1

INTRODUCTION

1.1 Objective and Scope

With an increasing number of large-scale excavation being done recently, the stability evaluation of such cut slopes is becoming more important. Consistent with this trend, excavation in diluvial soil layers such as highly-overconsolidated clay is also increasing in number. Therefore, the evaluation of the static and seismic stability of such cut slopes is one of the most important subjects in the construction industry.

A cut slope, especially one formed by highly overconsolidated clay, is characterized by the release of high horizontal earth pressures as a result of the excavation, as well as by the strain-softening of the soil. Because of the release of high horizontal pressures, stress concentration is likely to occur around the toe of a slope. Consequently, it is highly likely that local failure will occur around the toe and that the resulting unbalanced shear force will be redistributed to the adjacent regions along a potential failure surface, which could potentially cause total failure. This type of failure is called *progressive failure* in contrast to instantaneous failure. To evaluate the safety of slopes against progressive failure, therefore, requires methods of analysis different from the conventional methods that are applicable for instantaneous failure. In the extreme case, if the shear strength of the soil is known precisely prior to the excavation, the local failure zone caused by the excavation may be anticipated if the stress redistribution resulting from the local failure can be established. However, the shear strength of soil varies spatially and the uncertainties associated therewith

are unavoidable. Realistically, therefore, local failure caused by a cut may be evaluated only in terms of probability (Tang et al., 1985).

The first objective of this study is to modify and extend the model proposed by Tang et al. (1985) for more practical and general cases. For this purpose, the stress redistribution caused by a local failure is examined based on the results of finite-element analysis; the potential failure surface is modeled as joint elements (Goodman et al., 1968). Combining the stress redistribution rule with the inherent variability of the soil shear strength, a probabilistic model is established, through which the expected local failure zone and associated probability of failure can be evaluated.

Regarding the seismic stability of cut slopes, there is no satisfactory method or approach developed to date. Experiments on the dynamic shear strength of clay and soft rock have been performed by a few researchers (Seed and Chen, 1966; Ellis and Hartman, 1967; Nishi and Esashi, 1982). However, the pertinent failure mechanism has not been well defined; this is in contrast to the liquefaction failure of saturated sand under earthquake loadings.

The second objective of this study, therefore, is to develop a method for evaluating the seismic stability of cut slopes. The proposed method for this purpose involves the following: (1) convert the horizontal vibration of a sliding mass subjected to earthquake loadings into an equivalent single-degree-of-freedom (SDF) system with smooth hysteretic restoring force; (2) establish a failure criterion and a damage index for this converted SDF system; and (3) evaluate the safety based on the response statistics obtained through random vibration analysis of the system.

1.2 Related Previous Studies

1.2.1 Static Stability of Cut Slopes

The sliding of slopes that has never failed before is called *first—time slide*. It is difficult to explain the occurence of first-time slides, because the safety factors obtained from stability analyses of such slopes based on a peak shear strength of intact overconsolidated clay is invariably much greater than 1.0. Skempton (1964) analyzed many failures of slopes in London clay and compared the strength parameters with those from drained shear tests. It was found that the shear strength mobilized along the sliding surface is between the peak shear strength and the residual shear strength; the reason that the shear strength of clay drops from its peak value may be caused by shear stress concentration which, in turn, may be associated with the existence of fissures.

Based on case studies of sliding of excavated slopes composed of highly plastic overconsolidated clay, Bjerrum (1967) explained that sliding is initiated by local failure around the toe of a slope and subsequently extended to the whole area of the sliding mass in a progressive manner. Slope failures in Oxford clay (Burland et al., 1977) confirm the mechanism of progressive failure suggested by Bjerrum.

Duncan and Dunlop (1969), and Lo and Lee (1973) preformed finite-element analyses of excavated slopes to investigate the factors influencing progressive failure. These investigations showed that strain-softening of the clay, the magnitude of excavation and the release of horizontal earth pressures caused by the excavation have significant effects on the stability of slopes. In paticular, high earth pressures released as a result of the excavation leads to the stress concentration at the toe of a slope, which significantly influences

progressive failure. Chowdhury and A-Grivas (1982) and Tang et al. (1985) examined the reliability against progressive failures. In these models, the potential failure surface of a slope is divided into many segments, and the local safety factor is evaluated for each segment. Based on the distribution of the local safety factors along the potential failure surface, the most probable failure path is determined and the failure probability associated with that failure path is evaluated.

1.2.2 Seismic Stability of Cut Slopes

When a cut slope is located in a seismically active region, the evaluation of its seismic stability becomes important. For this purpose, it is necessary to carefully evaluate the dynamic shear strength of the soil.

Earthquake loadings are characterized by higher rate of loading compared to static loadings, as well as by repeated loadings and unloadings (cyclic loadings). The effect of the loading rate on the shear strength of soil depends on the type of soil considered (Casagrande and Shannon, 1948; Olson and Kane, 1965); the shear strength of clay tend to become stronger as the rate of loading increases, whereas the loading rate has almost no effect on the strength of sand. In the same way, cyclic loading effect differs according to the type of soil. Dense sand and clayey sand are insensitive to the effect of repeated loadings. On the other hand, the strength of loose saturated sand deteriorates drastically because of the buildup of pore water pressure caused by repeated shear loadings. Clay loses its shear strength gradually with the number of repeated cyclic loadings. Therefore, soils could be roughly classified into dense sand and clayey sand (type-1), loose to medium dense saturated sands (type-2), and clay (type-3). The dynamic shear strength of these three types of soil may be

summarized as follows: The dynamic shear strength of a type-1 soil is almost the same as its static shear strength; the dynamic strength of a type-2 soil decreases significantly under repeated loadings; whereas, the dynamic strength of a type-3 soil is higher than its static strength if the number of repeated loadings is small, but as the number of repeated loadings increases, the cyclic loading effect becomes more dominant than the loading rate effect, such that the dynamic shear strength may become lower than its static strength.

In the evaluation of the seismic stability of slopes, the so-called pseudo-static method (e.g., Terzaghi, 1950) has been used widely. This method, however, has shortcomings in the selection of the equivalent horizontal static force acting downhill on a sliding mass, as well as in the evaluation of the dynamic shear strength of the soil. In its place, Newmark (1965) proposed a method that combines two sets of data: (1) a critical acceleration, at which the slope would reach its ultimate strength, and (2) a representative strong-motion accelerogram. The Newmark method calculates the displacement of a rigid friction-block, with the same critical acceleration as the slope, subjected to the acceleration history defined by the given strong-motion accelerogram. This method has been applied mainly to the seismic stability of man-made soil structures such as dams and embankments that are usually formed by type-1 soil.

In the case of a slope composed of liquefaction-prone materials such as type-2 soil, the seismic stability of the slope can be evaluated (Seed, 1979) by a dynamic finite-element method combined with a model to evaluate the excess pore water pressure rise caused by earthquake loadings.

The above-mentioned methods, however, are not appropriate for evaluating the seismic stability of cut slopes formed by overconsolidated clay or soft rock which are basically type-3 soil. To date, no method is available for this

latter purpose.

1.3 Organization

The following chapters are divided into two parts; Chapters 2 and 3 deal with the static stability of cut slopes, whereas Chapters 4 through 7 deal with the corresponding seismic stability. Chapter 8 contains the main results and conclusions.

In Chapter 2, the important factors affecting the static stability of a cut slope composed of highly overconsolidated clay or soft rock are examined, and it is shown that failure is more likely to occur in a progressive manner.

In Chapter 3, the redistribution of the unbalanced force caused by a local failure to the adjacent regions are established by means of finite-element elasto-plastic analysis. The resulting stress redistribution is combined with the inherent variability of the shear strength of the soil to evaluate the probability of failure as well as the expected failure length of a cut slope.

Chapter 4 describes the seismic stability problem of a cut slope bounded by a potential failure surface, which is three dimensional in nature, and its conversion to an equivalent single-degree-of-freedom (SDF) system with nonlinear hysteretic properties. Also, the hysteretic energy dissipation statistics of the converted SDF system subjected to random vibration is examined.

Chapter 5 presents the dynamic stress-strain relation of soils, and the development of a technique for determining the damage of the converted SDF system caused by random loadings. The technique allows the utilization of data from dynamic shear tests, in which cyclic shear stress is superimposed on the initial shear stress already applied to the soil.

The methodology for the seismic reliability evaluation of a cut slope is formulated in Chapter 6. The technique for calculating the failure probability is described; the uncertainties in the soil properties as well as in the earthquake loading are included.

Examples of applications are illustrated in Chapter 7. The time to failure under an earthquake loading is compared with similar results obtained with other approaches.

1.4 Notation

The symbols and notations used in the text are summarized as follows (throughout the text, the time derivative of any quantity will be denoted with a dot over the symbol):

$A, \alpha, \beta, \delta, n$	=	parameters controlling the hysteretic stress strain relation.
a	=	input base acceleration.
a_{max}	=	peak base accleration.
A_m	=	seismic intensity measure.
$[B]$	=	covariance matrix of the random seismic loading.
c	=	coefficient of viscous damping.
c'	=	cohesion intercept in terms of effective stresses.
E	=	Young's modulus.
E_c	=	hysteretic energy dissipated per cycle.
E_T	=	total hysteretic energy dissipated.
$E[X]$, $\bar{X}$	=	expected or mean value of X.
$F(N)$	=	dynamic horizontal force to cause SDF-system to fail

with N cycles of loadings.

G = shear modulus.

G_o = shear modulus at very small strain.

h = equivalent viscous damping ratio.

K = stiffness.

K_0 = coefficient of earth pressure at rest.

M, m = mass.

OCR = overconsolidation ratio.

q = total restoring force.

S_0 = intensity scale of the double sided Kanai-Tajimi PSD function for earthquakes.

T_E = random duration of the strong motion part of an earthquake time history.

T_f = strong motion phase duration necessary to cause failure.

u = displacement of a vibrating system.

u_s = deformation of the skelton curve of a hysteretic spring.

$Var[X]$ = variance of X.

x_G = ground displacement.

$\hat{X}$ = estimated value of X.

Z = hysteretic component of displacement. The hysteretic restoring force is KZ.

β = reliability index against seismically-induced sliding failure of slopes.

β_V,β_H = parameters of autocorrelation function in the vertical and the horizontal directions, respectively.

γ = shear strain.

δ_X, Δ_X = coefficient of variation (COV) of X.

ζ_G, ω_G = parameters of the Kanai-Tajimi power spectral density function.

ν = Poisson's ratio.

$\rho_{i,j}$ = correlation coefficient between parameters i and j.

σ' = effective normal stress.

σ_X = standard deviation of X.

τ_P, τ_R = peak and residual shear strengths of soil.

$\tau_d(N)$ = dynamic shear stress to cause failure with N cycles of loadings.

τ = shear stress.

ϕ', ϕ_R' = peak and residual friction angles in terms of effective stresses, respectively.

CHAPTER 2

PROBLEMS OF CUT SLOPES

2.1 Introduction

In order to fully understand the potential failure modes of a cut slope, some background information relating to such slopes, especially those formed by highly overconsolidated clay, is necessary. The following describes the physical and mechanical properties pertinent to such cut slopes.

2.2 Shear Strength of Overconsolidated Clay

In Fig. 2.1, point (a) represents the state of a clay immediately after deposition. Further deposition of additional material will cause an increase in the effective pressure (effective normal stress) and a decrease in the water content. At a stage represented by point (b) the clay is normally-consolidated, in the sense that it has not been subjected to a pressure greater than the present overburden. The shear strength of normally-consolidated clay is proportional to the effective pressure, and the graph expressing the relation between the shear strength and effective pressure is, therefore, a straight line passing through the origin. In the process of continuing deposition, the state represented by point (b) is transformed to that of point (c). At this stage if a clay is subjected to erosion, the clay is then left in an overconsolidated state represented by point (d) in Fig. 2.1. The removal of pressure is accompanied by an increase in water content, but this increase is far less than the decrease in water content during consolidation. Thus, although the clay at point (d) is under the same effective pressure as the clay at point (b), the water content of the overconsolidated clay

is considerably lower. The particles are therefore in a denser state of packing and, not surprisingly, the shear strength is greater than that of a normally-consolidated clay.

The shear strength characteristics of an overconsolidated clay are shown in Fig. 2.2, which represent typical results obtained from slow drained tests in a simple shear test apparatus; the clay is subjected to displacements of several inches. As the clay is strained, it builds up an increasing resistance. However, under a given effective pressure, there is a definite limit to the resistance of the clay which is the peak strength τ_P. If the test is continued, the strength decreases as the displacement increases. This process is called strain-softening, eventually leading to a certain residual strength, τ_R, which the clay can maintain even when subjected to large displacements. If several such tests under different effective pressures are performed, the peak and residual strengths, when plotted against the effective pressure, would show a relationship approximately in accordance with the Mohr-Coulomb law. The peak strength can, therefore, be expressed by the equation

$$\tau_P = c' + \sigma' \tan\phi' \tag{2.1}$$

where: c' = cohesion intercept in terms of the effective stresses;

ϕ' = friction angle in terms of effective stresses.

and the residual strength is given by the equation

$$\tau_R = \sigma' \tan\phi'_R \tag{2.2}$$

where ϕ'_R = the residual friction angle in terms of effective stresses. In other words, in changing from the peak to the residual strength , the cohesion intercept c' disappears completely. During the same process, the angle of

shearing resistance also decreases-- in some clays by only 1 or 2 degrees, but in others by as much as 10 degrees. It is notable that during the shearing process overconsolidated clays tend to expand, especially if the peak strength is exceeded. Part of the drop in the strength from the peak value is, therefore, associated with an increasing water content.

2.3 Failure Modes of Cut Slopes

In the excavation of an overconsolidated clay, high horizontal earth pressures are released as a result of the cut. After the cut, negative pore pressures will build up in the soil. This makes the effective normal stress along a potential failure surface after the cut remain almost the same as that before the cut. There is, therefore, little reduction in the peak shear strength of the soil as denoted by point [1] in Fig. 2.3. However, as the pore pressure dissipates with time, the peak shear strength of the soil is reduced to that of point [2] in Fig. 2.3 corresponding to the effective normal stress following the cut. At that time, if the applied shear stress induced by the cut is larger than the peak drained strength somewhere along the potential failure surface, local failure can occur; as a consequence, the shear strength of that zone will drop gradually from its drained peak strength at point [2] to the drained residual strength at point [3] with its accompanying shear strain accumulation. An unbalanced shear force caused by the local failure is applied to the zone adjacent to the failure zone, thereby occasionally causing the local failure to extend into the adjacent zones. This is called *progressive failure*.

The same process depicted in Fig. 2.3 also holds for the excavation in normally consolidated clay. In this case, however, there is little difference between the peak and residual shear strengths, as shown on the right half of Fig. 2.3.

Therefore, the static stability of such a slope can be evaluated by the conventional circular method, which is based on the assumption that sliding along a failure circle occurs instantaneously.

As described above, in the safety evaluation of a cut slope formed by medium to highly overconsolidated clay, which is often encountered in practice, progressive failure should be considered as a critical failure mode.

2.4 Relation between OCR and K_0

The prediction of the in-situ state of stress in a soil deposit is of major importance in a wide variety of geotechnical problems. Although a substantial data base has been developed, it is still not possible to predict precisely the in-situ state of stress in most natural soil deposits because of a complex history of loading and unloading which is difficult to reconstruct.

The geostatic vertical stress can be estimated from a profile of the effective overburden stress with depth. The in-situ horizontal stress, however, is highly dependent on the geologic history of the soil. It is common to represent the ratio of the horizontal to vertical effective stresses by the at-rest coefficient

$$K_0 = \frac{\sigma'_h}{\sigma'_v} \tag{2.3}$$

where σ'_h and σ'_v are the horizontal and vertical effective stresses, respectively.

Consider the simplified stress history depicted in Fig. 2.4 for a homogeneous soil deposit with a horizontal ground surface. The stress path OA represents virgin loading of the soil deposit, associated with sedimentation and normally consolidated conditions. As represented by Fig. 2.4, the at-rest coefficient

remains constant during its virgin compression (K_{0nc}). Any reduction in the effective overburden stress will result in the overconsolidation of the soil, as represented by path ABC. The mechanisms causing an overconsolidated effect include erosion, excavation, etc. During unloading, the overconsolidation ratio, defined as

$$OCR = \frac{\sigma'_{v,max}}{\sigma'_v} \tag{2.4}$$

has a pronounced effect on the value of K_0. In Eq. 2.4, $\sigma'_{v,max}$ is the maximum effective overburden pressure to which the soil has been subjected, and σ'_v is the present effective overburden pressure.

For normally consolidated clays, K_{0nc} is usually evaluated by

$$K_{0nc} = 1 - \sin\phi' \tag{2.5}$$

Eq. 2.5 is an approximation to the theoretical formula of Jaky (1944). For overconsolidated clays, the corresponding coefficient, K_{0u}, is closely related to the OCR through the following relationship proposed by Schmidt (1966):

$$\frac{K_{0u}}{K_{0nc}} = OCR^{\alpha} \tag{2.6}$$

where α = an exponent defined as the at-rest rebound parameter of the soil. Schmidt proposed that the parameter α is uniquely related to the effective stress friction angle, ϕ', of the soil as follows:

$$\alpha = \sin\phi' \tag{2.7}$$

Eq. 2.7 applies quite well for a wide range of experimental data (Mayne, 1982). Therefore, during loading and unloading, K_0 may be related to ϕ' and OCR by

$$K_0 = (1-\sin\phi')\,OCR^{\sin\phi'} \tag{2.8}$$

The OCR of highly overconsolidated clay decreases gradually with depth from the ground surface. Strictly speaking, therefore, the corresponding K_0 also changes with depth. Fig. 2.5 shows measured values of K_0 varying with depth in London clay. Judging from this figure, K_0 may be taken as constant within some depth from the ground surface.

2.5 Shape and Location of Potential Failure Surface

In general, it is difficult to accurately predict the shape and location of the potential failure surface of any slope, natural or man-made. The location of a potential failure surface differs mainly depending on the subsoil conditions, whereas its shape is widely acknowledged to be nearly circular.

From actual observations of sliding of cut slopes in highly overconsolidated clay, the failure surface is nearly horizontal from the toe of a slope to some distance and then curved upward to the horizontal ground surface. On this basis, it appears reasonable to assume that the potential failure surface is circular passing through the toe of a slope with its center located above the toe of the slope.

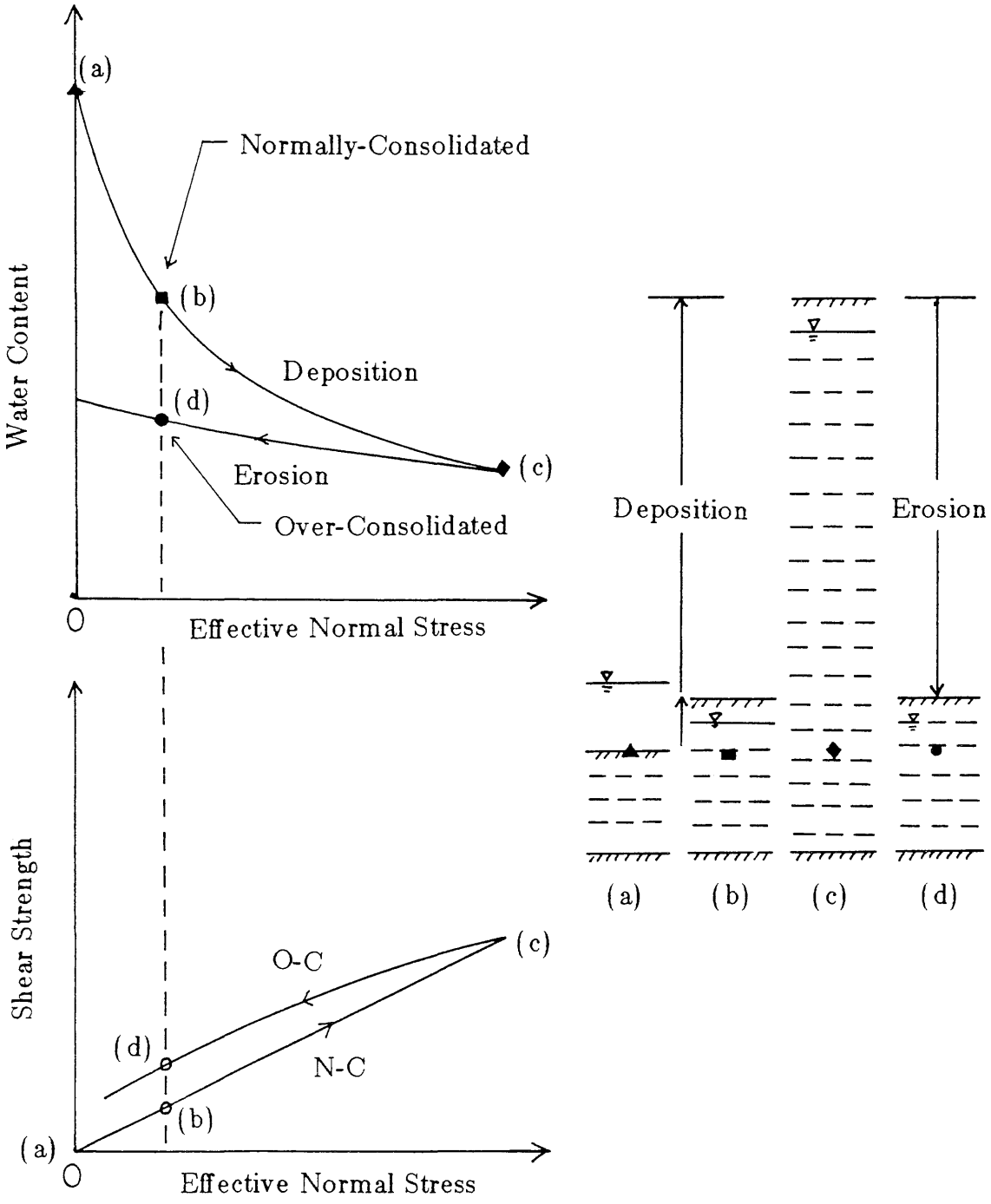

Fig. 2.1 Normally- and Over-Consolidated Clay

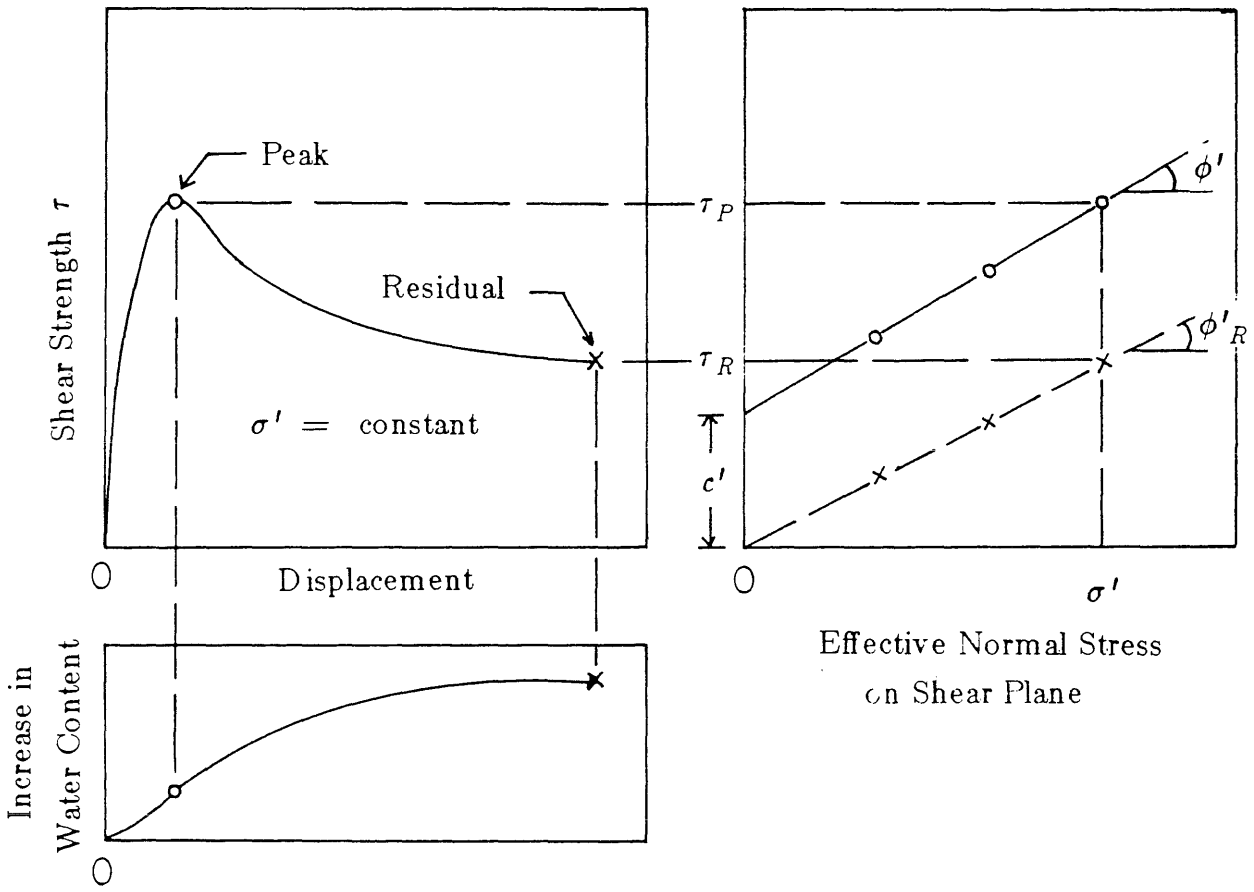

Fig. 2.2 Shear Characteristics of Over-Consolidated Clay

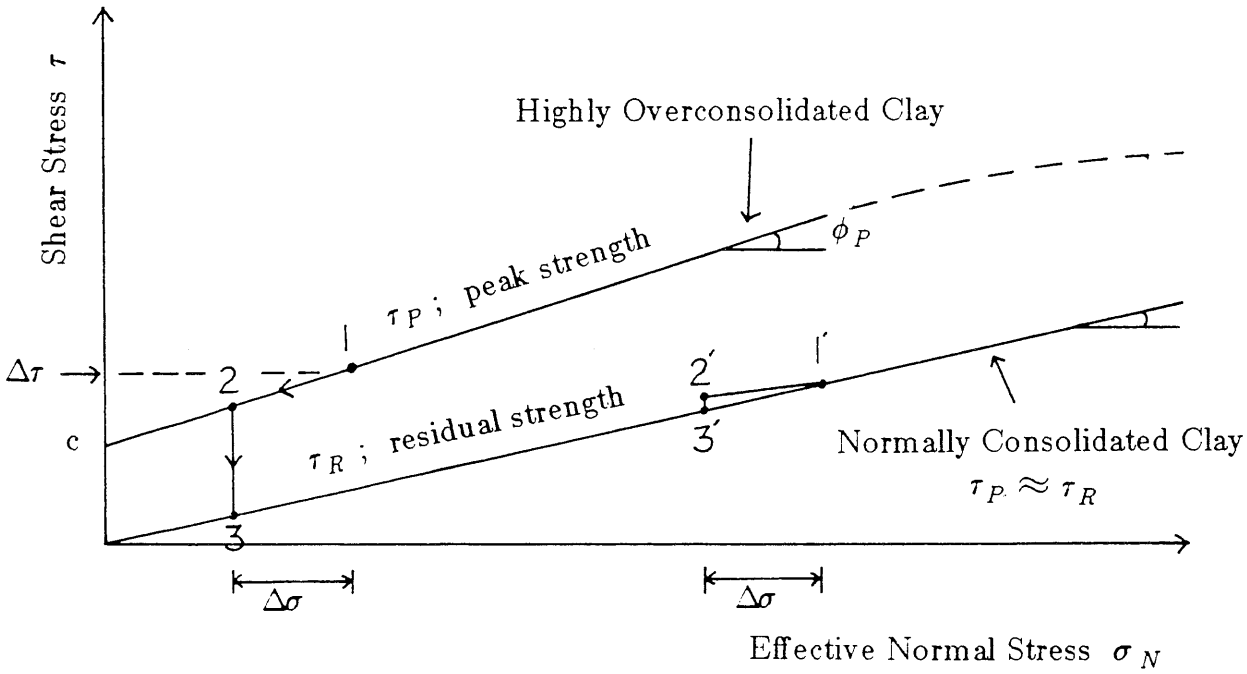

1, 1′ = stress condition before excavation

2, 2′ = stress condition after excavation

$\Delta\tau$ = excavation-induced shear stress

$\Delta\sigma$ = excavation-induced normal stress

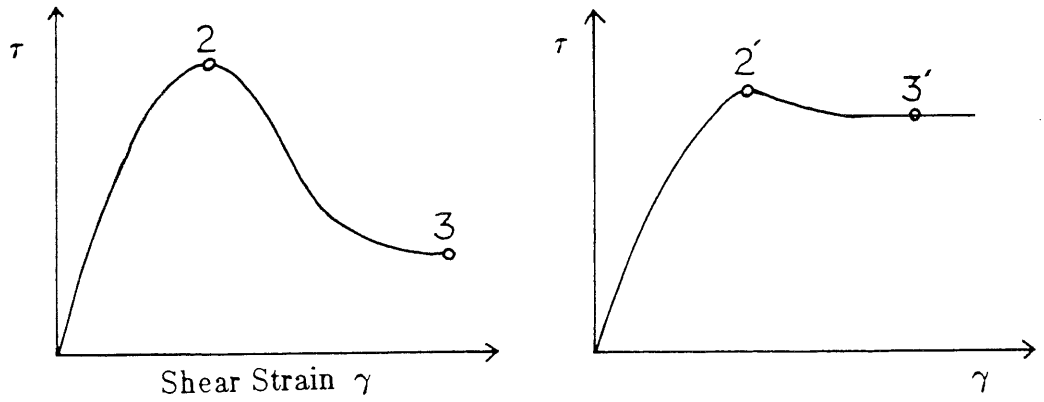

Fig. 2.3 Relation between Effective Normal Stress and Shear Stress

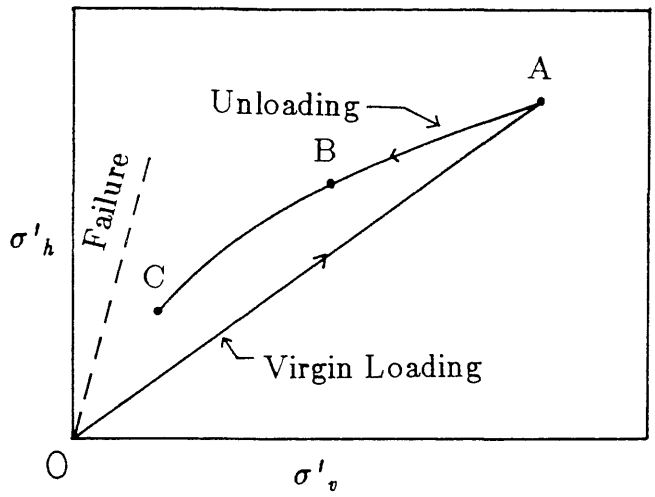

Fig. 2.4 Simplified Stress History of Soil under K_0 Conditions

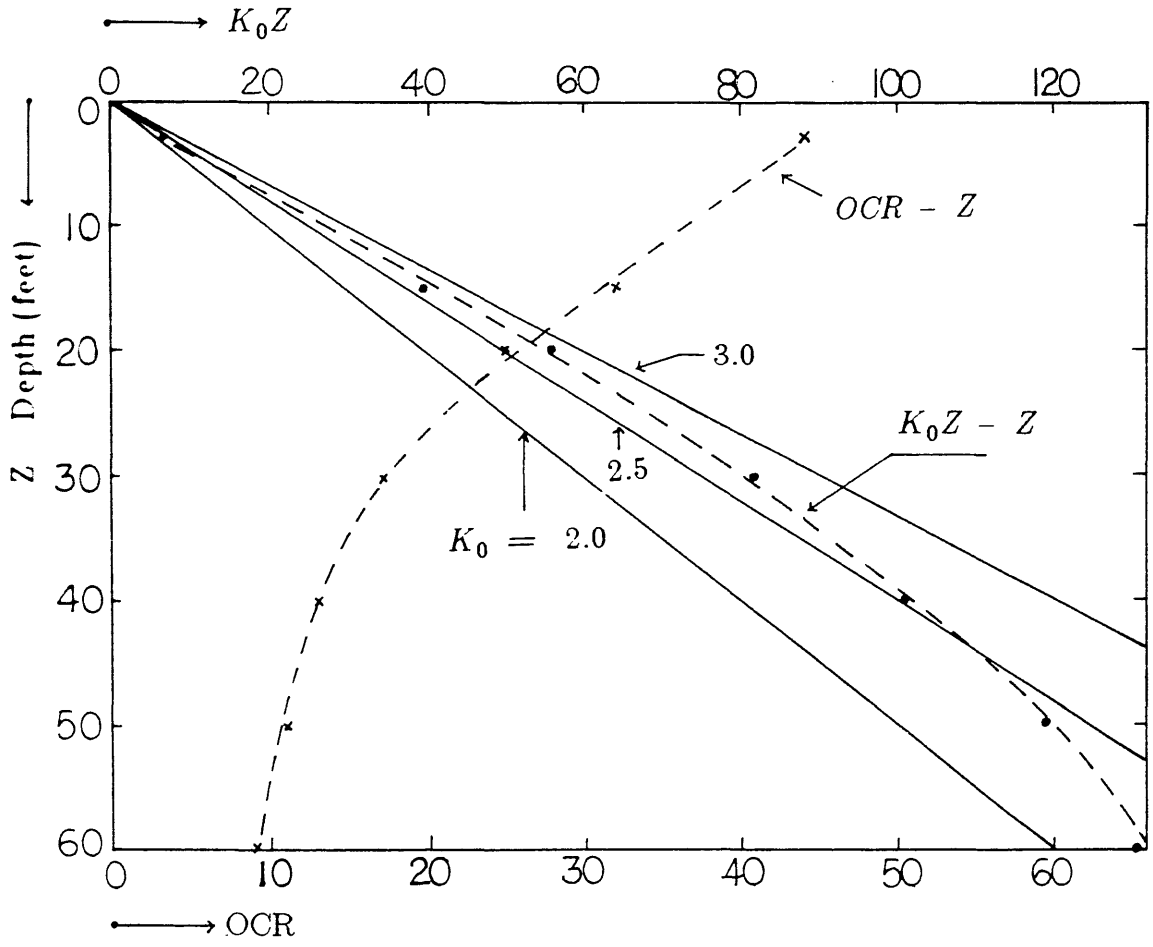

Fig. 2.5 Relation of K_0 with Depth (after Skempton, 1961)

CHAPTER 3

PROGRESSIVE FAILURE OF CUT SLOPES

3.1 Introduction

Progressive failure is more likely to occur in cut slopes where the released earth pressure resulting from the cut is very high, that is, K_0 is large, and there is great difference between the peak and residual strengths of the soil. If the stress condition subsequent to an excavation and the shear strength of the soil along a potential failure surface can be evaluated precisely, the local failure zone along the potential failure surface may be determined through finite-element analysis. The main factor complicating the problem is the inherent variability of the shear strength of the soil. Properly, the shear strength along a potential failure surface may be considered as a random process, and the stability analysis of cut slopes treated in terms of probability.

Conceivably, the problem could be treated by the following methods:

(1) The Failure Sequence Method -- Divide the potential failure surface of a slope into several segments. Failure of the slope could be defined as the event that the shear strength of all the segments comprising the slope is reduced to its residual strength. This system may be considered as an active redundant system, i.e., all the components (segments) participate actively in carrying the load (load-sharing system). In principle, the probability of failure of this system is obtained by considering all possible failure modes (Ang and Amin, 1967) with the aid of a failure graph (Henley and williams, 1973). However, the manner in which any unbalanced force due to the failure of a segment is transferred to the other segments is so complicated that the method does not appear to be

practical for this problem.

(2) Stochastic Finite-Element Method -- In this method, a sample distribution of the peak and residual strengths of the finite elements over the whole region satisfying specific probabilistic property is generated in each calculation. If finite-element elasto-plastic analysis is coupled with the above-generated soil condition, the local failure zone can be evaluated. Repeating the calculation a large number of times, useful results can be obtained. In practice, however, the method is very costly.

Alternatively, the problem may be considered as follows:

(i) Select a method to evaluate the stress condition after the cut. As will be shown later, the finite-element method is a viable method at present.

(ii) Apply finite-element elastic and elasto-plastic analyses in which the shear strength of the soil is given as a function of the normal stress. Through the results obtained, establish a method for determining the stress redistribution caused by a local failure.

(iii) Combine the method developed in step (ii) with the inherent variability of the shear strength along a potential failure surface. A practical simulation method may be developed to evaluate the probabilistic nature of a local failure zone.

(iv) Finally, establish a simulation-assisted approach suitable for evaluating the probability of progressive failure of the slope.

3.2 Stress Conditions of Cut Slopes

In order to evaluate the safety of cut slopes, it is essential that the stress condition of a slope after excavation be accurately assessed. In the

conventional method, the effective normal and shear stresses along a potential failure surface are evaluated, respectively, as follows (see Fig. 3.1):

$$\sigma' = \gamma R \cos^2\theta[\cos\theta - 1 + \min\{a\sin\theta, \frac{H}{R}\}] - u \tag{3.1}$$

$$\tau = \gamma R \sin\theta\cos\theta[\cos\theta - 1 + \min\{a\sin\theta, \frac{H}{R}\}] \tag{3.2}$$

The corresponding total effective normal and shear forces may be obtained by integrating Eqs. 3.1 and 3.2 over the entire failure surface; thus,

$$N = R\int_0^\theta \sigma' d\theta \tag{3.3}$$

$$S = R\int_0^\theta \tau d\theta \tag{3.4}$$

Fig. 3.2 shows the distributions of σ' and τ for a specified failure surface, where the ground water flow-net is assumed as shown in Fig. 3.3, obtained by means of the conventional method. These distributions are independent of the value of K_0. Strictly speaking, however, the stress condition will depend on K_0; in this light, therefore, this method is inappropriate for evaluating the stress conditions involved in the progressive failure of cut slopes.

The use of finite-element analysis may be a practical alternative, in which the potential failure surface is modeled by joint elements, whereas the remaining region of a slope is modeled by triangular elements. The analysis procedure is illustrated in Fig. 3.4, where the initial stresses of a slope prior to excavation are represented by σ_0; on the inclined surface, these initial stresses include both shear and normal components. Excavation of the slope may be simulated

analytically by applying stress changes, $\Delta\sigma$, to the excavated surface. Application of these changes in stress, which are equal and opposite to the initial stresses, σ_0, will yield a stress-free condition on the excavated surface. The applied stress changes on the excavated surface induce changes in the stresses away from the excavated surface. These induced changes in stresses are then added to the initial stresses to determine the final stresses, as indicated in Fig. 3.4. The initial effective normal and shear stresses along a potential failure surface may be evaluated following the notations of Fig. 3.1; that is,

$$\sigma'_i = \{1-(1-K_0)\sin^2\theta\}[\gamma R(\cos\theta-1+H/R)]-u \tag{3.5}$$

$$\tau_i = (1-K_0)\sin\theta\cos\theta[\gamma R(\cos\theta-1+H/R)] \tag{3.6}$$

The total initial effective normal and shear forces acting along a potential failure surface may be obtained as follows:

$$N_i = R\int_0^\theta \sigma'_i d\theta \tag{3.7}$$

$$S_i = R\int_0^\theta \tau_i d\theta \tag{3.8}$$

Additional normal and shear forces along a potential failure surface induced by the excavation may be evaluated from,

$$\Delta N = N - N_i \tag{3.9}$$

$$\Delta S = S - S_i \tag{3.10}$$

Let the horizontal and vertical forces released as a result of the cut be P_H and P_V, respectively. ΔS and ΔN are influenced by both P_H and P_V. However, ΔS

is mainly influenced by P_H, whereas ΔN is primarily a function of P_V. Accordingly, define the horizontal and vertical contributing factors, C_H and C_V, as follows:

$$C_H = \frac{\Delta S}{P_H} \tag{3.11}$$

$$C_V = \frac{\Delta N}{P_V} \tag{3.12}$$

The factors C_H and C_V will depend on the slope inclination, a, the radius of a circular potential failure surface relative to the depth of excavation, R/H, and K_0. In particular, these may be expressed as follows:

$$C_H = 1.0 - \frac{1}{3(R/H)}\left[1 + \frac{1}{a^2 K_0}\right] \tag{3.13}$$

$$C_V = 1.0 + aK_0 f(R/H) \tag{3.14}$$

where:

$$f(R/H) = 1/3[3(R/H)^2 - 2(R/H) + 1][2/(R/H) - 1/(R/H)^2]^{1/2} + [(R/H) - /(R/H)^2]\arcsin[2/(R/H) - 1/(R/H)^2]^{1/2}$$

C_H is less than 1.0, which means that some percentage of P_H gives rise to ΔN. The first term in Eq. 3.14 is the contribution of P_V, and this effect is closely related to changes in the normal stress of regions close to the excavated surface, whereas the second term is the contribution from P_H to ΔN and is mainly related to changes in the normal stress of a potential failure surface far from the excavated surface.

Finite-element elastic analyses were performed for several slopes with varying parameters. Figs. 3.5 through 3.8 show the distribution of the shear and

effective normal stresses along a potential failure surface for different values of K_0. From Fig. 3.8, it can be seen that (i) increasing values of K_0 lead to higher shear stress concentration at the toe of a slope ($x = 0$), (ii) there is little difference in the distribution of the effective normal stress for different values of K_0. Therefore, local failure at the toe of a slope is much more likely to occur with large K_0, which is representative of cut slopes formed by highly overconsolidated clay.

The distributions of the excavation-induced shear stresses along a potential failure surface (Fig. 3.9), $\Delta\tau$, can be approximated quite well with an exponential function especially for $K_0 \geq 1.0$. On the other hand, the distribution of the excavation-induced normal stress, $\Delta\sigma$, cannot be expressed by a specific function as that of $\Delta\tau$ (Fig. 3.10). Therefore, the distribution of σ' should be evaluated directly by the results obtained from finite-element elastic analysis.

Elastic finite-element analyses were performed to investigate the effects of K_0, a and H on the shape of the distribution of the excavation-induced shear stress. Doubling the height of a slope will yield the following results:

$$\Delta\tau(x\ ;\ 2H) = 2\ \Delta\tau(x/2\ ;\ H) \tag{3.15}$$

In the same way, the effect of doubling K_0 can be expressed as follows:

$$\Delta\tau(x\ ;\ 2K_0) = 2\ [C_H(2K_0)/C_H(K_0)\ ]\Delta\tau(x\ ;\ K_0) \tag{3.16}$$

In the case where R/H is large and/or $K_0 \geq 1.0$, it is reasonable to assume that $C_H(2K_0) \approx C_H(K_0)$ according to Eq. 3.13. Therefore, Eq. 3.16 is reduced to,

$$\Delta\tau(x\ ;\ 2K_0) \approx 2\ \Delta\tau(x\ ;\ K_0) \tag{3.17}$$

From induction, the distribution of $\Delta\tau$ for a slope with inclination, a, and given R/H can be evaluated by

$$\Delta\tau(x) = C_1 (K_0\gamma H)\, e^{-\frac{C_2}{H}x} \tag{3.18}$$

where C_1 and C_2 are interrelated because of the constraint $\Delta S = C_H P_H$, where $P_H = 1/2K_0\gamma H^2$. Thus, it can be shown that C_1 and C_2 satisfy the following equation:

$$C_H = 2\frac{C_1}{C_2}[1-e^{-C_2\frac{R}{H}\theta}] \tag{3.19}$$

where $\theta = x/R$. Therefore, given C_2, C_1 could be evaluated through Eq. 3.19. Table 3.1 shows C_2 for different combinations of a and R/H. Therefore, the distribution of $\Delta\tau$ along a potential failure surface for any cut slope can be evaluated approximately by Eqs. 3.13, 3.18, 3.19 and Table 3.1.

Table 3.1 Value of Coefficient C_2

Slope ; a	R/H		
	1.8	2.5	3.5
0.67	0.96	0.80	0.72
1.0	1.02	0.88	0.82

3.2.1 Stress Redistribution

To determine the redistribution of the unbalanced force to the adjacent regions resulting from the local failure around the toe of a slope, elasto-plastic finite-element analysis is necessary that takes into account the shear strength property of the soil. For this purpose, the potential failure surface is represented by joint elements, originally developed for modeling joints or cracks in rocks (Goodman, 1968). Such joint elements model the sliding failure in a manner that a sliding soil mass is almost intact except for a thin-layered slip zone, and thus the resulting stress distribution along the failure surface should be more representative of a slope failure. Each joint element has three deformation modes: (i) deformation in the direction parallel to the element, (ii) deformation in the direction normal to the element, and (iii) rotation about the center of the element. Therefore, a joint element has shear stiffness, K_s, normal stiffness, K_n, and rotational stiffness, K_w, corresponding to the respective deformation modes. K_w may be related to K_n based on reasonable assumptions about the deformation pattern of the joint element, and thus each joint element can be described with two independent stiffnesses, K_s and K_n. In the elasto-plastic analysis, the relation between shear stress and shear strain is modeled as shown in Fig. 3.10. The calculation is carried out by means of the variable stiffness method (e.g., Zienkiewicz, 1971); shear stiffness of each joint element is changed iteratively so that the calculated shear stress and strain follow the stress-strain curve of Fig. 3.11.

The soil parameters appropriate for the finite-element analysis are listed in Table 3.2. Young's modulus, E, is taken as constant for the whole region considered; E for clays are nearly proportional to the square root of the maximum

overburden stress to which the clay has been subjected and, therefore, in highly overconsolidated clay E is almost constant irrespective of the depth. For slopes formed by soils with constant E, the calculated results are identical for any value of E used in the computations. The value of Poisson's ratio, ν, is assumed to be 0.475, a value appropriate to represent a saturated clay with low bulk compressibility. It was observed that the calculated stresses are insensitive to ν.

Table 3.2 Input Conditions for FEM

Property of Soil		Type of Analysis	
		Elastic	Elasto-Plastic
Young Modulus ; E (psf)		60000	60000
Poisson Ratio ; ν		0.475	0.475
Shear Strength	c' (psf)		500.0
	ϕ'_P $(deg.)$		35.0
	ϕ'_R $(deg.)$		30.0

Results obtained for a slope with $K_0 = 1.0$ are shown in Fig. 3.12. In the elastic analysis, as pointed out earlier, the distribution of the excavation-induced shear stress along the potential failure surface, $\Delta\tau(x)$, may be approximated reasonably well with an exponential function, $\Delta\tau(x) = \tau_0 \, e^{-\alpha x}$. The results of the elasto-plastic analysis indicate that failure has occured in some region from the toe of a slope and that the distribution of the shear stress along the unfailed zone of the potential failure surface is similar in shape to the shear

stress distribution obtained in the elastic analysis. Accordingly, the unbalanced force may be redistributed to the unfailed adjacent regions in an exponential form. With this information, therefore, the length of the local failure from the toe of a slope can be determined only through finite-element elastic analysis. As shown in Fig. 3.12, it is convenient to define the modified peak and residual shear strengths, $\tau'_P(x)$ and $\tau'_R(x)$, respectively; both include the initial shear stress, $\tau_i(x)$, that existed along a potential failure surface before excavation.

$$\tau'_P(x) = \tau_P(x) - \tau_i(x) \tag{3.20a}$$

$$\tau'_R(x) = \tau_R(x) - \tau_i(x) \tag{3.20b}$$

Based on the results of the above finite-element analyses, an algorithm for evaluating the length of local failure may be developed as follows:

(i) Divide a prescribed potential failure surface into n segments, each of which has the same length Δl, numbered from the toe of a slope.

(ii) Based on the distribution of the initial shear stress, τ_i, and the distribution of the effective normal stress, σ', after the cut obtained through finite-element elastic analysis, evaluate the corresponding modified peak and residual shear strengths at the I-th segment, $\tau'_P(I)$ and $\tau'_R(I)$ respectively.

(iii) Evaluate the excavation-induced shear stress for the I-th segment, $\Delta\tau(I)$, I=1,n.

(iv) For segment I=1, which is located at the toe of the slope, compare $\Delta\tau(I)$ and $\tau'_P(I)$ to determine whether there is local failure. If failure occurs, the unbalanced force, $[\Delta\tau(I) - \tau'_R(I)]\ \Delta l$, is redistributed to the adjacent segments according to the exponential function. This process is repeated

for the next segment (I+ 1) until no further local failure occurs.

The length of the local failure and the redistribution of the excavation-induced shear stresses obtained through the above algorithm are the same as those obtained with finite-element elasto-plastic analysis.

3.3 Evaluation of Failure Probability

3.3.1 Simulation Method

Up until now, it is assumed that the shear strength of the soil can be expressed exactly by shear strength parameters such as those in Table 3.2. In reality, however, the shear strength of the soil varies spatially, and may be expressed only in terms of probability. Therefore, the peak and residual shear strengths, τ_P and τ_R, respectively, should be modeled as random variables. Assuming that the respective coefficients of variation of τ_P and τ_R are constant everywhere, the peak and residual shear strengths along the potential failure surface may be expressed as follows:

$$\tau_P(x) = \overline{\tau}_P(x) + \overline{\tau}_P(x)\delta_P S_P(x) \tag{3.21a}$$

$$\tau_R(x) = \overline{\tau}_R(x) + \overline{\tau}_R(x)\delta_R S_R(x) \tag{3.21b}$$

where:

x = distance from the toe along the potntial failure surface;

$\overline{\tau}_P(x)$ = mean peak shear strength at x;

$\overline{\tau}_R(x)$ = mean residual shear strength at x;

δ_P, δ_R = coefficients of variation of τ_P and τ_R;

$S_P(x), S_R(x)$ = normal variate; N(0,1).

The values of $S(x)$ at different points are correlated as a function of the separation distance. In general, the correlation between $S(v_1)$ and $S(v_2)$ at two depths v_1 and v_2 is commonly expressed by,

$$\rho_{S(v_1),S(v_2)} = e^{-\beta_V |v_1 - v_2|} \tag{3.22}$$

where β_V is a measure of correlation in the vertical direction. The value of β_V ranges from 0.1 to 0.8 (ft^{-1}) for clay layers (Matsuo, 1976; Wu, 1974; Lumb, 1970). In the same way, the correlation of $S(u_1)$ and $S(u_2)$ between two horizontal points u_1 and u_2 can be expressed as,

$$\rho_{S(u_1),S(u_2)} = e^{-\beta_H |u_1 - u_2|} \tag{3.23}$$

where $\beta_H \leq 0.003\ (ft^{-1})$ for clays. So, $S(u_1)$ and $S(u_2)$ can be considered to be prefectly correlated. On the basis of the above, the correlation for $S(x)$ between two points x_1 and x_2 along a circular potential failure surface may be expressed by (see Fig. 3.13)

$$\rho_{S(x_1),S(x_2)} \approx e^{-\beta_V |v_1 - v_2|} \tag{3.24a}$$

$$\approx e^{-\beta_V \sin\left(\frac{x_1+x_2}{2R}\right) |x_1 - x_2|} \tag{3.24b}$$

Principally, the length of the local failure from the toe of a slope may be evaluated by comparing the modified shear strengths defined in Eq. 3.20 and the excavation-induced shear stress. This evaluation, however, eludes analytical treatment because the modified shear strengths along a potential failure surface is a random process. Simulation may be the only way of treating this problem, in which sample functions of $S(x)$ can be generated through the following

steps:

(i) Generate a sample function of $S(v)$ in the vertical direction over an excavated depth, H, which is a stationary response of a linear system subjected to white noise as shown below:

$$\frac{dS(v)}{dv} + \beta_V S(v) = \xi(v) \tag{3.25}$$

where $\xi(v)$ = a stationary white noise with power spectral density β_V/π.

(ii) Project a sample function of $S(v)$ in the horizontal direction onto a circular potential failure surface to obtain a sample function of $S(x)$.

The spatial distributions of the modified peak and residual shear strengths can be obtained by substituting the generated sample functions of $S(x)$ into Eqs. 3.21 and 3.20. Combining the generated soil condition with the stress redistribution caused by the local failure at the toe of a slope, the length of the local failure from the toe as well as the local failure zones in the interior of the potential failure surface can be obtained. Repeating the simulation a large number of times, the expected value of the length of the local failure from the toe of a slope and the associated failure probability may be evaluated. This simulation method is applied to the same slope considered earlier. The result is shown in Fig. 3.14; the dark zone denotes a local failure zone. From this figure, it can be observed that (i) the toe failure zone accounts for about 99 % of total failure zone; that is, local failure zone other than the toe-failure zone is negligilbe, (ii) the average toe failure length is almost the same as that calculated with a deterministic shear strength of the soil following the procedure in the Sect. 3.2.1.

3.3.2 Simulation-Assisted Approach

The simulation method of Sect. 3.3.1 is appropriate for the probabilistic evaluation of the local failed length from the toe of a slope. However, it may be costly for the evaluation of the failure probability, P_F, because accurate evaluation of P_F requires a large number of repeated simulations. This section develops an alternative simulation method suitable for evaluating P_F.

A clear-cut definition of the entire failure of a cut slope is essential to the evaluation of P_F of the cut slope. As seen in the previous sections, the resisting force provided by a soil is divided into two parts: one is the contribution from the failed region; the other is from the exponentially-distributed shear resistance in the unfailed region. Thus, the resisting force corresponding to an assumed toe-failure length l_f can be evaluated as

$$R(l_f) = \int_0^{l_f} \tau'_R(x)\, dx + \tau'_P(l_f) \cdot \int_{l_f}^{l} e^{-\frac{C_2}{H}(x-l_f)}\, dx \tag{3.26}$$

where l = length of a potential failure surface. The available maximum resisting force provided by a soil, $R_{\max}$, can be obtained as the maximum of $R(l_f)$ for $0 \leq l_f \leq l$. Total failure occurs if $R_{\max}$ is less than the excavation-induced shear force, ΔS. $R_{\max}$ is a random variable because of the inherent variability of the shear strength of a soil. Therefore, the corresponding probability of failure, P_F, can be defined as

$$P_F = P(R_{\max} < \Delta S) \tag{3.27}$$

$R_{\max}$ can be evaluated through the simulation procedure in which the spatial distribution of the shear strength of a soil is generated. Simulation is

performed for the slope with a specific potential failure surface in Fig. 3.12. $R_{\max}$ may be considered to be log-normal, type-1 or type-2 distributed. Goodness of fit analysis was performed for the simulated $R_{\max}$ (see Table 3.3 and Fig. 3.15); the log-normal distribution can be seen to be the best distribution for $R_{\max}$. Combining Eq. 3.27 with the obtained log-normal parameters (λ,ζ) for the distribution of $R_{\max}$, P_F is evaluated simply as

$$P_F = \Phi(\frac{\ln\Delta S - \lambda}{\zeta}) \tag{3.28}$$

where $\Phi(\ )$ = CDF of standard normal variate.

Table 3.3 Fitness Analysis of $R_{\max}$

Distribution	Parameters		Correlation Coefficient
Log-Normal	λ	ζ	0.9968
	11.140	0.1245	
Type-1	α	u	0.9808
	1.483×10^{-4}	65600	
Type-2	K	V	0.9671
	10.391	65270	

3.3.3 Influence of Ground Water Level on Failure Probability

Steady-state ground water condition within a slope is difficult to predict precisely. In other words, the prediction of the ground water condition involves

errors or uncertainties. Therefore, the water table, H_w, should be treated as a random variable in the evaluation of the failure probability, P_F, of a slope, obtaining

$$P_F = \int P_F(h_w) f_{H_w}(h_w)\, dh_w \tag{3.29}$$

where:

$P_F(h_w)$ = P_F with $H_w = h_w$;

$f_{H_w}(h_w)$ = PDF of H_w .

The evaluation of $P_F(h_w)$ requires the distribution of pore water pressure along a potential failure surface, $u(x)$, which may be evaluated through the flow-net corresponding to the case of $H_w = h_w$.

In place of Eq. 3.29, an approximate formula may be used, in which $u(x)$ is taken directly as a random variable, and the corresponding P_F evaluated as

$$P_F \approx \int P_F[C \cdot \mu_u(x)] f_C(C)\, dC \tag{3.30}$$

where:

$\mu_u(x)$ = $u(x)$ corresponding to the expected water table;

$P_F[C \cdot \mu_u(x)]$ = P_F with $u(x) = C \cdot \mu_u(x)$;

C = positive random variable with $\mu_C = 1.0$.

In Eq. 3.30, the COV of C represents the degree of disbelief about the expected steady-state hydraulic condition within the slope.

3.4 Illustrative Example

This section illustrates through specific examples the usefulness and advantages of the proposed method over the conventional methods.

In the first example, the safety of an excavated slope shown in Fig. 3.12 is evaluated with the proposed method as well as the reliability-based conventional method. The results are shown in Table 3.4.

Table 3.4 Comparison of Results with both Conventional and Proposed Methods

Method	Potential Failure Surface R/H	F_S	P_F	$E[l_f]$ (f)
Conventional Method (Peak Strength)	1.78	1.911	0.150×10^{-5}	
	2.12	1.866	0.263×10^{-5}	
	2.50	1.890	0.203×10^{-5}	
	2.92	1.969	0.884×10^{-6}	
	3.38	2.061	0.354×10^{-6}	
Conventional Method (Residual Strength)	1.78	0.703	0.999	
	2.12	0.784	0.995	
	2.50	0.856	0.942	
	2.92	0.944	0.711	
	3.38	1.025	0.413	
Proposed Method	1.78		0.856×10^{-3}	18.5
	2.12		0.104×10^{-2}	18.9
	2.50		0.154×10^{-3}	24.1
	2.92		0.309×10^{-4}	24.9
	3.38		0.120×10^{-4}	23.5

The probability of failure P_Fs obtained with the conventional method based on the assumption that the available shear strength of a soil is its peak or residual shear strength give merely the upper and lower bounds of P_F. The difference

between the bounds is so large that the results obtained with the conventional method is almost useless. In contrast, the proposed method can evaluate P_F as well as the probabilistic nature of the toe-failure length, which can not be obtained with other existing methods. It is worthy to note that the critical failure surface, i.e., the most probable potential failure surface, obtained with both the conventional and the proposed methods are very close. Therefore, the safety of cut slopes can be evaluated by applying the proposed method to several potential failure surfaces around the most critical failure surface determined by means of the conventional method.

The second example shows the effects of the COV of shear strengths (δ) and β_V on P_F along the most critical failure surface of the same cut slope discussed in the first example. Table 3.5 shows the results for several combinations of δ and β_V; δ is strongly related to P_F, and β_V is equally influential on P_F if δ is relatively small.

Table 3.5 Sensitivity of COV of Shear Strength and β_V to P_F

COV of Shear Strength	β_V (ft^{-1})	P_F
0.1	0.1	0.388×10^{-3}
0.1	0.3	0.327×10^{-6}
0.1	0.5	0.151×10^{-8}
0.2	0.1	0.231×10^{-1}
0.2	0.3	0.104×10^{-2}
0.2	0.5	0.791×10^{-4}

The third example shows the effects of the difference of the steady-state water condition on P_F along the most critical failure surface in terms of Eq. 3.30. The calculation is made for different combinations of the expected water level as shown in Fig. 3.15 including the one shown in Fig. 3.3 and the COV of C. The results are shown in Table 3.6; the difference in the expected water level has marked effect on P_F whereas the difference in COV of C, that is, the degree of uncertainty about the expected water level is much less influential on P_F.

Table 3.6 Influence of Difference of Water Table on P_F

Expected Water Level	COV	P_F
1	0.0	0.997×10^{-5}
	0.1	0.998×10^{-5}
	0.2	0.999×10^{-5}
	0.3	0.100×10^{-4}
2	0.0	0.429×10^{-4}
	0.1	0.444×10^{-4}
	0.2	0.485×10^{-4}
	0.3	0.538×10^{-4}
3	0.0	0.104×10^{-2}
	0.1	0.125×10^{-2}
	0.2	0.232×10^{-2}
	0.3	0.396×10^{-2}

3.5 Summary

In an excavated slope which is composed of a seemingly strong soil such as highly overconsolidated clay, its critical failure mode is progressive failure, which is different from the usually-assumed instantaneous failure. Existing methods are inapplicable for evaluating the static stability of this type of slopes.

To tackle this problem, the pattern of the stress redistribution of the unbalanced force caused by a local failure along a potential failure surface is first investigated in some detail using finite-element elasto-plastic analysis. Then, the established stress redistribution is combined with the inherent variability of the shear strength of a soil along a potential failure surface to determine the failure probability P_F. Reliability-based conventional method can evaluate only the lower and upper bounds of P_F, whereas the proposed method can evaluate the failure probability as well as the expected toe-failure length.

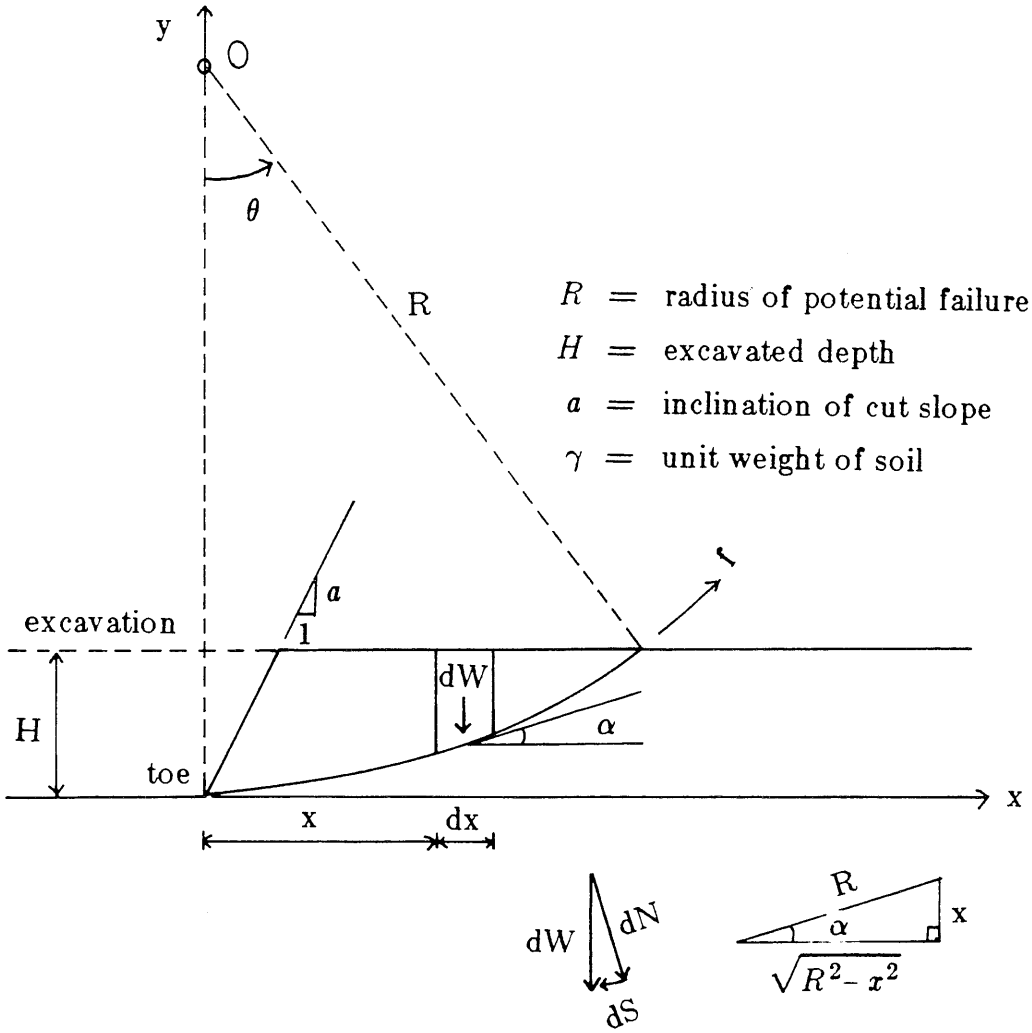

$$dW = \gamma[\sqrt{R^2-x^2} + Min\{H, ax\} - R]\,dx$$

where $dN = dW\cdot\cos\alpha = dW\cdot\sqrt{R^2-x^2}/R$

$$dS = dW\cdot\sin\alpha = dW\cdot x/R$$

$$\sigma = \frac{dN}{dx}\frac{\sqrt{R^2-x^2}}{R} = \gamma R[\cos\theta + Min\{a\sin\theta, H/R\} - 1]\cos^2\theta$$

$$\sigma' = \sigma - u$$

$$\tau = \frac{dS}{dx}\frac{\sqrt{R^2-x^2}}{R} = \gamma R[\cos\theta + Min\{a\sin\theta, H/R\} - 1]\sin\theta\cos\theta$$

where $\theta = f/R$

Fig. 3.1 Conventional Method

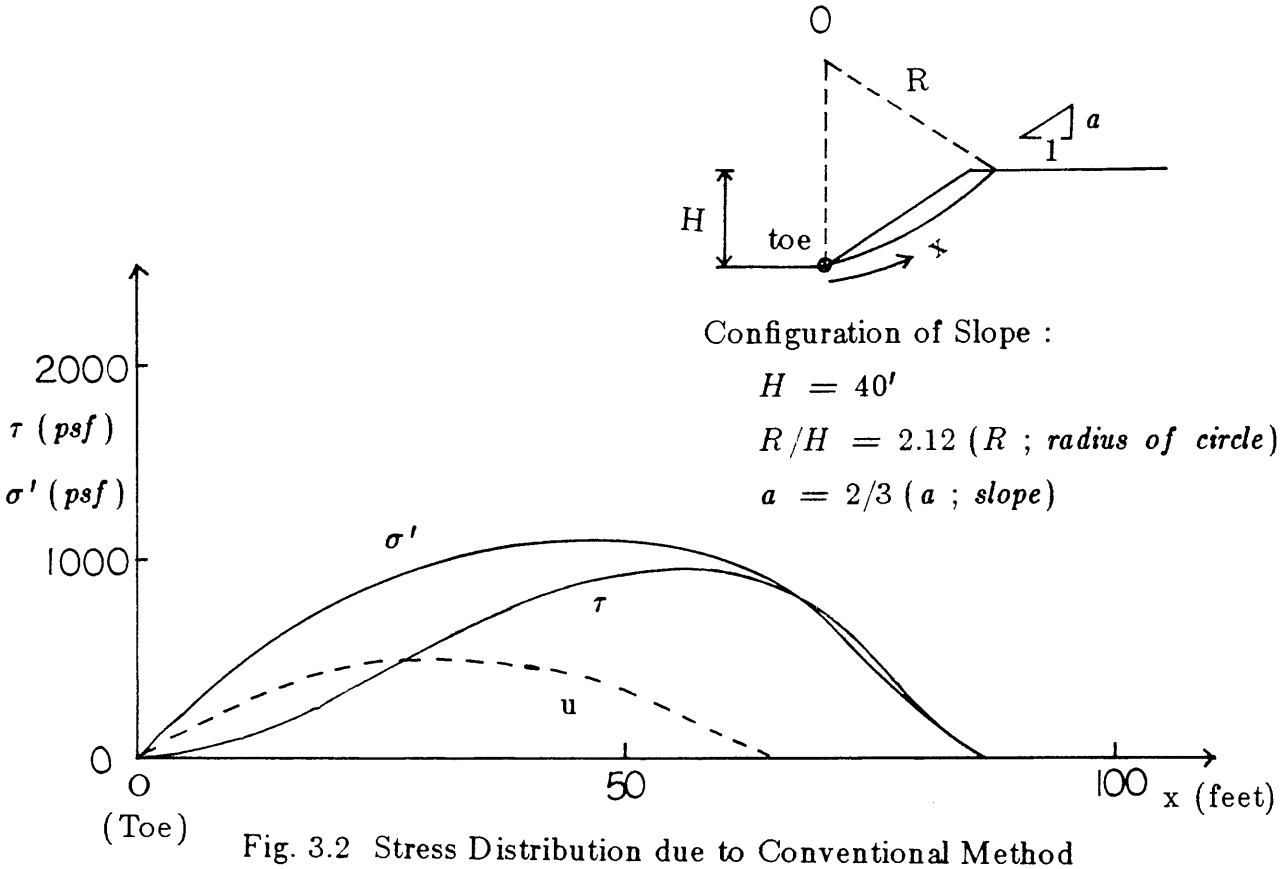

Fig. 3.2 Stress Distribution due to Conventional Method

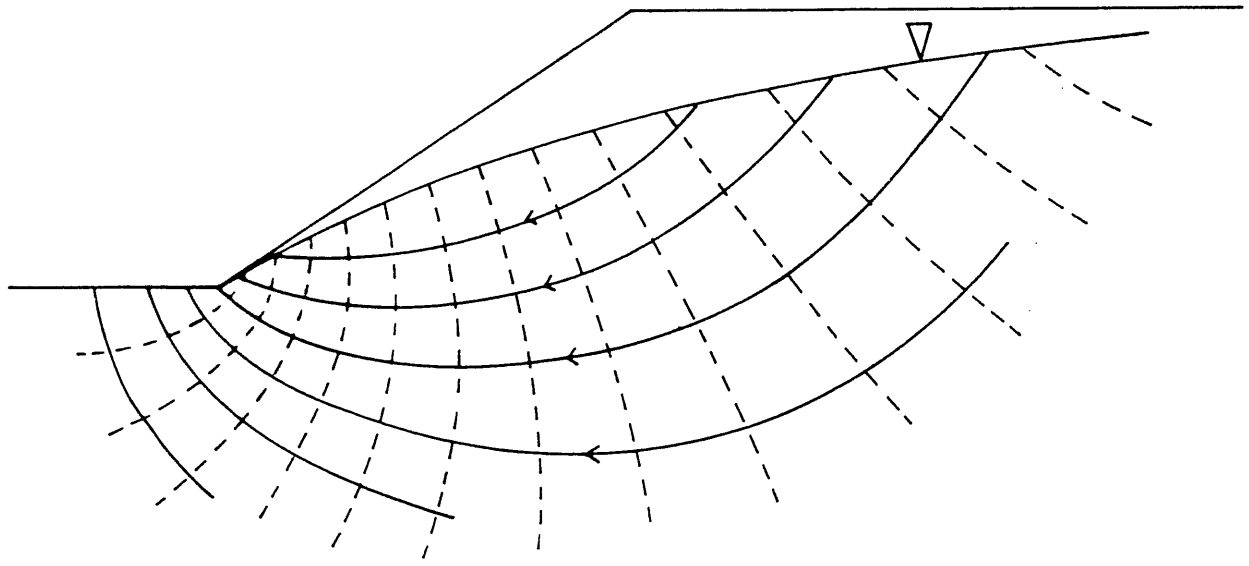

Fig. 3.3 Assumed Flow-Net

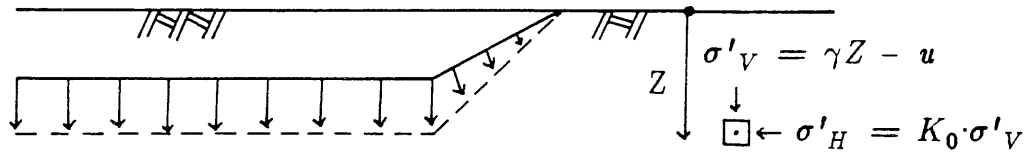

(a) σ_0 : initial stress

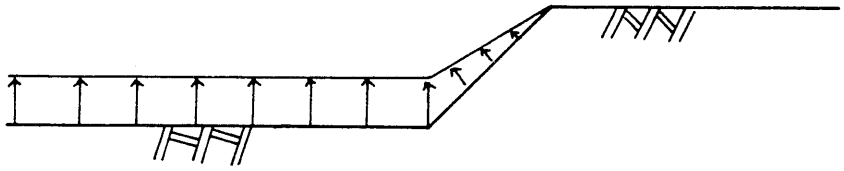

(b) $\Delta\sigma$: excavation-induced stress

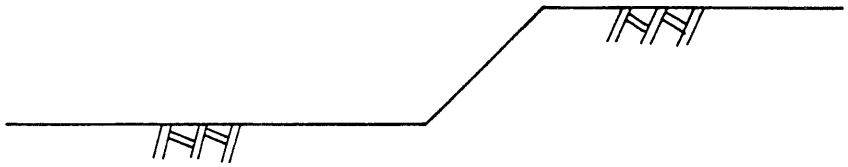

(c) σ : stress after excavation

$$\sigma = \sigma_0 + \Delta\sigma$$

Fig. 3.4 Analytical Simulation of Excavation

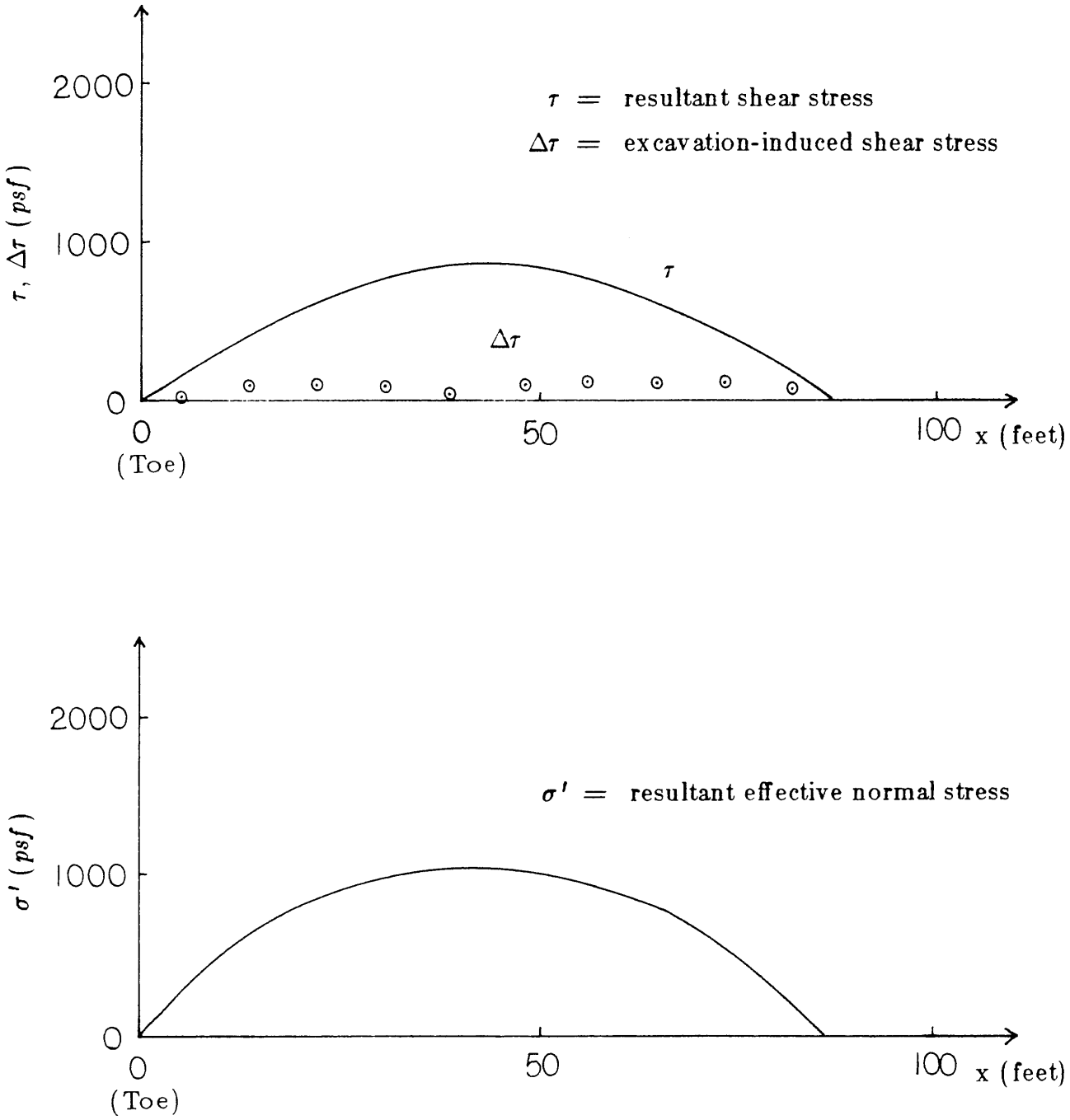

Fig. 3.5 Stress Distribution obtained from Finite-Element Elastic Analysis ($K_0 = 0.5$)

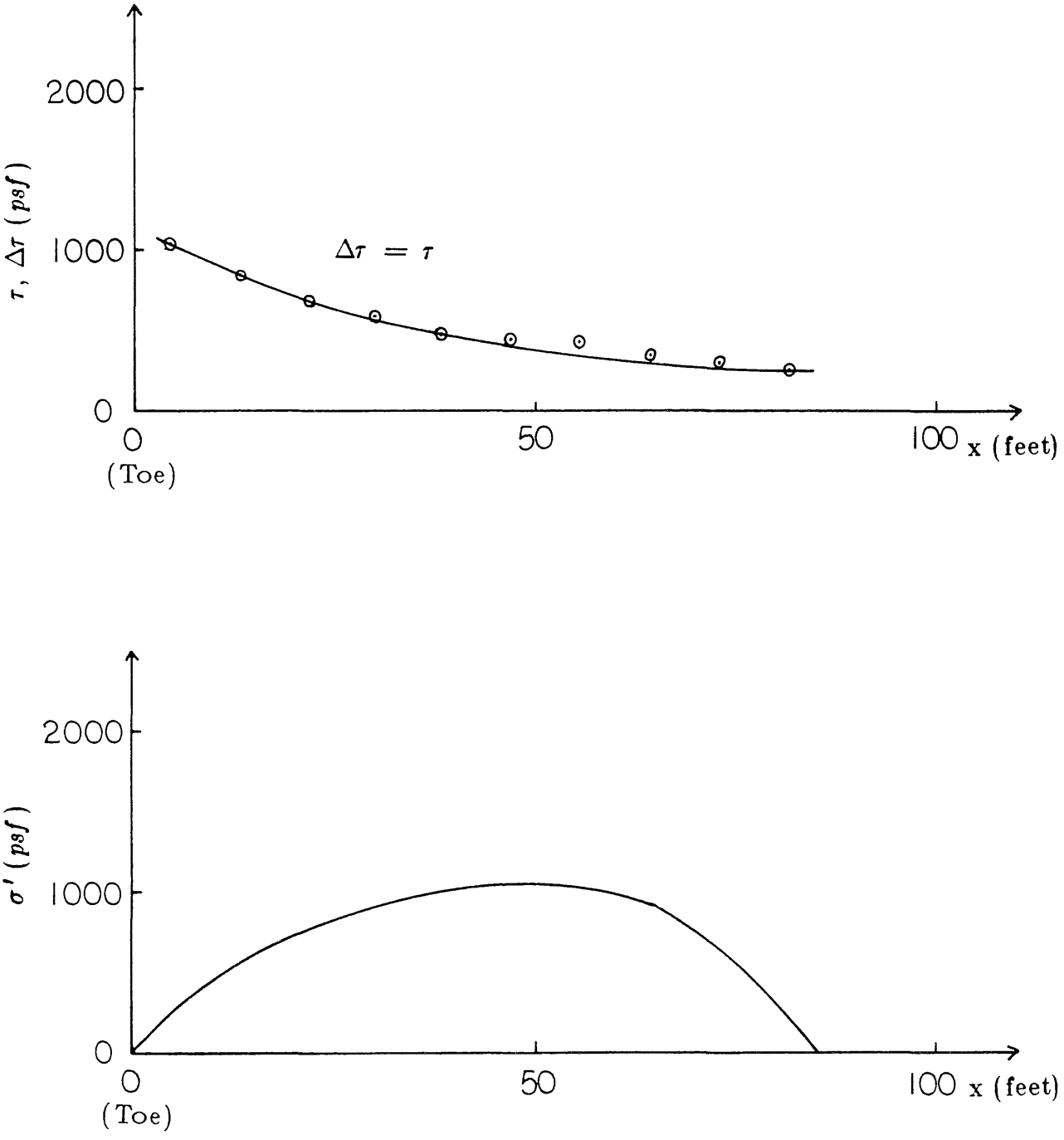

Fig. 3.6 Stress Distribution obtained from Finite-Element Elastic Analysis ($K_0 = 1.0$)

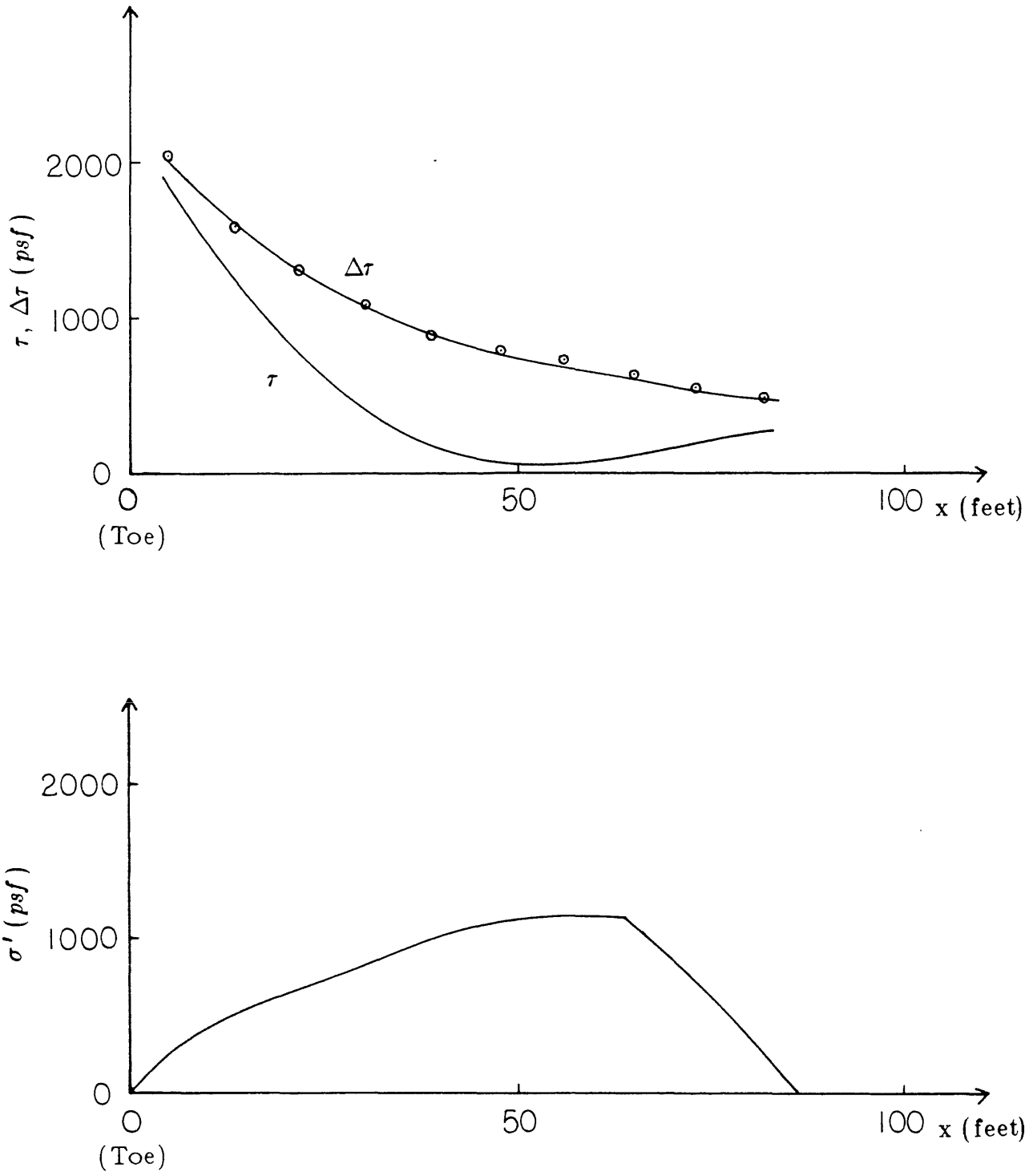

Fig. 3.7 Stress Distribution obtained from Finite-Element Elastic Analysis ($K_0 = 1.5$)

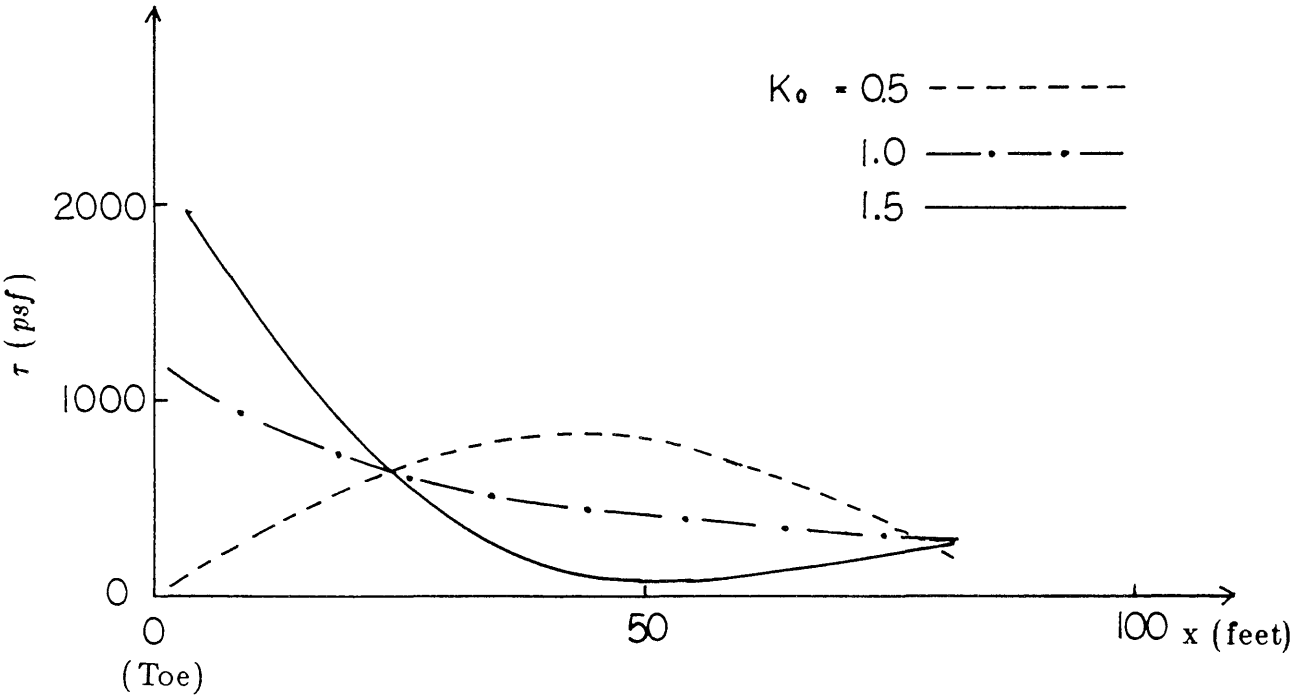

Fig. 3.8 Summary of Shear Stresses from Finite-Element Elastic Analysis

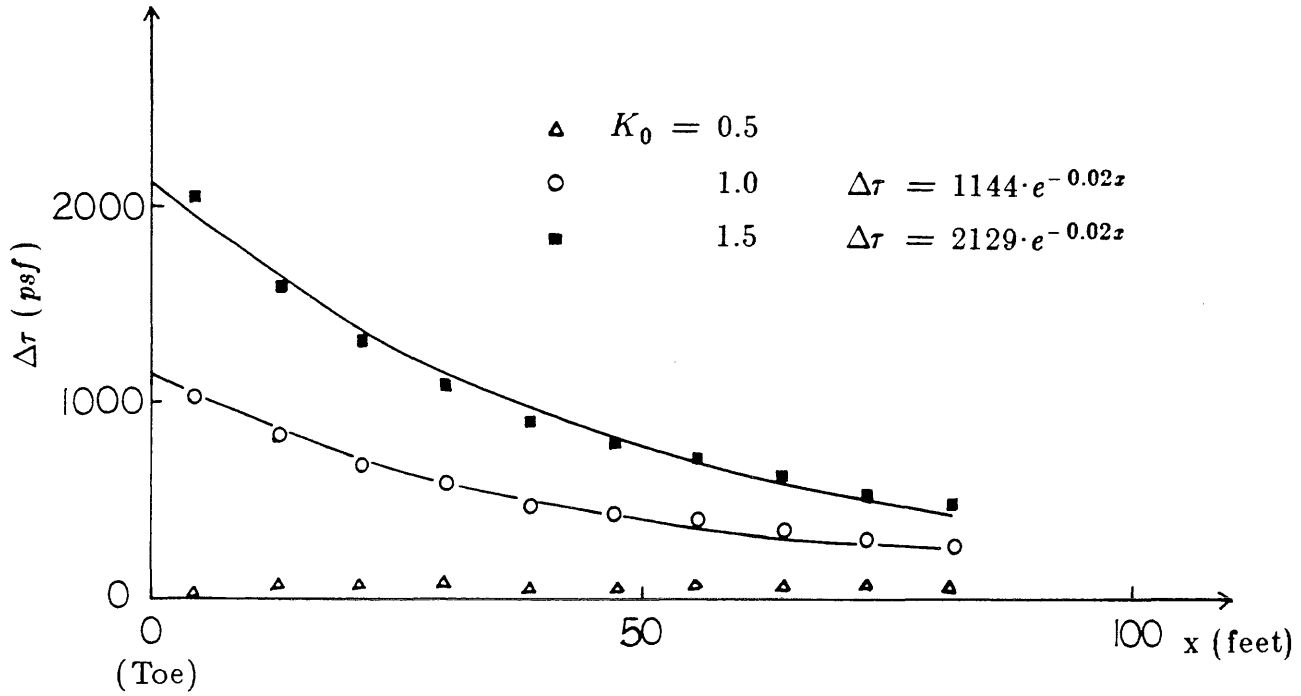

Fig. 3.9 Excavation-Induced Shear Stresses along Failure Surface

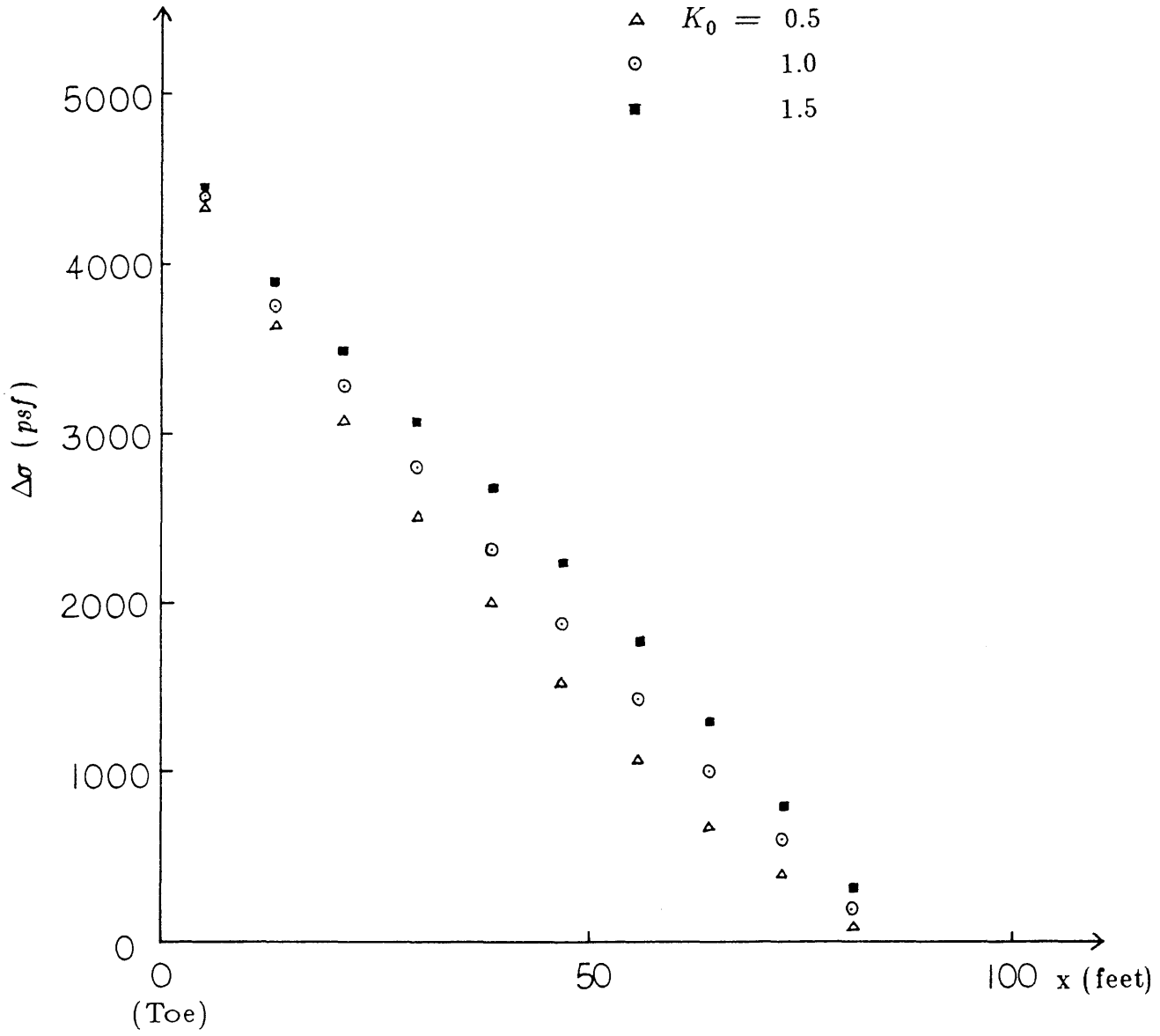

Fig. 3.10 Excavation-Induced Normal Stresses along Failure Surface

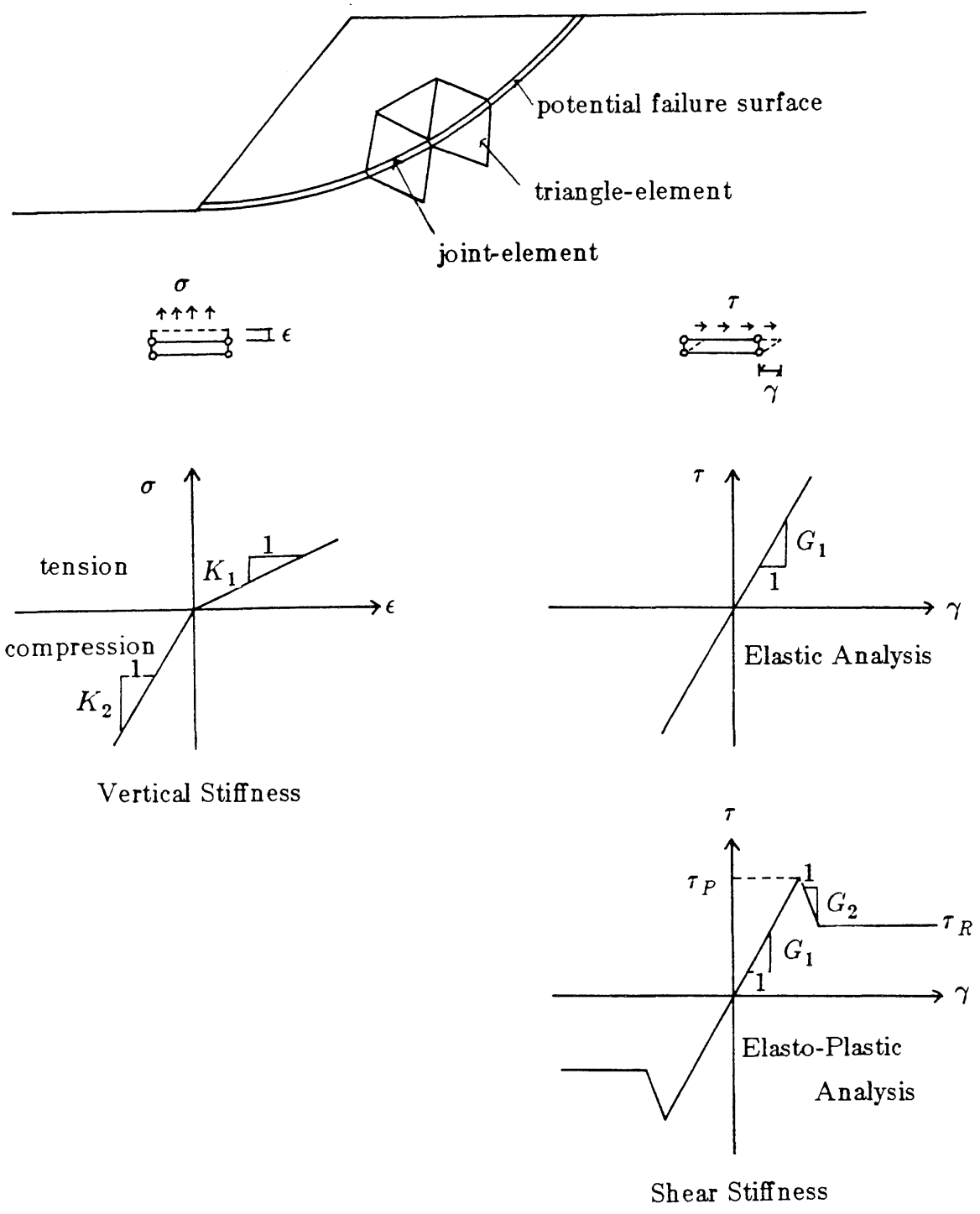

Fig. 3.11 Modeling of Potential Failure Surface

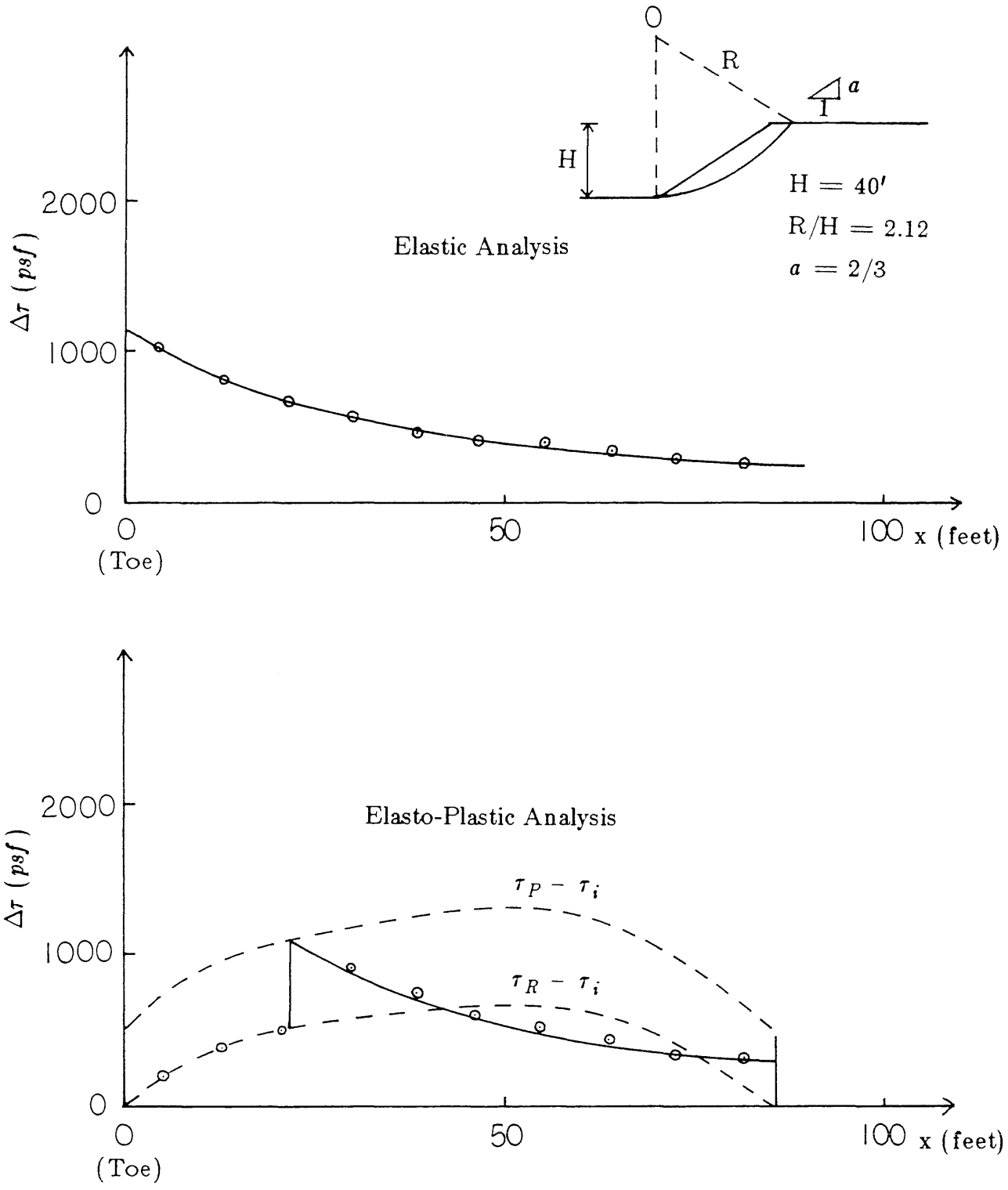

Fig. 3.12 Results of Finite-Element Analysis ($K_0 = 1.0$)

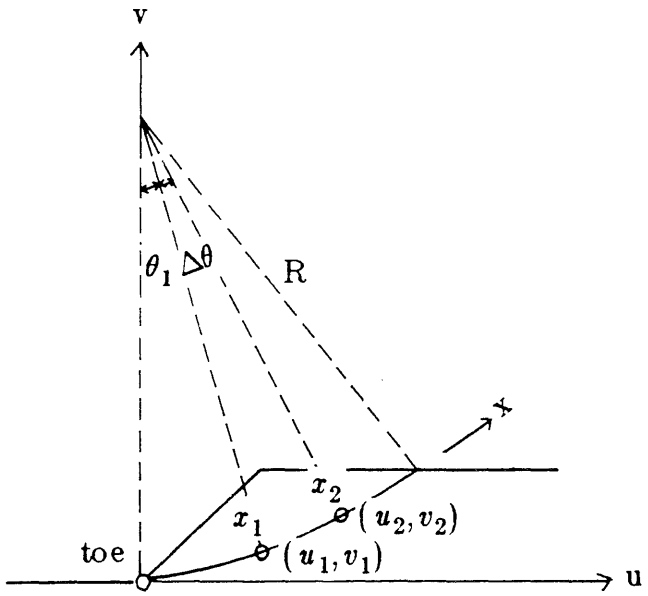

$$\rho(x_1, x_2) \approx e^{-\beta_V |v_1 - v_2|}$$

$$|v_1 - v_2| = R\{\cos\theta_1 - \cos(\theta_1 + \Delta\theta)\}$$

$$= 2R\sin(\frac{\Delta\theta}{2})\sin(\theta_1 + \frac{\Delta\theta}{2})$$

In case of $\Delta\theta$ being relatively small,

$$\sin(\frac{\Delta\theta}{2}) \approx \frac{\Delta\theta}{2} = \frac{|x_2 - x_1|}{2R}$$

$$\theta_1 + \frac{\Delta\theta}{2} = \frac{x_1 + x_2}{2R}$$

Therefore, $\rho(x_1, x_2) \approx e^{-\beta_V \sin(\frac{x_1+x_2}{2R})|x_1 - x_2|}$

Fig. 3.13 Correlation between Two Points on a Circular Potential Failure Surface

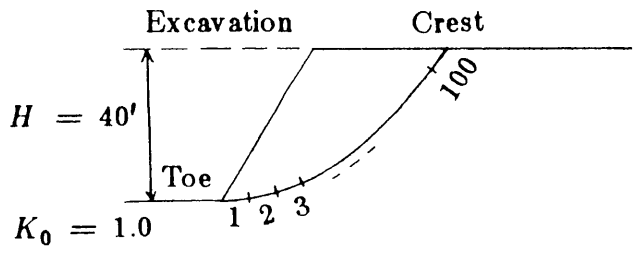

Input Soil Conditions:

c' = 500 psf

ϕ' = 35 degree

ϕ'_R = 30 degree

COV (peak) = 0.2

COV (residual) = 0.2

β_V = 0.3 ft^{-1}

Segments divided along a Potential Failure Surface

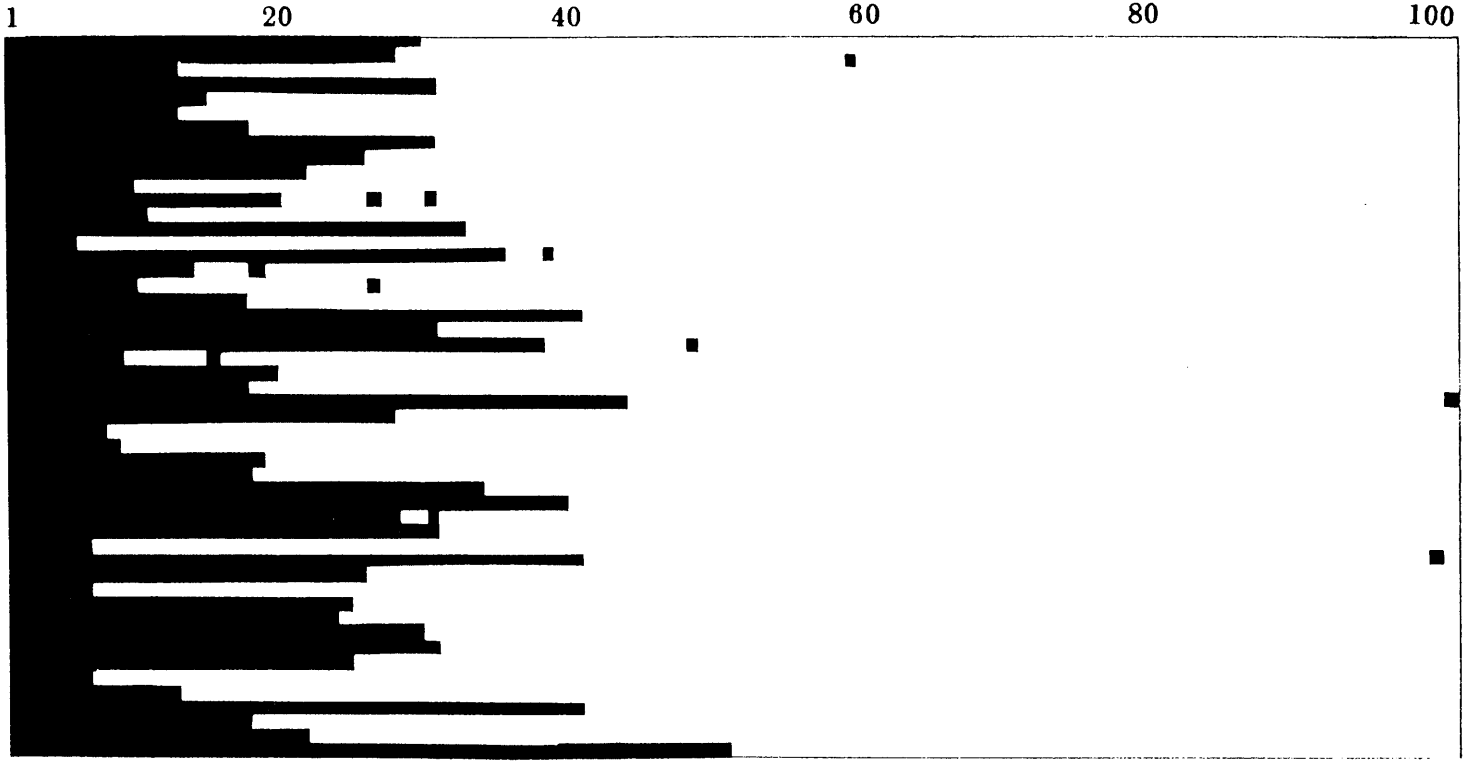

*) Each row shows the corresponding simulation result in which dark zone denotes a local failure.

Fig. 3.14 Failed Zone obtained by Simulation

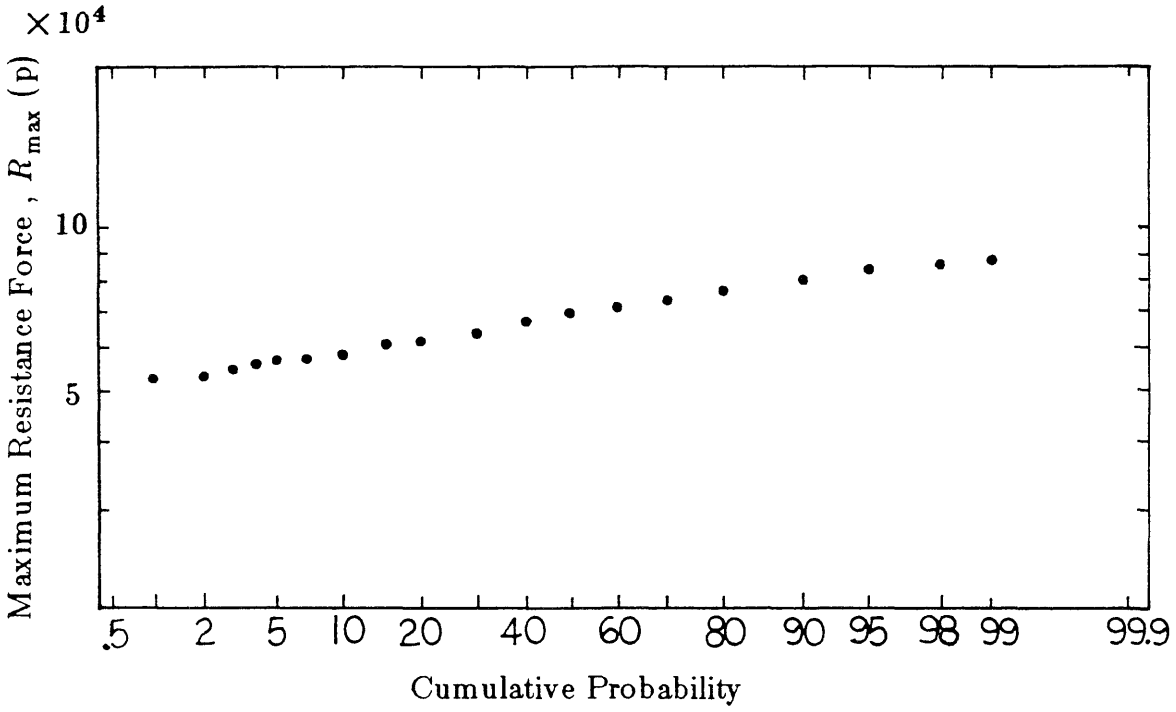

Fig. 3.15 R_{max} plotted on Log-normal Probability Paper

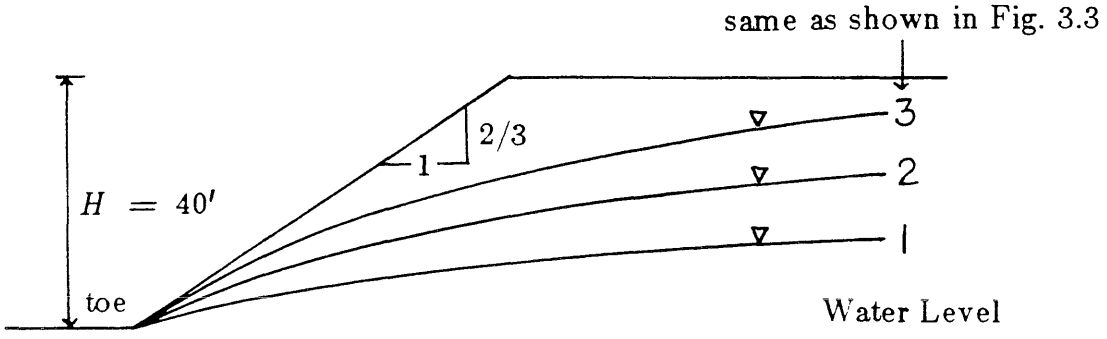

Fig. 3.16 Assumed Water Levels

CHAPTER 4

SEISMIC STABILITY OF CUT SLOPES

4.1 The Analytical Model

In general, earthquake-induced horizontal accelerations within a slope vary spatially. However, dynamic finite-element analyses of earth slopes (e.g., Idriss and Seed, 1966) show that the root-mean-square horizontal accelerations at various points within a slope can be expressed approximately as a function of the depth from the crest of the slope, regardless of the horizontal distance from the slope surface. This implies that the seismic stability of a slope, which is two or three-dimensional in nature, may be converted into a one-dimensional vibration system.

In light of the above information, the seismic slope stability problem can be modeled as follows:

(i) As shown in Fig. 4.1, the distribution of the amplification factor A_f, which may be defined as the root-mean-square (RMS) absolute acceleration normalized by the acceleration at the toe of a slope, and the dominant frequency ω_1 could be obtained from the dynamic analysis of a multi-degree-of-freedom (MDF) system subjected to a filtered shot noise.

(ii) As will be shown later, the first mode of vibration is invariably dominant, and thus the shape of the amplification factor simply represents the mode shape of the horizontal acceleration of the MDF system. Therefore, the system can be converted into an equivalent single-degree-of-freedom (SDF) system, in which a concentrated mass M, equivalent height H_{eq} and

average amplification factor A_{av} are evaluated considering the equilibrium of force and moment applied to a sliding mass, as shown in Fig. 4.2.

(iii) Based on the distribution of the dynamic shear strength corresponding to N cycles of uniform loadings $\tau_d(N)$ along a potential failure surface, the horizontal force F(N) that will cause failure of the SDF system in N cycles of uniform loadings (Fig. 4.3) is evaluated.

(iv) The shearing stress-strain relation of this converted system is modeled by the smooth hysteretic model proposed by Wen (1976, 1980). In this regard, the system must satisfy the following conditions: the RMS absolute acceleration of the concentrated mass is A_{av} times as large as that at the base level; the expected frequency is the same as ω_1; and the ultimate hysteretic restoring force is equal to F(N=1). Through random vibration analysis coupled with equivalent linearization (Atalik and Utku, 1976), the system parameters can be determined to satisfy the above-mentioned conditions, and the corresponding response statistics can be oftained for the purpose of assessing the damage of the system subjected to an earthquake. In this analysis, an earthquake ground motion is modeled as a filtered shot noise stationary random process.

4.2 Dynamic Analysis of Nonlinear MDF System

In the dynamic system shown in Fig. 4.4, the governing equations of motion are as follows:

$$[M]\{\ddot{u}\} + [C]\{\dot{u}\} + [K]\{u\} = -[M]\ddot{x}_G \tag{4.1}$$

where:

$[M]$ = mass matrix;

$[C]$ = damping matrix;

$[K]$ = stiffness matrix;

$\{\ddot{u}\}$ = vector of acceleration relative to that at the toe of a slope;

$\{\dot{u}\}$ = vector of velocity relative to that at the toe;

$\{u\}$ = vector of displacement relative to that at the toe.

Absolute acceleration at the toe of a slope, $\ddot{x}_G$, is generated artificially as follows:

(1) The stationary wave form is generated having a constant power spectral density function (white noise) of intensity S_0 over a wide range of frequencies.

(2) The resulting wave form of shot noise is then passed through a second-order filter (Kanai-Tajimi filter) which amplifies the frequency content in the neighborehood of a characteristic frequency and attenuates the high frequencies.

Second-order filtering is accomplished digitally by solving numerically the second-order differential equation relating the filter output to its corresponding input (Clough and Penzien, 1975). This solution is obtained numerically by the standard linear acceleration method using constant integration time intervals of 0.01 seconds.

If the i-th layer of a soil column is subjected to a shear strain as shown in Fig. 4.5, the shear stress induced in the i-th layer is

$$\tau_i = \frac{P_i}{(Unit\ Area)} = G_i \gamma_i \tag{4.2}$$

where:

P_i = shear force applied at the top of the i-th layer;

G_i = shear modulus of the i-th layer;

γ_i = shear strain at the i-th layer.

γ_i is given by

$$\gamma_i = \frac{\Delta u_i}{l_i} \tag{4.3}$$

where:

Δu_i = difference in horizontal displacement between the top and bottom of the i-th layer;

l_i = thickness of the i-th layer.

Substituting Eq. 4.3 into Eq. 4.2, the following is obtained

$$P_i = \frac{G_i(\textit{Unit Area})}{l_i}\Delta u_i \tag{4.4}$$

Therefore, the shear stiffness of the i-th layer is

$$K_i = \frac{G_i}{l_i}(\textit{Unit Area}) \tag{4.5}$$

The viscous damping coefficient, C_i, is related to the hysteretic damping ratio, h_i, of the i-th layer as follows:

$$C_i = 2\sqrt{M_i K_i}\, h_i \tag{4.6}$$

where M_i = mass of the i-th layer.

The relation between shear stress and strain of soils is highly nonlinear as shown in Fig. 4.6. The secant modulus G, and damping ratio h (defined in Fig. 4.7), are expressed as a function of the shear strain, γ. The dynamic response

of the nonlinear system can be evaluated efficiently through equivalent linearization. The procedure is as follows:

(i) Select the first trial values of G and h corresponding to an assumed level of γ. Through Eqs. 4.5 and 4.6, K and C are evaluated. With these parameters, perform the linear analysis to obtain the root-mean-square absolute acceleration, the displacement of each layer relative to that of the toe of the slope and the inter-layer drift, $d_{i,rms}$. The RMS shear strain in the i-th layer is then evaluated as follows:

$$\gamma_{i,rms} = \frac{d_{i,rms}}{l_i} \tag{4.7}$$

(ii) Using updated values of G_i and h_i corresponding to $\gamma_{i,rms}$ obtained in the previous step, linear vibration analysis is repeated until convergence is achieved.

4.3 Nonlinear Random Vibration Method

Soil deposits subjected to earthquake loadings are often likely to undergo shear deformations of the order of 0.01 to 0.5 %, which is well in the nonlinear inelastic range. In addition, the behavior of the material is hysteretic. Thus, an accurate analysis of the seismic response of such soil deposits requires a structural model capable of including the nonlinear-inelastic and hysteretic behavior.

Faccioli and Ramirez (1976) analyzed the seismic response of horizontally layered soil deposits with a Ramberg-Osgood shearing stress-strain behavior using a random vibration model, in which the parameters of an equivalent linear system were obtained by a harmonic linearization technique. Gasetas, Debchaudhury and Gasparini (1981) obtained the statistics of the response of

earth dams excited by strong motions consisting of vertically propagating shear waves using a linear random vibration model. In general, however, to obtain the statistics and probabilities of the response with the above nonlinear models, repeated time-history analysis, i.e., Monte Carlo simulation, must be performed. Recently, Wen (1976, 1980), and Baber and Wen (1979, 1981) proposed a hysteretic restoring force model, and an analytical method for the solution of the required statistics and probabilities without statistical simulation. The following sections will briefly describe this latter model.

4.3.1 The Smooth Hysteretic Model

The equation of motion of a single-degree-of-freedom system subjected to ground excitations can be written as

$$m\ddot{u} + c\dot{u} + q(u, t) = -m\ddot{x}_G \tag{4.8}$$

where the restoring force is

$$q(u, t) = \alpha K u + (1 - \alpha) K Z \tag{4.9}$$

The nonlinear differential equation governing Z is given by

$$\dot{Z} = A\dot{u} - \beta |\dot{u}| |Z|^{n-1} Z - \delta \dot{u} |Z|^n \tag{4.10}$$

where:

$\alpha, A, \beta, \delta, n$ = parameters describing the shape of the hysteretic loop;

u = the relative displacement of the mass;

Z = the hysteretic component of the displacement;

m = mass;

$\ddot{x}_G$ = base accleration;

c = coefficient of viscous damping;

K = initial stiffness of linear system.

The total restoring force, q(u, t), has a hereditary property because of the inclusion of the Z term, which is the solution of the nonlinear differential equation, Eq. 4.10. A large number of hysteresis shapes can be described by varying the parameters A, β, δ and n, where A, β and δ must satisfy certain criteria to assure that the total energy dissipated over a loading cycle is positive. Some of the possible hysteretic loops are shown in Fig. 4.8, among which (b) is the most suitable for modeling soil behavior.

The skeleton curve, defined as the locus of the tips of the hysteresis loops with different amplitudes, is given by

$$u_s(Z) = \frac{1}{2}\left[\int_o^Z \frac{d\varsigma}{A-(\delta+\beta)\varsigma^n} + \int_0^Z \frac{d\varsigma}{A-(\delta-\beta)\varsigma^n}\right] \tag{4.11}$$

The incremental work done by hysteretic action is

$$dE_T = (1-\alpha)KZ\,du \tag{4.12}$$

and the energy dissipated per cycle of amplitude Z, $E_c(Z)$, is given by (Baber and Wen, 1979)

$$E_C(Z) = 2(1-\alpha)K\left[\int_0^Z \frac{\varsigma\, d\varsigma}{A-(\delta+\beta)\varsigma^n} - \int_0^Z \frac{\varsigma\, d\varsigma}{A-(\delta-\beta)\varsigma^n}\right] \tag{4.13}$$

For a softening system, Z attains a maximum value when $dZ/du = 0$ in Eq. 4.10. For positive $\dot{u}$ and Z, this gives

$$Z_u = \left(\frac{A}{\delta+\beta}\right)^{1/n} \tag{4.14}$$

Therefore, the ultimate hysteretic restoring force, f_u, is given as follows:

$$f_u = (1-\alpha)KZ_u = (1-\alpha)K\left(\frac{A}{\delta+\beta}\right)^{1/n} \tag{4.15}$$

The total energy dissipated by hysteretic action is

$$E_T = \int_0^t (1-\alpha)K(Z\dot{u})\, dt \tag{4.16}$$

4.3.2 Stochastic Equivalent Linearization

The response statistics may be obtained by the method of equivalent linearization (Atalik and Utku, 1976). The special form of the nonlinear hysteretic model presented in Sect. 4.3.1 permits the linearization of the equation of motion in closed form, without resorting to the Krylov-Bogoliulov (KB) approximation.

Examining the equations of motion of a SDF system, Eqs. 4.8 through 4.10, reveals that the differential equation for Z, Eq. 4.10, is the source of nonlinearity. Hence, only Eq. 4.10 needs to be linearized. The linearized form of Eq. 4.10 was obtained by Baber and Wen (1980) as follows:

$$\dot{Z} = C_e \dot{u} + K_e Z \tag{4.17}$$

where C_e and K_e are equivalent linear coefficients, chosen such that the resulting solution for $\dot{Z}$ is as close to that obtained with the original nonlinear equation as possible. The general expressions for C_e and K_e, in terms of the response statistics, are given in the Appendix.

The earthquake base excitation may be modeled as a filtered white noise (Amin and Ang, 1966, 1968; Shinozuka and Sato, 1967; Liu, 1970; Clough and

Penzien, 1975) with the Kanai-Tajimi filter (Tajimi, 1965). The equation of motion, expressed in matrix form, is

$$\{\dot{y}\} = [G]\{y\} + \{F\} \tag{4.18}$$

in which,

$$\{y\}^T = [u, Z, x_G, \dot{u}, \dot{x}_G]$$

$$[G] = \begin{bmatrix} 0 & 0 & 0 & 1 & 0 \\ 0 & -K_e & 0 & -C_e & 0 \\ 0 & 0 & 0 & 0 & 1 \\ -\alpha K/m & -(1-\alpha)K/m & \omega_G^2 & -c/m & 2\zeta_G\omega_G \\ 0 & 0 & -\omega_G^2 & 0 & -2\zeta_G\omega_G \end{bmatrix}$$

and,

$$\{F\}^T = [0,0,0,0,\ddot{x}_G]$$

The zero time lag covariance matrix, [S], of the system of equations defined by Eq. 4.18 is the solution of the following differential equation (Lin, 1967):

$$[\dot{S}] = [G][S] + [S][G]^T + [B] \tag{4.19}$$

where:

$[S(t)] = E[\{y(t)\}\{y(t)\}^T]$;

$B_{ij} = 0$ except $B_{55} = 2\pi S_0$;

S_0 = the two-sided power spectral density of a white noise.

The system of equations defined by Eq. 4.19 is a system of nonlinear ordinary differential equations, because [G] depends on the response statistics, and its solution requires numerical integration in the time domain. The stationary solution for nondeteriorating systems, i.e., $[\dot{S}] = 0$, may be obtained iteratively using the algorithm reported by Bartels and Stewart (1972).

4.3.3 Energy Dissipation Statistics

The rate of energy dissipated by hysteresis is given by

$$\dot{E}_T(t) = (1-\alpha)KZ\dot{u} \tag{4.20}$$

The expected rate of hysteretic energy dissipated is, therefore, given by

$$E[\dot{E}_T(t)] = (1-\alpha)K\ E[\dot{u}Z] \tag{4.21}$$

The value of $E[\dot{u}Z]$ is an element of the zero time lag covariance matrix [S(t)]. The mean square value of $\dot{E}_T(t)$ is given by

$$E[\dot{E}_T^2(t)] = (1-\alpha)^2K^2E[\dot{u}^2Z^2] \tag{4.22}$$

Assuming that Z and $\dot{u}$ are jointly Gaussian, the expected value of $\dot{E}_T^2(t)$ may be calculated by

$$E[\dot{E}_T^2(t)] = (1-\alpha)^2K^2(1+2\rho_{\dot{u}Z}^2)\sigma_Z^2\sigma_{\dot{u}}^2 \tag{4.23}$$

The coefficient of variation of $\dot{E}_T(t)$ is

$$\delta_{\dot{E}_T(t)} = \sqrt{1+1/\rho_{Z\dot{u}}{}^2} \tag{4.24}$$

The mean total hysteretic energy dissipated up to time t, $E[E_T(t)]$, is

$$E[E_T(t)] = (1-\alpha)K\int_0^t E[Z(\tau)\dot{u}(\tau)]\ d\tau \tag{4.25}$$

whereas the corresponding mean square of the total energy dissipated is

$$E[E_T^2(t)] = (1-\alpha)^2K^2E\left[\int_0^t\int_0^t Z(s)\dot{u}(s)Z(v)\dot{u}(v)\ ds\ dv\right] \tag{4.26}$$

Evaluation of the right-hand side of Eq. 4.26 requires the knowledge of the two time joint probability distribution of $\dot{u}$ and Z, and involves the calculation of a six fold integral. However, if jointly Gaussian behavior is assumed for the two time joint probability distribution of $\dot{u}$ and Z, calculations may be performed without difficulty. With this latter assumption (Pires et al., 1983),

$$E[E_T^2(t)] = (1-\alpha)^2K^2\int_0^t\int_0^t \{E[Z(s)\dot{u}(s)]E[Z(v)\dot{u}(v)] + E[\dot{u}(s)\dot{u}(v)]E[Z(s)Z(v)] + E[\dot{u}(s)Z(v)]E[Z(s)\dot{u}(v)]\}\, ds\, dv \quad (4.27)$$

Hence, only the two time covariance matrix of the response, [S(s,v)], is necessary. For the stationary case, the above expression is simplified to

$$E[E_T^2(t)] = 2(1-\alpha)^2K^2\left\{\int_0^t (t-\tau)E[\dot{u}(\tau)\dot{u}(0)]E[Z(\tau)Z(0)]\, d\tau + \int_0^t (t-\tau)E[\dot{u}(\tau)Z(0)]E[Z(\tau)\dot{u}(0)]\, d\tau\right\} + \{E[E_T(t)]\}^2 \quad (4.28)$$

The two-time covariance matrix for the stationary case is obtained from:

$$\frac{d}{d\tau}[S(\tau,0)] = [G]\,[S(\tau,0)] \quad ; \quad \text{for} \quad \tau \geq 0 \quad (4.29)$$

The solution of Eq. 4.29 is as follows:

$$[S(\tau,0)] = [T]\,\exp\{[\Lambda]\tau\}\,[T]^{-1}\,[S(0,0)] \quad (4.30)$$

where:

$[T]$ = the eigenmatrix of [G];

$[\Lambda]$ = a diagonal matrix, with the eigenvalues of [G] along its diagonal;

$[T]^{-1}$ = the inverse matrix of [T].

The coefficient of variation of E_T is necessary for calculating the variance of the strong motion duration that will cause sliding failure, and for evaluating the seismic reliability of a cut slope against sliding.

The variance of E_T as obtained with the procedure presented previously was compared with the results of simulations. The results of this investigation are summarized in Fig. 4.9. The coefficient of variation, δ_{E_T}, decreases rapidly with time for the first few seconds of excitation.

4.3.4 The Expected Frequency

The expected frequency of a SDF system subjected to random excitations is defined as

$$E[\omega] = \left\{\frac{E[K_{eq}]}{M}\right\}^{1/2} \tag{4.31}$$

where:

$E[K_{eq}]$ = expected equivalent stiffness;

M = mass.

The restoring force, q, in Eq. 4.9 is composed of two parts: the first part, αKu, is a linear restoring force component q_1 (Fig. 4.10a); and the second part, $(1-\alpha)KZ$, is a hysteretic restoring force component q_2. The skelton curve of q_2 is shown in Fig. 4.10b. The ultimate restoring force f_u in the hysteretic restoring force component is given by Eq. 4.15.

The hysteretic model used herein exhibits smooth yielding and, therefore,

does not have a clearly defined yield point. However, the yield displacement, δ_y, in q_2 may be defined as the ultimate restoring force f_u divided by the initial stiffness in q_2; thus,

$$\delta_y = Z_u/A = \frac{1}{A}\left(\frac{A}{\beta+\delta}\right)^{1/n} \tag{4.32}$$

Adopting δ_y as the yield displacement with the initial stiffness $K_i = [\alpha+(1-\alpha)A]K$, the yield resistance q_y may be defined as

$$q_y = \delta_y K_i = [\alpha+(1-\alpha)A]KZ_u/A \tag{4.33}$$

On the basis of the above, the idealized bilinear skelton curve of the restoring force q can be obtained as shown in Fig. 4.10c. The equivalent stiffness of the hysteresis loop may be defined by the secant stiffness of the hysteresis loops at the peak as

$$K_{eq}(u_P) = q_P/u_P \tag{4.34}$$

where q_P and u_P are the restoring force and displacement at the peak of the hysteresis, respectively. From Fig. 4.10c,

$$K_{eq}(u_P) = K_i\,, \quad \text{for } 0 \leq u_P \leq \delta_y \tag{4.35a}$$

$$K_{eq}(u_P) = K_f + (q_y - \delta_y K_f)/u_P\,, \quad \text{for } \delta_y < u_P \tag{4.35b}$$

where $K_f = \alpha K$

In the case of a stationary random response, the expected stiffness may be defined as a function of the RMS response u in the following form:

$$E[K_{eq}(\sigma_u)] = \int_0^\infty K_{eq}(u_P)p(u_P,\sigma_P)\, du_P \tag{4.36}$$

where the probability density of u_P was proposed by Rice (1954) for the narrow band response as

$$p(u_P,\sigma_u) = (u_P/\sigma_u^2)\exp\{-u_P^2/(2\sigma_u^2)\} \tag{4.37}$$

Substituting Eqs. 4.37 and 4.35 into Eq. 4.36 yields

$$E[K_{eq}(\sigma_u)] = K_i\{1-(1-\alpha)\exp[-(\frac{\delta_y}{\sqrt{2}\sigma_u})^2] + \sqrt{\pi}(1-\alpha)A(\frac{\delta_y}{\sqrt{2}\sigma_u})[1-erf(\frac{\delta_y}{\sqrt{2}\sigma_u})]\} \tag{4.38}$$

where $erf(\ )$ is the error function.

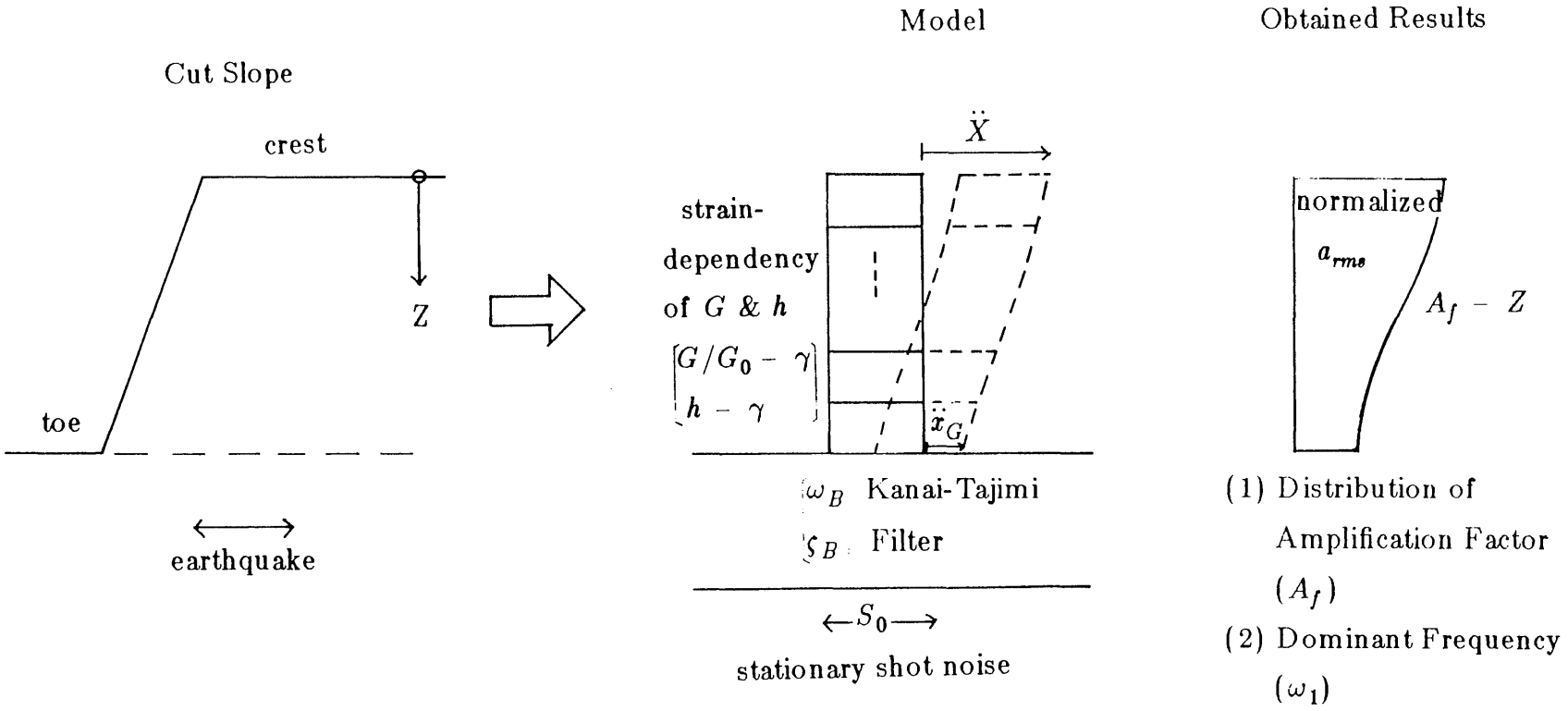

Fig. 4.1 Determination of Amplification Factor (A_f) with Depth (Z) and Dominant Frequency (ω_1)

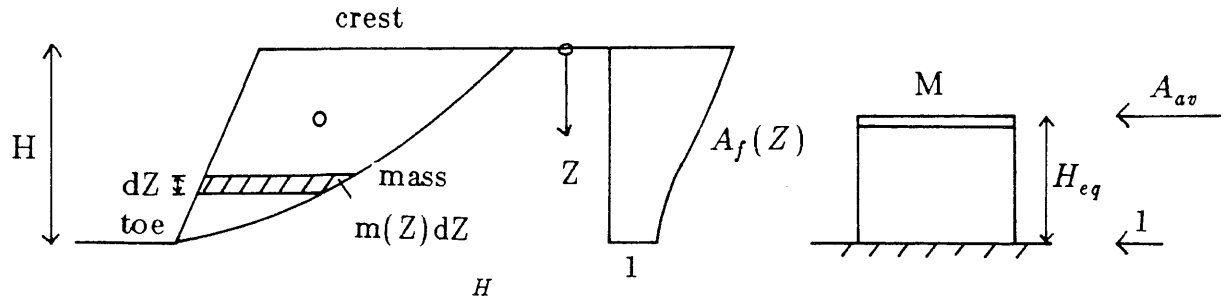

$$M = \int_0^H m(Z)\, dZ$$

$$H_{eq} = H - \frac{1}{M}\int_0^H Z \cdot m(Z)\, dZ$$

$$A_{av} = \frac{1}{M}\int_0^H m(Z) \cdot A_f(Z)\, dZ$$

Fig. 4.2 Conversion of Seismic Slope Stability into Equivalent SDF System

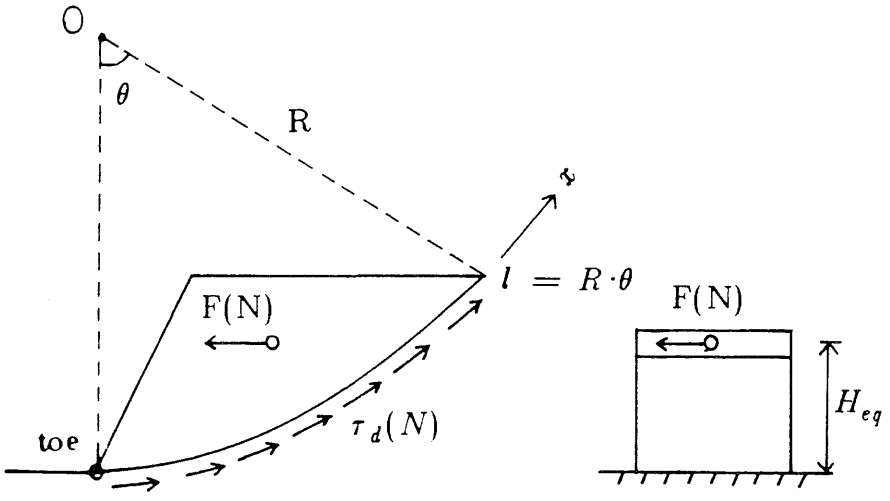

$$F(N) = \left(\frac{R}{R - H_{eq}}\right)\int_0^l \tau_d(N,x)\, dx$$

Fig. 4.3 Determination of F(N) in the Converted SDF System

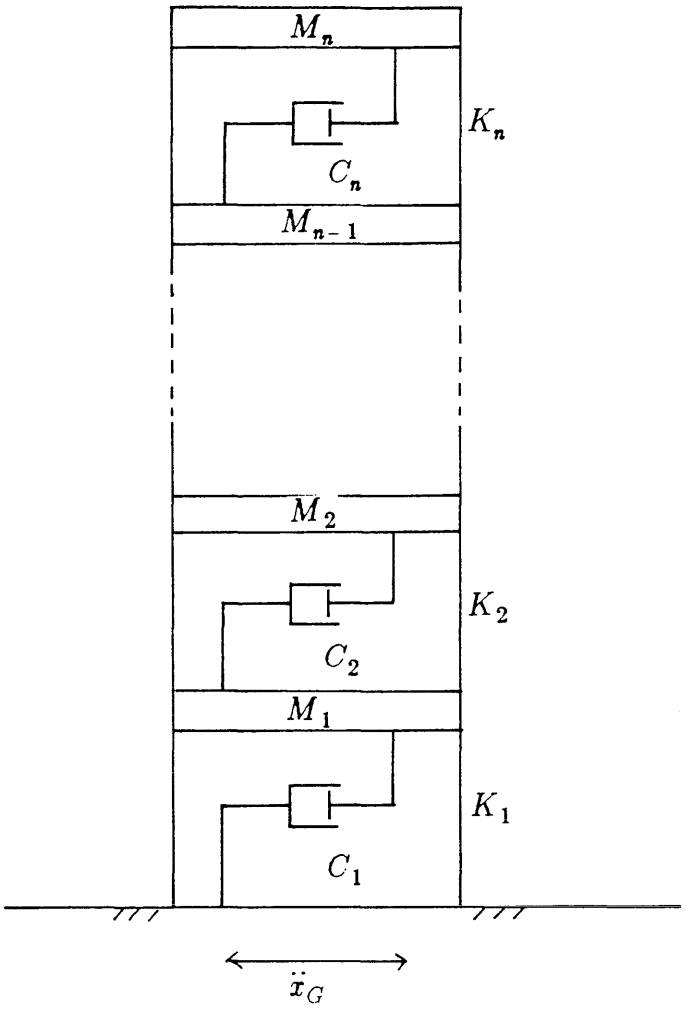

Fig. 4.4 Lumped Mass Model

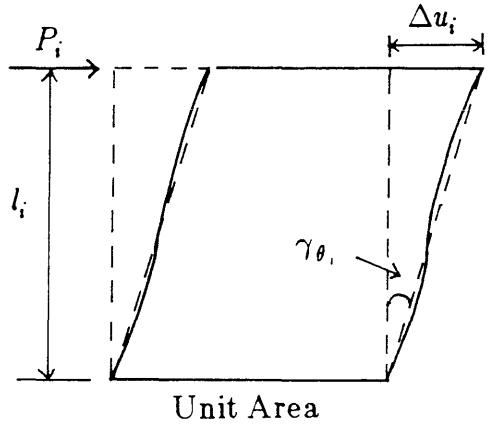

Fig. 4.5 Shear Deformation at the i-th Soil Layer

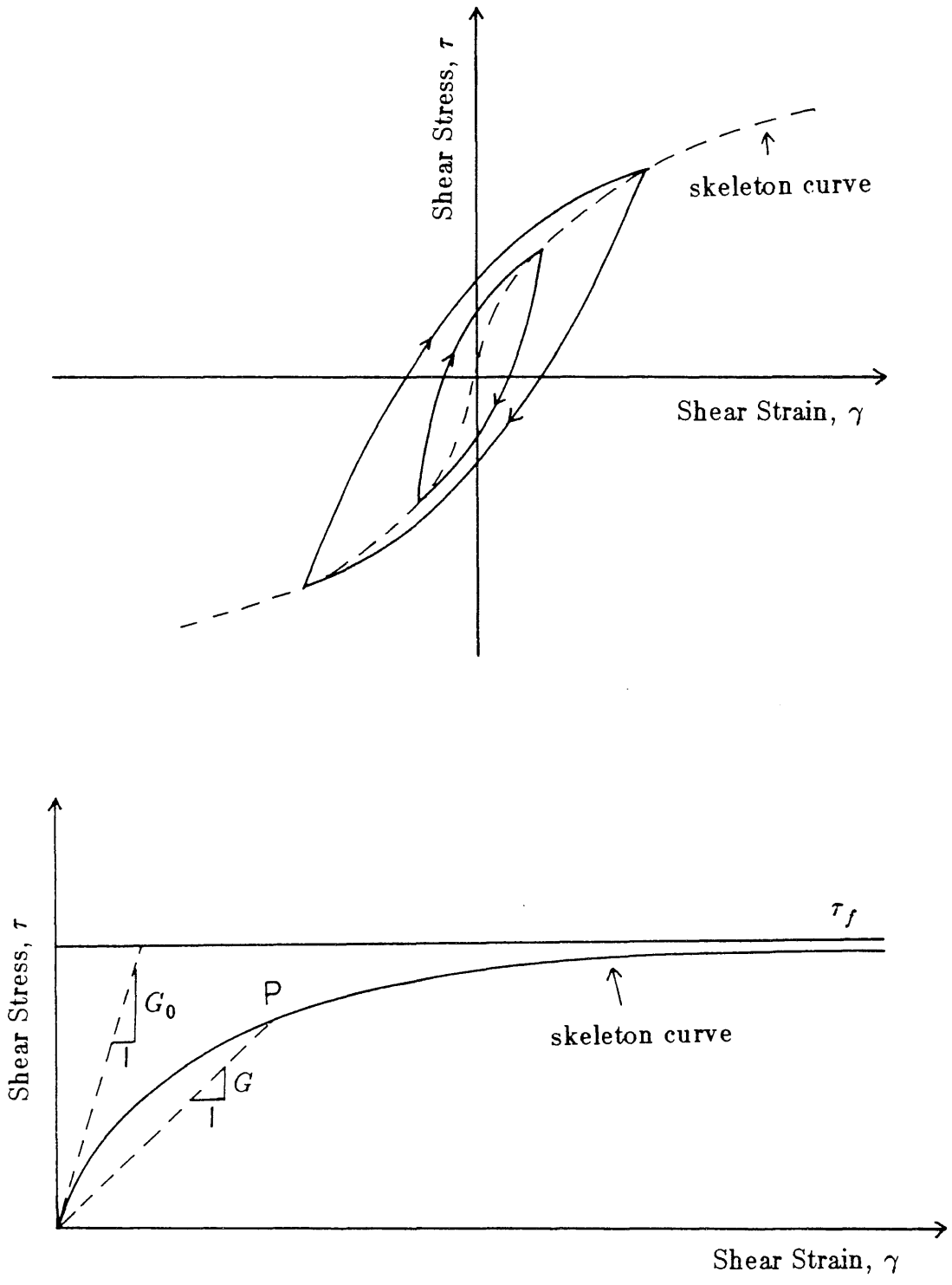

Fig. 4.6 Dynamic Shear Stress-Strain Relation for Soils

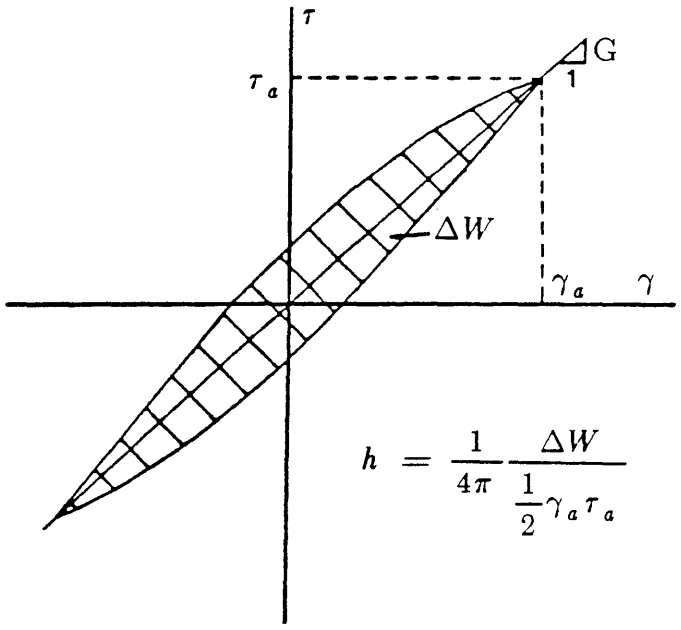

Fig. 4.7 Equivalent Viscous Damping Ratio h

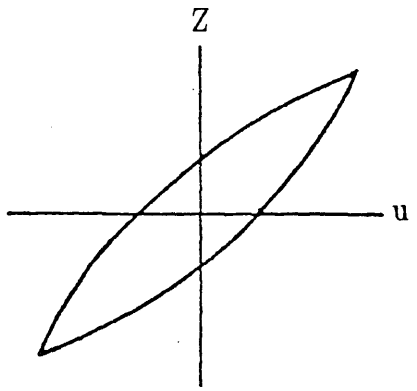

(a) $\beta+\delta>0,\ \delta-\beta<0$

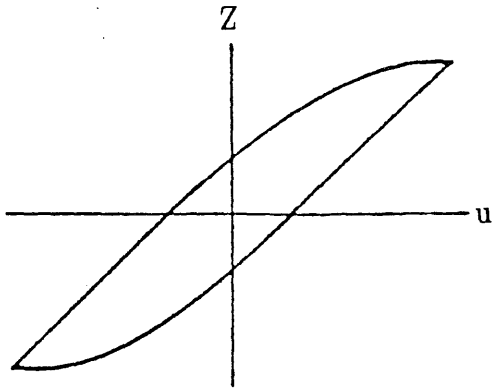

(b) $\beta+\delta>0,\ \delta-\beta=0$

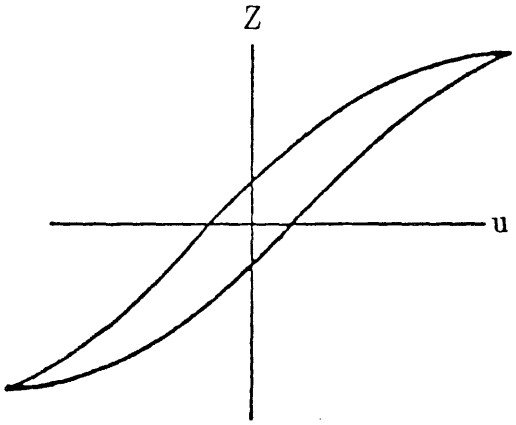

(c) $\beta+\delta>\delta-\beta>0$

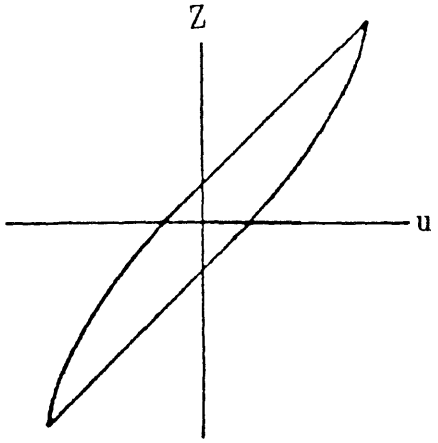

(d) $\beta+\delta=0,\ \delta-\beta>0$

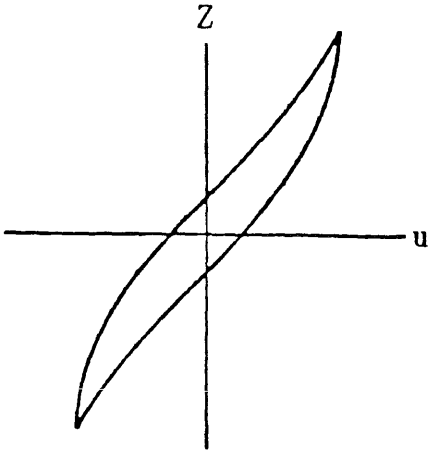

(e) $0>\beta+\delta>\delta-\beta$

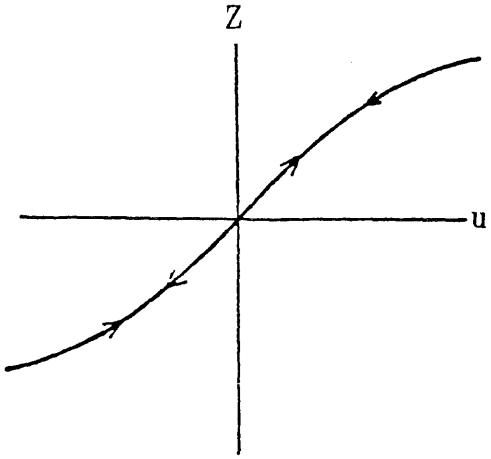

(f) $\beta=0,\ \delta>0$

Fig. 4.8 Possible Combination of β and δ

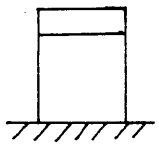

$A = 1.0$
$\delta = \beta = 1.0$
$n = 1.0$
$\alpha = 0.01$
$T = 0.3$ sec

Filtered White Noise
$S_0 = 100\ in^2/\text{sec}^3$
$\omega_B = 15.6\ rad/sec$
$\zeta_B = 0.64$
○○○ *Simulation* ($n = 100$)
—— *Analytical Results*

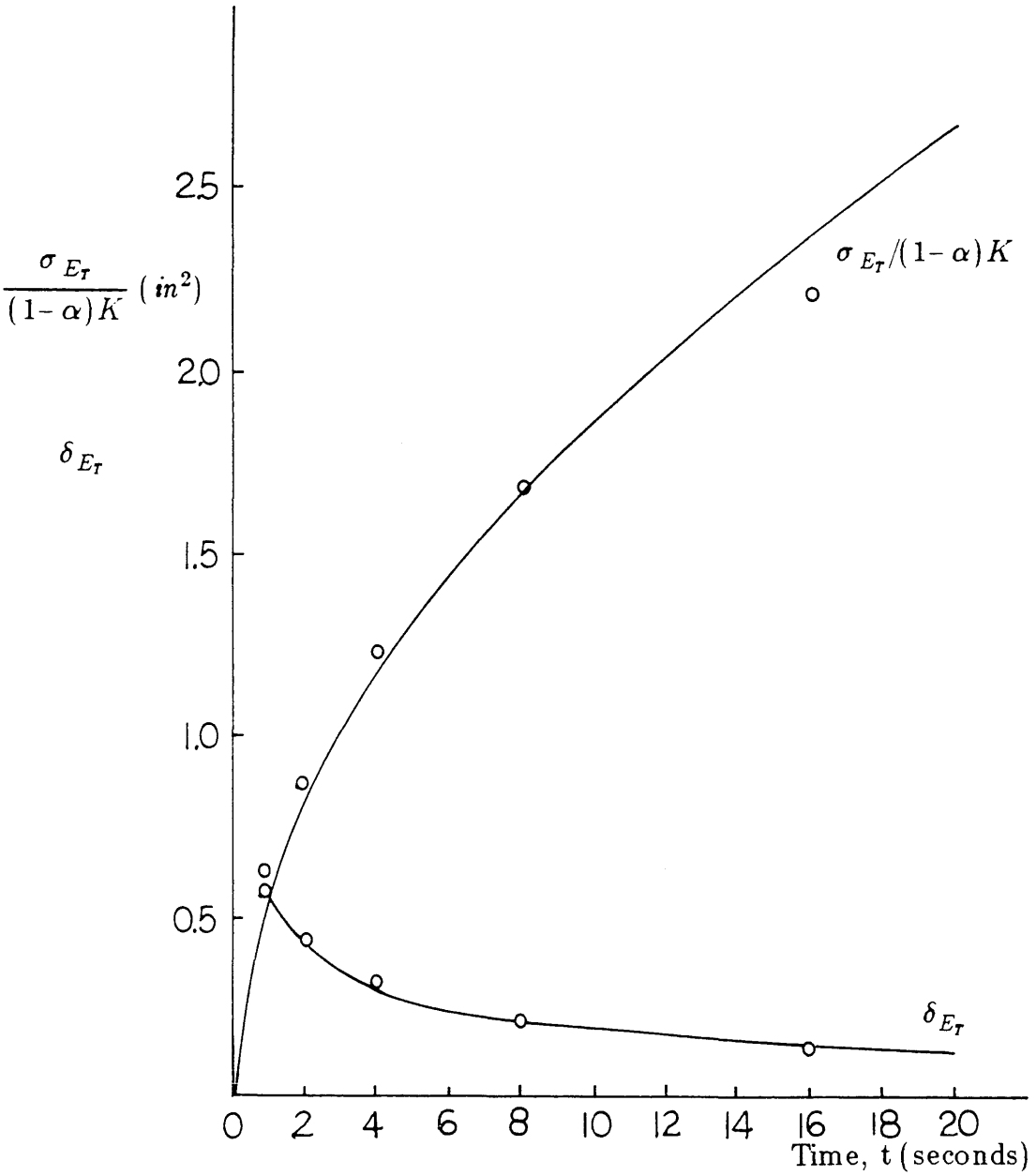

Fig. 4.9 σ_{E_T} and δ_{E_T} for a SDF System

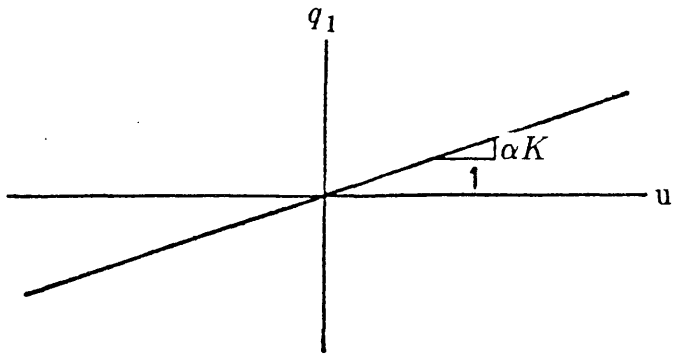

(a) Linear Restoring Force q_1

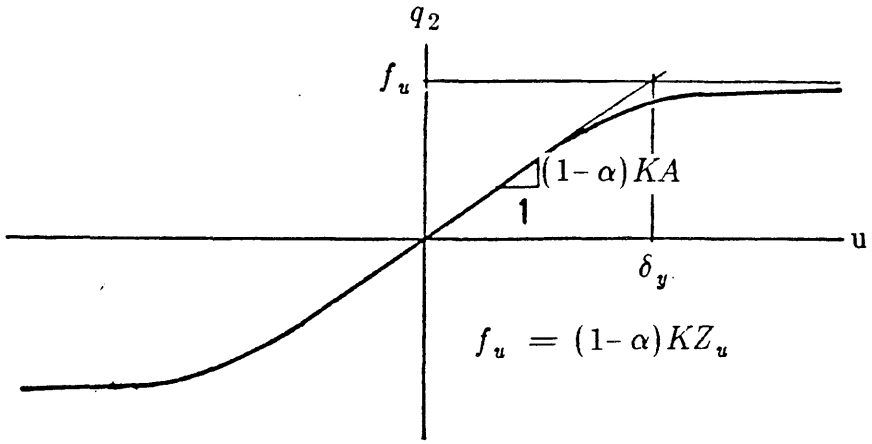

(b) Hysteretic Restoring Force q_2

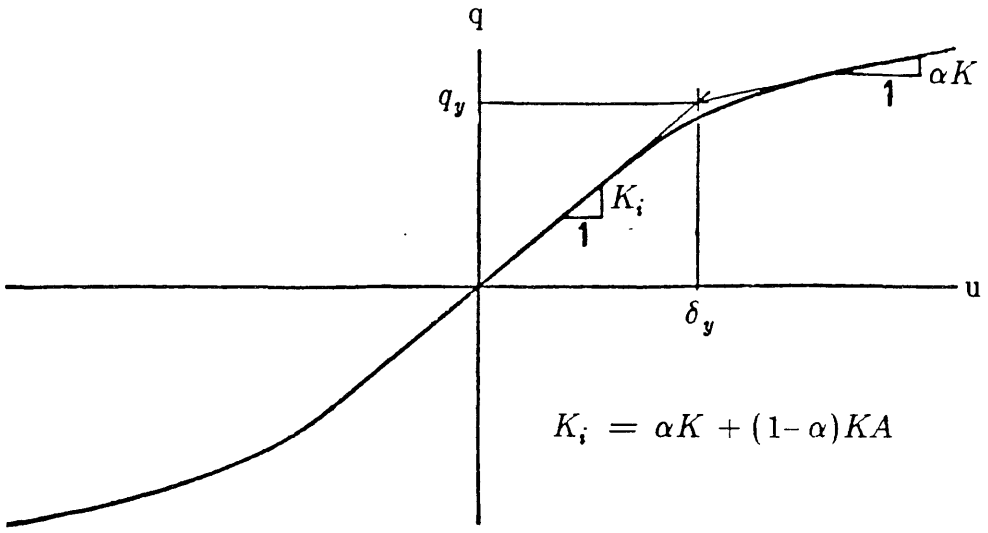

(c) Total Restoring Force q

Fig. 4.10 Relationship between Restoring Force and Displacement

CHAPTER 5

SOIL CHARACTERIZATION AND DAMAGE MODEL

5.1 Dynamic Shear Stress-Strain Relation of Clays

The shear modulus of a soil at infinitesimally small strain, G_0, is obtained through in-situ investigation using shear wave propagation or laboratory tests of undisturbed soil samples taken from the site. According to results obtained from laboratory tests, G_0 is highly dependent on the void ratio, e, effective confining pressure, σ'_0, and the OCR of the soil. Hardin and Black (1969) proposed the following empirical equation for normally-consolidated clay,

$$G_0 = C\ F(e)\ (\sigma'_0)^{1/2} \tag{5.1}$$

where:

C = constant;

$F(e) = (2.97-e)^2/(1+e)$.

The effect of OCR on G_0 depends strongly on the plasticity index, I_P, of a soil, as shown schematically in Fig. 5.1. For overconsolidated clay, $G_{0,OC}$, can be expressed as follows:

$$G_{0,OC} = C_{OC}\ F(e)\ (\sigma'_0)^{n_0} \tag{5.2}$$

where n_0 is a constant depending on I_P. In the special case if σ'_0 is equal to the maximum pressure to which the soil has ever been subjected, σ'_P, G_0 evaluated with both Eqs. 5.1 and 5.2 should be the same. Therefore, the following equation for C_{OC} can be obtained by equating Eq. 5.1 to Eq. 5.2:

$$C_{OC} = C\,(\sigma'_P)^{1/2-n_0} = C\,(\sigma'_P)^{K_S} \tag{5.3}$$

where $K_S = 1/2 - n_0$. Substituting Eq. 5.3 into Eq. 5.2 yields

$$G_{0,OC} = C\,F(e)\,(OCR)^{K_S}\,(\sigma'_0)^{1/2} \tag{5.4}$$

The relation between K_S and I_P can be obtained from the experimental results of Fig. 5.2 (Hardin and Black, 1969). Values of K_S ranges from 0 to 0.5. In general, overconsolidated clays that are susceptible to progressive failure are highly plastic (Bjerrum, 1967). Therefore, with $K_S = 0.5$, Eq. 5.4 is reduced to

$$G_{0,OC} = C\,F(e)\,(\sigma'_P)^{1/2} \tag{5.5}$$

Thus, for such a highly overconsolidated clay as shown in Fig. 2.5, G_0 is almost constant with depth.

The shear stress-strain curve of soils is nonlinear and hysteretic, as shown in Fig. 4.6. At zero shearing strain the tangent to the curve establishes the maximum value of the shear modulus, G_0. The secant shear modulus corresponding to an intermediate point on the curve, such as point P in Fig. 4.6, is denoted by G. τ_f is the strength of the soil. The skelton curve shown by the dashed line in Fig. 4.6 describes the variation of the secant shear modulus, G, with the respective shearing strain, γ. The loop shape and width describe the increase in the equivalent damping as a function of the shearing strain, γ.

It is often convenient to approximate the strain-softening behavior of soils analytically, as shown in Fig. 4.6. Hardin and Drnevich (1972) adopted the hyperbolic stress-strain relationship originally formulated by Kondner and Zelasko (1963). Richart (1975), and Streeter, Wylie and Richart (1974) used the equations proposed by Ramberg and Osgood (1943); other expressions

were also suggested by Martin (1976) and Pender (1977). Hardin and Drnevich (1972) determined the variation of the ratio G/G_0 and the equivalent viscous damping ratio, h (defined in Fig. 4.7), with the shearing strain, γ, by the following equations:

$$\frac{G}{G_0} = \frac{1}{1+\frac{\gamma}{\gamma_r}} \tag{5.6}$$

$$h = h_0 \left(1-\frac{G}{G_0}\right) \tag{5.7}$$

in which γ_r is a reference strain defined as τ_f/G_0, and h_0 is the equivalent viscous damping ratio for the limiting case of G = 0. The strain dependency of G and h, i.e., G/G_o - γ and h - γ, is important in the dynamic analysis for the amplification factor A_f.

5.2 Dynamic Shear Strength of Clays

5.2.1 Uniform Cyclic Loading

Nishi and Esashi (1982) conducted comprehensive research on the static and dynamic properties of mudstone (soft rock) at low confining pressures, which has mechanical properties similar to those of overconsolidated clays. On the basis of the static tests for mudstone, certain conclusions can be drawn as follows:

(i) The stress-strain curve shows strong strain-softening property.

(ii) The axial strain at failure, ϵ_f, corresponding to the peak shear strength ranges from 0.8 to 1.0 %.

(iii) The peak shear strength is dependent on the speed at which the shear stress is applied, whereas its residual shear strength is almost independent of the rate of loading.

Conclusion (iii) means that the soil that has already failed in the static condition cannot provide any resistance against earthquake loadings. On the other hand, the dynamic shear strength of a soil that has not failed prior to an earthquake may be evaluated through the test scheme shown in Fig. 5.3; a static shear stress is applied under a drained condition before uniform cyclic shear stress is applied to the soil specimen. One example of the dynamic test performed on a mudstone with a frequency of 1.0 hz is shown in Fig. 5.4; the axial strain accumulation seems to occur suddenly at a certain number of cycles, N, and the accumulated axial strain at this stage is around 1.0 %, which is almost the same as that at failure under a static load. Therefore, failure is considered to take place with N cycles of loadings. It is also reported that the effect of different frequencies ranging from 0.1 to 3.0 hz is negligible. In this way, the dynamic shear strength under N cycles of uniform loadings, $\tau_d(N)$, with different initial static shear stress, τ_S, can be evaluated. Based on the results of dynamic shear tests for saturated clays (Seed and Chen, 1966), the dynamic shear strength may be expressed in the following form:

$$\frac{\tau_d(N)}{\tau_f} = a \left\{1-\left(\frac{\tau_S}{\tau_f}\right)\right\}^b \tag{5.8}$$

where a and b are functions of N. Fig. 5.5 shows Eq. 5.8 graphically for several N's; as pointed out in Chapter 1, $\tau_S+\tau_d(N)$ is larger than τ_f for small N because of the loading rate effect, whereas $\tau_S+\tau_d(N)$ decreases gradually with increasing N because of the dominant effect of cyclic loading.

As explained in Sect. 4.1, the distribution of $\tau_d(N)$ along a potential failure surface is used to evaluate a horizontal force F(N) that will cause failure with N cycles of uniform loadings. F(N=1) represents the maximum restoring force of the system. The degree to which the system approaches failure is considered to be closely related to the total energy dissipated. In this sense, the value of $N \cdot E_C(Z)$ may be an indicator of damage. However, it is reasonable to assume that the percentage of $E_C(Z)$ that can contribute to the damage accumulation increases with the amplitude of cyclic loadings. To account for this latter effect, the weight function $h(Z)$ may be introduced such that $h(Z) \cdot N \cdot E_C(Z)$ is the same for different amplitude Z. Therefore, the damage index necessary for failure in the system may be expressed by

$$D_f = N \cdot h(Z) \cdot E_C(Z) \tag{5.9}$$

5.2.2 Irregular and Random Dynamic Loading

Nishi and Esashi (1982) performed dynamic loading tests using ground motion records from actual earthquakes. Fig. 5.6 shows one of the results obtained for the El Centro earthquake, in which the vertical axis represents the stress ratio (the maximum applied shear stress to the static shear strength), and the horizontal axis represents the strain ratio (the maximum axial strain to the static axial strain at failure). The residual strain ϵ_r after the dynamic loading of the non-failure cases shown in Fig. 5.6 is as low as 15 % of ϵ_f. Therefore, in practice, the residual strain ϵ_r prior to failure is negligible. Nishi and Esashi (1982) showed that the damage induced by irregular loadings can be evaluated through an accumulated damage rule (e.g., Miner, 1945) based on the results of uniform cyclic loadings. The energy-based damage index introduced in the

previous section is basically a form of accumulated damage rule. Accordingly, the applicability of the damage index is reasonable. The damage accumulated under a nonuniform loading may be computed as follows:

(i) Damage required for failure is calculated by Eq. 5.9.

(ii) For the first to the i-th cycles of loadings, calculate the damage D_i as follows:

$$D_i = \sum_{j=1}^{i} h(\tau_j) E_C(\tau_j) \tag{5.10}$$

where τ_j is the amplitude of the j-th cycle of loading.

(iii) Eqs. 5.9 and 5.10 are sufficient to calculate the level of damage.

For random loadings, steps (i) and (iii) remain the same; step (ii) is replaced by the following:

(ii) The damage accumulated up to time t, D(t), is calculated as

$$D(t) = \int_0^t X(s) \dot{E}_T(s)\, ds \tag{5.11}$$

where $\dot{E}_T(t)$ is the rate of hysteretic energy dissipated by a soil caused by shearing, and X(t) is a function analogous to $h(\tau_P)$ as follows:

$$X(t) = \frac{\int_0^{\tau_{P,max}} h(\tau_P) E_C(\tau_P) p(\tau_P, \sigma_\tau, \sigma_{\dot{\tau}}, \rho_{\tau\dot{\tau}})\, d\tau_P}{\int_0^{\tau_{P,max}} E_C(\tau_P) p(\tau_P, \sigma_\tau, \sigma_{\dot{\tau}}, \rho_{\tau\dot{\tau}})\, d\tau_P} \tag{5.12}$$

where $p(\ )$ is the probability density function of the peaks of the hysteretic restoring shear stress, τ_P (Kobori and Minai, 1967; and Lin, 1967), and is

expressed as follows:

$$p(\tau_P,\sigma_\tau,\sigma_{\dot\tau},\rho_{\tau\dot\tau}) = \exp(-\frac{\tau_P^2}{2\sigma_\tau^2})\left[\frac{\tau_P}{\sigma_\tau^2}\exp\{\frac{\rho_{\tau\dot\tau}^2\tau_P^2}{2(1-\rho_{\tau\dot\tau}^2)\sigma_\tau^2}\}\right.$$

$$\left. + \frac{\rho_{\tau\dot\tau}}{\sqrt{1-\rho_{\tau\dot\tau}^2}}\sqrt{\pi/2\sigma_\tau^2}(\frac{\tau_{P_2}}{\sigma_\tau^2}-1)\,erf\{\frac{\rho_{\tau\dot\tau}\tau_P}{\sqrt{2(1-\rho_{\tau\dot\tau}^2)\sigma_\tau^2}}\}\right] \quad (5.13)$$

Steps (ii) and (iii) are repeated until failure occurs or until the excitation stops. In the case of a stationary excitation, Eq. 5.13 is reduced to the classical Rayleigh distribution (Rice, 1954) with $\rho_{\tau\dot\tau} = 0$ and $X(t)$ and $\dot E_T(t)$ are constants for any given loading.

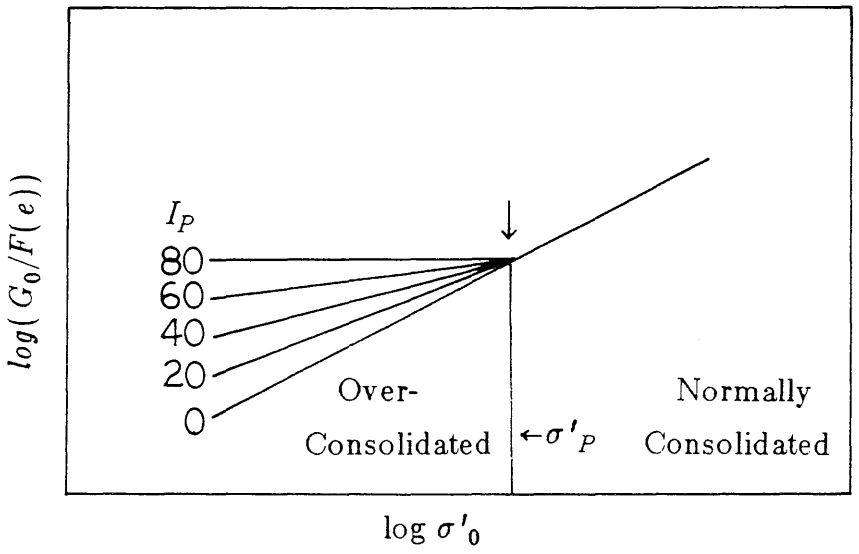

Fig. 5.1 Effect of OCR on G_0

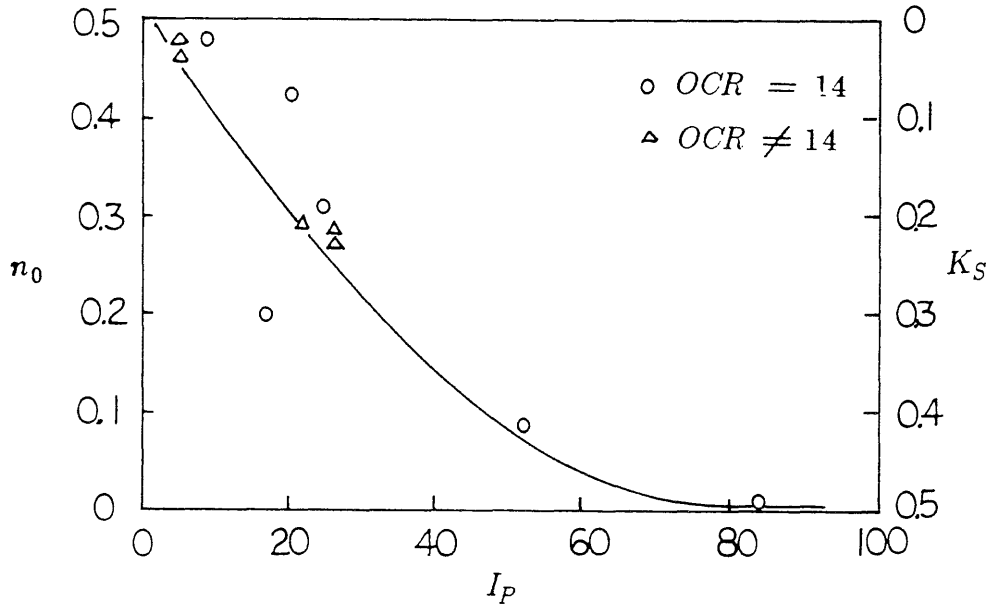

Fig. 5.2 Relation between K_S and I_P
(Hardin and Black, 1969)

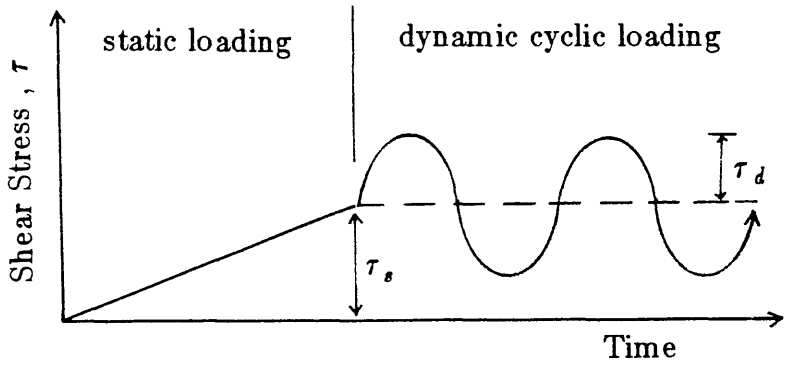

Fig. 5.3 Dynamic Shear Test

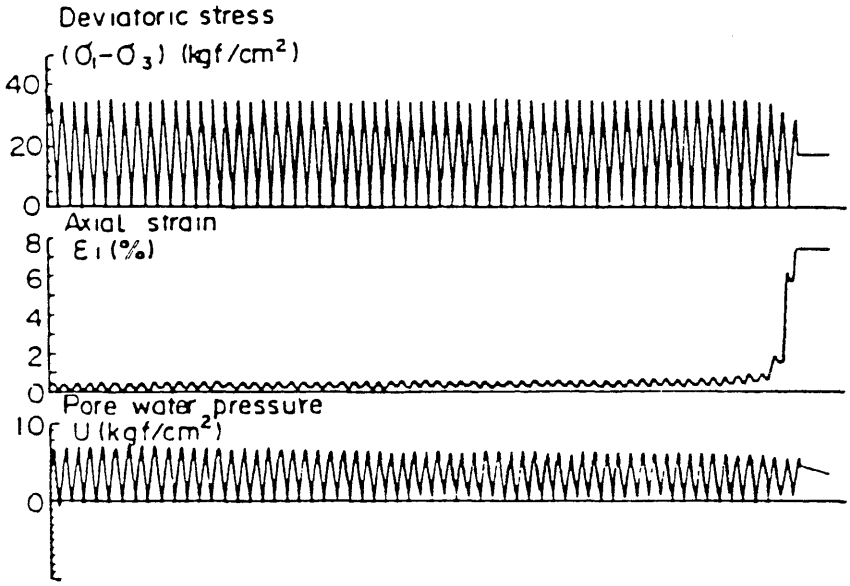

Fig. 5.4 Variation of Axial Strain with Time
(Nishi and Esashi, 1982)

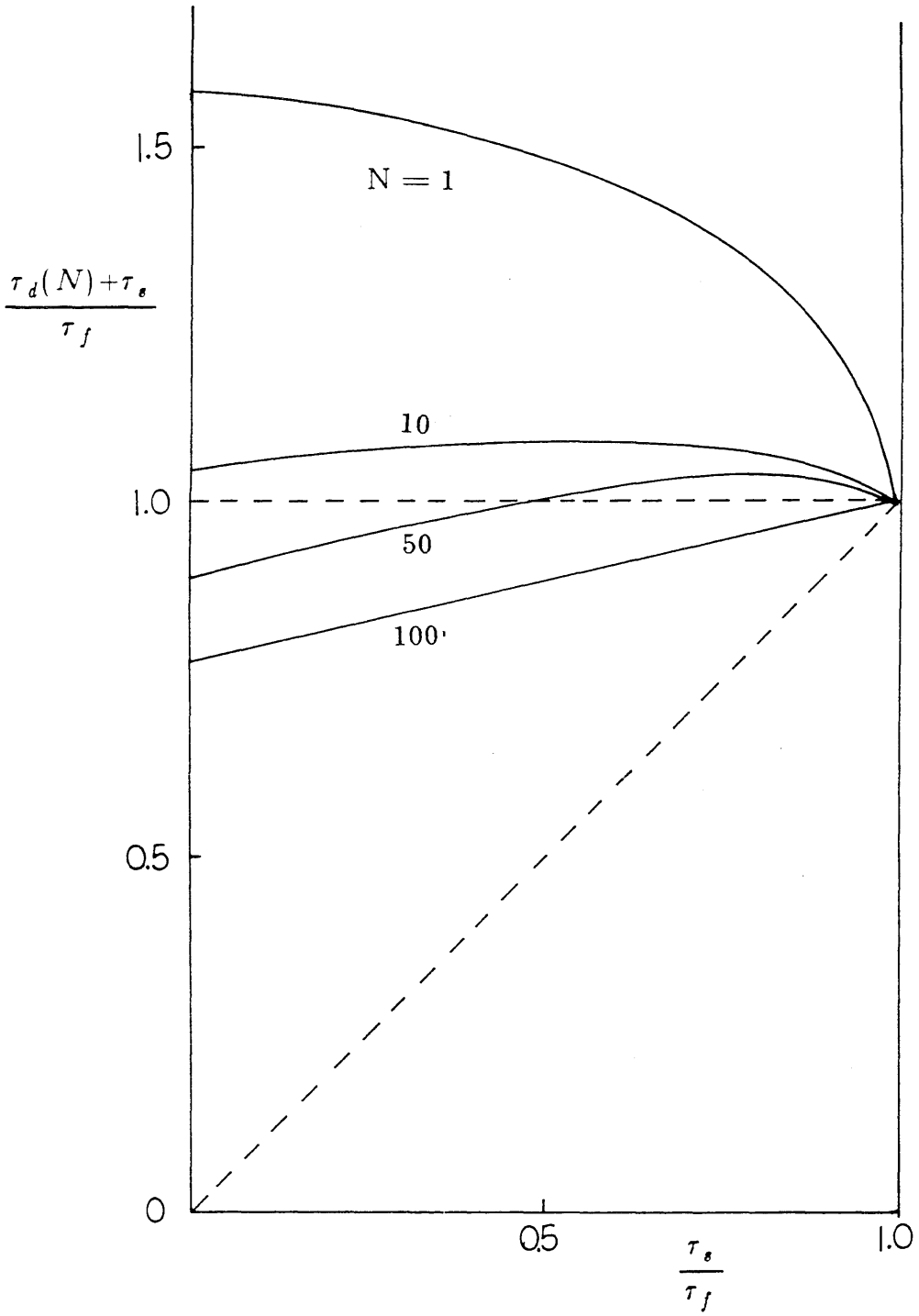

Fig. 5.5 Relation between Dynamic Shear Strength and Initial Shear Stress

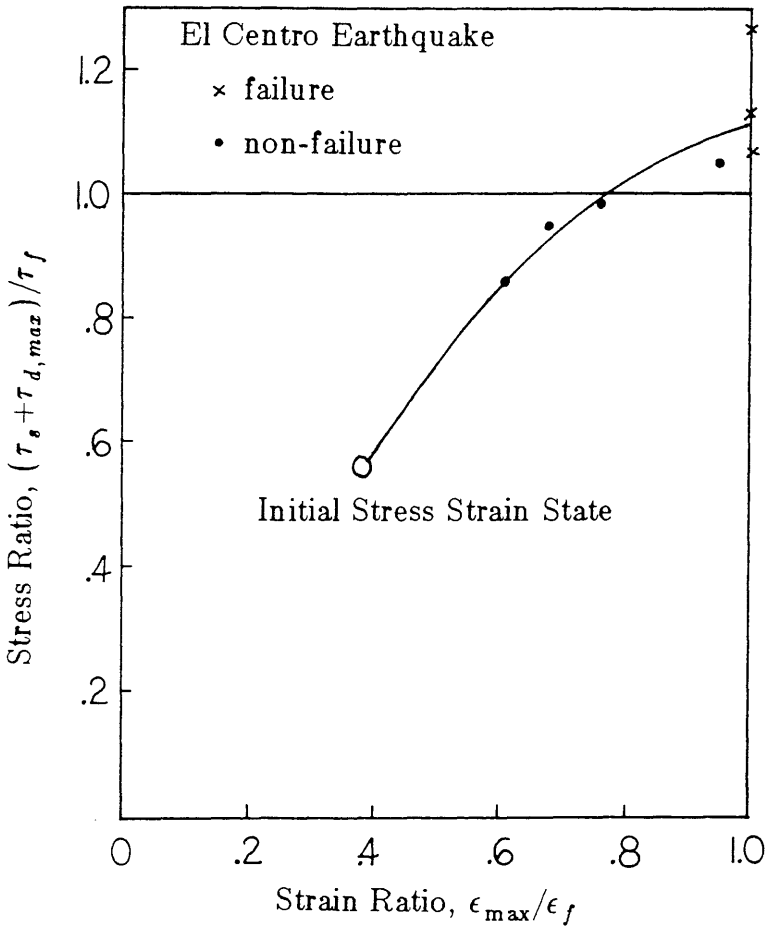

Fig. 5.6 Relation of Stress and Strain Ratio for Mudstone (Nishi and Esashi, 1982)

CHAPTER 6

SEISMIC RELIABILITY ANALYSIS

6.1 Introduction

The uncertainties underlying the slope-stability model developed in the previous chapters arise from the randomness in the frequency content and duration of the strong ground motion, as well as from the dynamic soil properties. The randomness in the occurrence of the earthquake loading is also important for the lifetime reliability evaluation against sliding failure.

The required dynamic soil properties are divided into two types: one is the dynamic deformation property (such as the variation of G_0 with depth and the strain dependency of G/G_0, h) which is used to determine the average amplification factor A_{av} and the dominant frequency ω_1; the other is the dynamic shear strength used in the construction of the F(N)-N relation for the converted SDF system. It is difficult to generalize the uncertainties associated with the dynamic properties of a soil, because they differ greatly from site to site, depending on the physical and mechanical properties of the soil. Therefore, the uncertainties of the dynamic properties of the soil should be determined on a site-by-site basis. The degree to which the final results are influenced by the uncertainty in the G/G_0 - γ relation will be illustrated in Chapter 7; whereas, the uncertainty in the F(N)-N relation associated with the dynamic shear strength of the soil is discussed in Sect. 6.3.

6.2 Reliability Evaluation

Given the occurrence of an earthquake with a given intensity, $A_m = a$, and a strong motion duration, $T_E = t$, the performance function of a cut slope against sliding failure is

$$Z = D_f - D(t) \tag{6.1}$$

where:

D_f = measure of resistance capacity defined by Eq. 5.9;

$D(t)$ = damage index defined by Eq. 5.11.

Failure is then defined as,

$$Z(a,t) < 0 \tag{6.2}$$

The response of a converted SDF system depends on other uncertainties such as the dynamic soil properties. Let the vector of such uncertain properties be denoted by $\tilde{R}$ with mean $\mu_{\tilde{R}}$, and let σ_{R_i} be the standard deviation of the i-th component of $\tilde{R}$, and ρ_{ij} be the correlation coefficient between the i-th and j-th component of $\tilde{R}$. Then, the quantity $Z(a,t)$ is also a function of $\tilde{R}$, and failure is

$$Z(a,t,\tilde{R}) < 0 \tag{6.3}$$

The time necessary to cause failure, T, is obtained by solving $Z(a,t,\tilde{R}) = 0$ for t as follows:

$$T = T(a,\tilde{R}) \tag{6.4}$$

Using first-order approximation (Ang and Tang, 1975), the mean and coefficient of variation (COV) of T can be calculated from

$$\mu_T(a,\tilde{R}) \approx \mu_T(a,\mu_{\tilde{R}}) \tag{6.5}$$

$$\Omega_T^2(a,\tilde{R}) \approx \delta_T^2(a,\mu_{\tilde{R}}) + \frac{1}{\mu_T^2(a,\mu_{\tilde{R}})} \sum_i \sum_j \rho_{ij} \left[\frac{\partial T(a,\tilde{R})}{\partial R_i}\right]_{\mu_{\tilde{R}}} \left[\frac{\partial T(a,\tilde{R})}{\partial R_j}\right]_{\mu_{\tilde{R}}} \sigma_{R_i}\sigma_{R_j} \tag{6.6}$$

where:

$$\mu_T(a,\mu_{\tilde{R}}) = E[T(a,\mu_{\tilde{R}})] = \frac{D_f(a,\mu_{\tilde{R}})}{X(a,\mu_{\tilde{R}})E[\dot{E}_T(a,\mu_{\tilde{R}})]} \tag{6.7}$$

$$\delta_T^2(a,\mu_{\tilde{R}}) = \frac{1}{\mu_T^2(a,\mu_{\tilde{R}})} \left\{ \int_0^{\mu_T\mu_T} \int_0 X(s,a,\mu_{\tilde{R}})X(v,a,\mu_{\tilde{R}}) E[\dot{E}_T(s,a,\mu_{\tilde{R}})\dot{E}_T(v,a,\mu_{\tilde{R}})]\, ds\, dv - \mu_T^2(a,\mu_{\tilde{R}}) \right\} \tag{6.8}$$

$\mu_T(a,\mu_{\tilde{R}})$ and $\delta_T^2(a,\mu_{\tilde{R}})$ are obtained from random vibration analysis, and the derivatives in Eq. 6.6 may be evaluated by finite-differences. An analytical technique to obtain the derivatives in Eq. 6.6 was recently proposed by Sues et al. (1983). This study considers the randomnesses in the G/G_0 - γ relation in the preliminary analysis (R_1), the F(N)-N relation in a converted SDF system (R_2) and the uncertainties in the frequency content of an earthquake loading (R_3) as components of $\tilde{R}$. The uncertainty in the prediction of T as a result of these three components cannot be evaluated through Eq. 6.6. Assuming that

the R_is are independent of one another, modification of Eq. 6.6 yields the following:

$$\Omega_T^2(a,\tilde{R}) = \delta_T^2(a,\mu_{\tilde{R}}) + \frac{1}{\mu_T^2(a,\mu_{\tilde{R}})}\sum_{i=1}^{3} Var[\mu_T]_i$$

$$= \delta_T^2(a,\mu_{\tilde{R}}) + \sum_{i=1}^{3}\Delta_i^2 \qquad (6.9)$$

where the Δ_is are uncertainties in the prediction of $\mu_T(a,\mu_{\tilde{R}})$ arising from the randomness in the corresponding R_is. Therefore, through the Eqs. 6.5 and 6.9, T is reduced to only a function of a, $T = T(a)$. Thus, the probability of failure with given $A_m = a$ and $T_E = t$ becomes

$$P_F(a,t) = P[Z(a,t) < 0] = P[t > T(a)]$$

$$= \Phi\left[\frac{\ln t - \ln\mu_T(a)}{\Omega_T(a)}\right] \qquad (6.10)$$

in which the log-normal distribution is assumed for T.

The lifetime probability of failure P_F, unconditional on A_m and T_E may be evaluated by

$$P_F = \int_{A_{m,mm}}^{A_{m,max}} \int_{T_{E,min}}^{T_{E,max}} P_F(a,t)\, p_{A_m T_E}(a,t)\, da\, dt \qquad (6.11)$$

where $p_{A_m T_E}(a,t)\,dadt$ is the joint probability that $a < A_m < a+da$ and $t < T_E < t+dt$ at the site. So far, available seismic hazard models deal only with the earthquake intensity A_m, and not with its duration T_E. For the purpose of this study the statistics of T_E will be conditional on the value of A_m, and the

results suggested by Lai (1980) will be used. The probability of failure conditional on A_m is evaluated by

$$P_F(a) = \int_{T_{E,min}}^{T_{E,max}} P_F(a,t) p_{T_E|A_m}(t|a)\, dt \tag{6.12}$$

where $p_{T_E|A_m}(t|a)$ = the conditional probability density function of T_E. Finally, the lifetime probability of failure can be calculated as

$$P_F = \int_{A_{m,min}}^{A_{m,max}} P_F(a) p_{A_m}(a)\, da \tag{6.13}$$

where $p_{A_m}(a)$ is the probability density function of A_m for a given lifetime, which may be obtained with the fault-rupture seismic hazard model of Der Kiureghian and Ang (1977). The measure of earthquake intensity used in this study is the peak acceleration at the toe level of a slope. The statistics of T_E conditional on A_m, and the randomness associated with the frequency content of the earthquake ground motion are examined in Sect. 6.4.

6.3 Uncertainties in Dynamic Shear Strength of Soil

The dynamic shear strength of a clay for N cycles of uniform loading, $\tau_d(N)$, can be expressed approximately in the form of Eq. 5.8. Now, suppose the case where the coefficients a and b in Eq. 5.8 are determined from n sample tests. Taking the logarithm on both sides of Eq. 5.8 and introducing new notations, Eq. 5.8 is reduced to

$$Y = \alpha + \beta X; \tag{6.14}$$

where:

$$Y = \ln\{\tau_d(N)/\tau_f\};$$

$$X = \ln\{1-(\tau_S/\tau_f)\} - \overline{\ln\{1-(\tau_S/\tau_f)\}};$$

$$\overline{\ln\{1-(\tau_S/\tau_f)\}} = \frac{1}{n}\sum_{i=1}^{n}\ln\{1-(\tau_S/\tau_f)\}_i;$$

$$\beta = b;$$

$$\alpha = \ln a + \beta\overline{\ln\{1-(\tau_S/\tau_f)\}}.$$

α and β are random variables whose expected values are

$$E[\alpha] = \hat{\alpha} = \overline{Y} = \frac{1}{n}\sum_{i=1}^{n} Y_i \tag{6.15}$$

$$E[\beta] = \hat{\beta} = \sum_{i=1}^{n} Y_i X_i / \sum_{i=1}^{n} X_i^2 \tag{6.16}$$

The mean and variance of Y for a specific X_0 are as follows (denoting $Y_0 = Y(X_0)$):

$$E[Y_0] = \hat{\alpha} + \hat{\beta}X_0 \tag{6.17}$$

$$Var[Y_0] = \sigma^2\left[\frac{1}{n} + \frac{X_0^2}{\sum_{i=1}^{n} X_i^2}\right] + \sigma^2 \tag{6.18}$$

where $\sigma^2 \approx s^2 = \frac{1}{n-2}\sum_{i=1}^{n}(Y_i - \hat{Y}_i)^2$; where $\hat{Y}_i = \hat{\alpha} + \hat{\beta}X_i$. The first term of the right-hand side of Eq. 6.18 represents the error in the estimation of the parameters α and β, and the second term represents the inherent variability of Y. Therefore, given τ_S/τ_f, i.e. X_0, at point x along a potential failure surface, $\tau_d(N,x)$ at the point can be evaluated through the following equation:

$$\tau_d(N,x) = \exp\{E[Y_0] + \sqrt{Var[Y_0]}\cdot S(x)\}\,\tau_f(x) \tag{6.19}$$

where $S(x)$ is a standard normal variate. $\tau_d(N,x)$ with different values of N can be evaluated by the same type of equation as Eq. 6.19. In order to evaluate F(N) for a converted SDF system, which is proportional to the integration of $\tau_d(N,x)$ along a potential failure surface (see Fig. 4.3), the correlation between the $\tau_d(N,x_1)$ and $\tau_d(N,x_2)$ at any two points along the potential failure surface should be taken into account. Assuming that the correlation structure of $S(x)$ in Eq. 6.19 is the same as Eq. 3.24 and that the $\tau_d(N,x)$s for different values of N are perfectly correlated, a sample of F(N)-N relation can be generated through the following simulation procedure:

(i) Divide a potential failure surface into m segments with equal length $\Delta l = l/m$ where l is the length of the potential failure surface.

(ii) Generate the sequences of correlated $S(i)$; $i = 1,m$ satisfying Eq. 3.24 by following the algorithm shown in Sect. 3.3.1.

(iii) By substituting $S(i)$ into Eq. 6.19 for several values of N, evaluate $\tau_d(N,i)$; $i = 1,m$.

(iv) Finally, evaluate F(N) corresponding to the given values of N through the equation in Fig. 4.3 in which $\int_0^l \tau_d(N,x)\,dx$ is replaced by $\sum_{i=1}^{m}\tau_d(N,i)\cdot\Delta l$.

By repeating the process, a number of F(N)-N relations are obtained. Through random vibration analysis for a number of F(N)-N relations generated above, the COV of the mean time necessary for failure, Δ_2, can be evaluated.

6.4 Earthquake Loading

6.4.1 Ground Motion Model

For the purpose of this study the earthquake-induced strong ground motion should be specified in terms of its amplitude frequency content and duration. The intensity of the earthquake loading is characterized by its peak ground acceleration, $a_{\max}$, and the frequency content by its power spectral density function (PSD function). The Kanai-Tajimi PSD function

$$S(\omega) = 2S_0 \frac{1 + 4\zeta_B^2(\omega/\omega_B)^2}{[1-(\omega/\omega_B)^2]^2 + 4\zeta_B^2(\omega/\omega_B)^2} \tag{6.20}$$

is used to model the frequency content of the earthquake loading. The parameter S_0 is the intensity scale of the PSD function; and, ω_B and ζ_B are the natural frequency and damping coefficient of the ground.

The peak ground acceleration $a_{\max}$ has been related to the root mean square ground acceleration a_{rms}, and excellent correlations have been found by Lai (1980), Vanmarke and Lai (1980), Moayyad and Mehraz (1982), and Hanks and McGuire (1981). In particular, Vanmarke and Lai (1980) suggested the following relationship:

$$a_{\max} = a_{rms}\sqrt{2\ln(\frac{2T_E}{T_0})} \tag{6.21}$$

where:

T_E = duration of the strong-motion phase ground excitation;

T_0 = predominant period of the ground motion, defined as

$$T_0 = \frac{2\pi}{\omega_C} \tag{6.22}$$

in which ω_C is calculated from

$$\omega_C = 0.89 \cdot \omega_B + 4.6 \tag{6.23}$$

The duration of the strong-phase motion is determined from Eq. 6.21 on the condition that the total energy of the ground motion is retained, i.e. with

$$I_0 = a_{rms}^2 T_E \tag{6.24}$$

where I_0 is the Arias intensity (time integral of the squared accelerations). In this manner, the expected peak ground acceleration and the energy of the recorded accelerograms are reproduced by the model.

When the parameters of the Kanai-Tajimi PSD function are known, the root mean square ground acceleration can be calculated by

$$a_{rms}^2 = 2S_0 \frac{\pi \omega_B}{4\zeta_B}(1+4\zeta_B^2) \tag{6.25}$$

and the peak ground acceleration may be obtained from

$$a_{max} = (PF) \cdot a_{rms} \tag{6.26}$$

where (PF) is a peak factor, as defined in Eq. 6.21; this peak factor is insensitive to the duration and predominant period of the ground motion, and is taken as 2.9 in this study following the recommendation of Sues et al. (1983).

6.4.2 Uncertainties in Earthquake Load Parameters

Power Spectral Density Function -- Housner and Jennings (1964) have initially suggested the values of $\omega_B = 5\pi$ *rad/sec* and $\zeta_B = 0.64$ in the specification of the PSD for "firm" ground conditions; whereas based on 140 horizontal accelerograms Lai (1980) found ω_B to vary from 5.7 rad/sec to 51.7 rad/sec, and ζ_B between 0.10 and 0.90. For 22 "rock" site records ω_B had a mean of 26.7 rad/sec and COV of 0.40, and ζ_B had a mean of 0.35 and COV of 0.36. For "soft" site records the corresponding means and COVs are 19 rad/sec and 0.43 for ω_B and 0.32 and 0.36 for ζ_B.

Moayyad and Mohraz (1982) obtained average shapes of the PSD function for vertical and horizontal accelerations. When a Kanai-Tajimi PSD function, Eq. 6.20, is fitted to the average shape for "rock" sites proposed by Moayyad and Mohraz (1982), ω_B and ζ_B were found to be $\omega_B = 16.9$ *rad/sec* and $\zeta_B = 0.94$ (Sues, 1983). The Kanai-Tajimi PSD function with these values of ω_B and ζ_B is used in this study to model the earthquake ground motion except as otherwise stated.

The Kanai-Tajimi PSD function with $\omega_B = 16.9$ *rad/sec* and $\zeta_B = 0.94$, and the Housner-Jennings PSD function are shown in Fig. 6.1. The average PSD function for "rock" sites obtained using the statistics and distributions for ω_B and ζ_B proposed by Lai (1980) is also shown in Fig. 6.1.

The PSD function with $\omega_B = 16.9$ *rad/sec* and $\zeta_B = 0.94$, and the average PSD function obtained with Lai's data are similar, implying that the response statistics may be calculated with either proposed PSD. However, the study of Lai (1980) shows that the large COV in ω_B implies the high likelihood of occurrence of earthquakes with very different frequency content. The effect

of these differences on the seismic response of a cut slope is evaluated in Sect. 7.2.4; a COV of the time to failure, Δ_3, was found to be of the order of 0.2.

Peak Ground Acceleration -- The probabilities of exceedance of all significant intensities at a site during the lifetime of a project are calculated with the fault-rupture seismic hazard model of Def Kiureghian and Ang (1977). The probabilities calculated with this model will depend on the physical relations assumed in the model (e.g., the intensity attenuation equation, and the slip-length magnitude relation) as well as the values of the parameters including the occurence rate and the slope of the "magnitude recurrence" curve (Der Kiureghian and Ang, 1977). The effect of these uncertainties on the calculated probabilities can be systematically evaluated. In general, the uncertainties in the intensity attenuation equation will tend to dominate. The COV of the peak ground acceleration obtained with the attenuation equation may be as high as 0.70 (Der Kiureghian and Ang, 1977).

Duration of Strong Phase Motion -- Lai (1980) suggested the following relationship between the expected peak ground acceleration and the mean duration of the strong phase motion,

$$\mu_{T_E}(a_{max}) = 30 \cdot \exp(-3.254 \cdot a_{max}^{0.35}) \quad , \text{sec} \tag{6.27}$$

where a_{max} is in terms of g. The COV of T_E conditional on the value of a_{max} is $\delta_{T_E} = 0.804$, and the gamma distribution is considered appropriate for T_E. For "rock" site conditions the strong motion durations are slightly shorter (Moayyad and Mohraz, 1982; Lai, 1980). However, because of scarcity of data for "rock" sites Eq. 6.27 is retained.

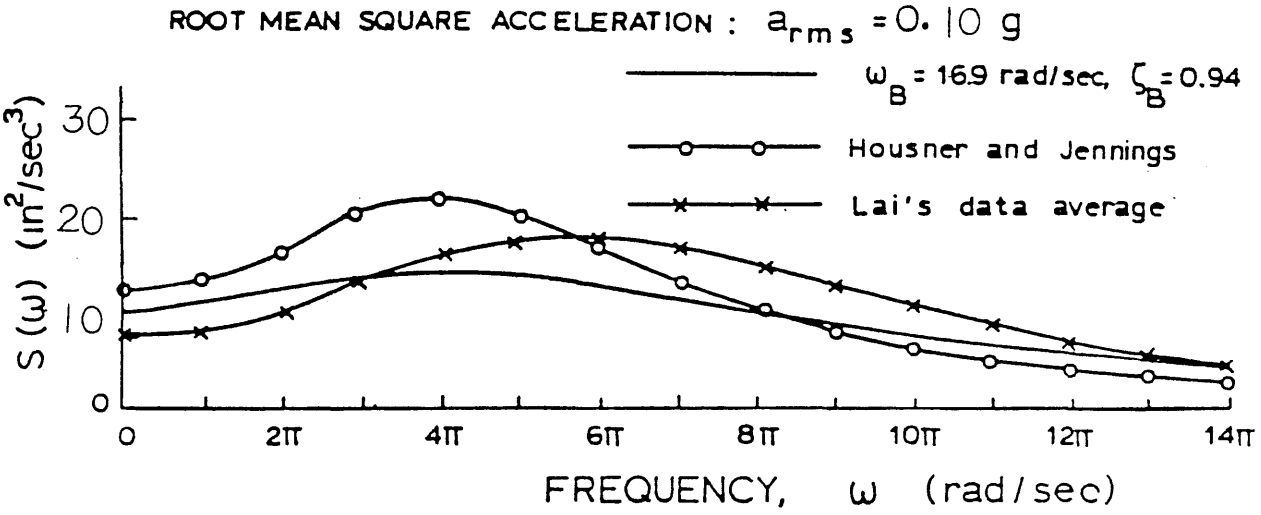

Fig. 6.1 PSD Function for "Rock" Sites

CHAPTER 7

ILLUSTRATIVE EXAMPLES

7.1 Introduction

In the previous several chapters, a method for evaluating the seismic stability of a cut slope has been developed. For the purpose of illustration, the seismic stability of the same cut slope that was considered in the static stability analysis is examined herein.

The procedures developed in the previous chapters are applied to the calculation of the mean and standard deviation of the duration of strong motion with a specified intensity necessary to cause sliding failure.

The same problem is also examined using the alternate approach, which is more direct but less sophisticated in the probabilistic sense.

Finally, the lifetime reliability of a cut slope is evaluated taking into account the uncertainties associated with several parameters such as strain dependency of G, the F(N)-N relation and the variability in the frequency content of the ground excitation.

7.2 Seismic Stability Evaluation of Cut Slopes

7.2.1 Problem Description

The seismic stability of the same cut slope analyzed earlier for static stability is considered. The cut slope with $K_0 = 1.0$ is shown in Fig. 3.12 with the static shear strength of the soil listed in Table 3.2. The stress conditions along the most probable potential failure surface prior to an earthquake are shown in

Figs. 3.6 and 3.12. The dynamic properties of the soil are assumed to be as follows: the variation of G_0 with depth Z is expressed as 2050000 + 2500·Z, in psf; $G/G_0 - \gamma$ is of hyperbolic form with its reference strain $\gamma_r = 0.001$, and $h_0 = 0.20$; the dynamic shear strength follows the results shown in Fig. 5.5.

7.2.2 Evaluation of Time to Failure

In order to determine the most susceptible potential failure surface under earthquake loadings, the expected strong-phase durations with different values of the expected $a_{\max}$ at the base necessary to cause failure are evaluated for several potential failure surfaces including the most probable failure surface determined in the static analysis. Table 7.1 shows the results; the most probable sliding mass is identical irrespective of the magnitude of earthquake loadings, and is larger than that determined from the static analysis. Subsequent dynamic analysis is performed for the above-determined most probable failure surface.

The dynamic analysis with different root-mean-square (RMS) base accelerations, $a_{rms,base}$, is performed for a one-dimentional MDF system. The profile of the RMS absolute accelerations is shown in Fig. 7.1 for expected $a_{\max}$ at the base of 0.1, 0.2, 0.3 and 0.4 g. The nonlinear behavior is apparent in the variation of the ratio of the RMS absolute acceleration at the top to the RMS base acceleration, $a_{rms,base}$. The RMS absolute accelerations with depth Z in Fig. 7.1 can be normalized with respect to $a_{rms,base}$ to obtain the relation of A_f with Z. Fig. 7.2 shows the comparison of the normalized RMS relative displacements with the fundamental mode shape obtained from the modal analysis using G with Z corresponding to the RMS shear strain, γ_{rms}. The agreement appears to be quite good, implying that the first mode is extremely dominant and that, therefore, the seismic stability of a cut slope can be reasonably

represented with a SDF system. Combining the relation of the dynamic shear strength ratio $\tau_d(N)/\tau_f$ with the number of cyclic loadings N, the stress condition along a potential failure surface prior to an earthquake, and the $A_f - Z$ relation obtained in the preliminary analysis indicated above, A_{av} and F(N)-N relation in the converted SDF system are obtained as indicated in the last column of Table 7.2 and in Fig. 7.3, respectively.

Table 7.1 Time (second) of Strong Phase Motion Necessary for Failure

R/H^*	Expected a_{max} at the Toe			
	0.1 g	0.2 g	0.3 g	0.4 g
2.12	1810.5	51.82	20.07	7.94
2.50	965.2	29.53	11.07	4.82
2.92	821.9	21.89	9.41	4.10
3.38	535.8	14.43	6.46	3.08
3.88	632.7	17.14	7.04	3.66
4.42	1158.4	30.36	12.84	5.56

* see Fig. 3.12

Table 7.2 Average Amplification Factor A_{av} and Dominant Frequency ω_1

Case	S_0 (f^2/sec^3)	Expected a_{max} at the Toe (g)	ζ_B	ω_B (rad/sec)	Obtained Results	
					ω_1 (rad/sec)	A_{av}
1	0.0096	0.1	0.94	16.9	25.95	3.020
2	0.0385	0.2			23.49	3.108
3	0.0866	0.3			22.60	2.526
4	0.1540	0.4			19.64	2.436

On the condition that c = 0, A = 1.0, α = 0.01 and $\delta = \beta$, the system parameters n, β and K in the converted SDF system are determined uniquely through the random vibration analysis by satisfying the following equations:

$$E[\omega] = \omega_1 \tag{7.1}$$

$$f_u = F(N = 1) \tag{7.2}$$

$$\frac{\sigma_{\ddot{X}}}{\sigma_{\ddot{x}_G}} = A_{av} \tag{7.3}$$

where:

$E[\omega]$ is defined by Eq. 4.31;

f_u is defined by Eq. 4.15;

$\sigma^2_{\ddot{X}} = \sigma^2_{\ddot{u}+\ddot{x}_G} = E[\{\frac{c}{m}\dot{u}+\alpha\frac{K}{m}u+(1-\alpha)\frac{K}{m}Z\}^2]$;

$\sigma^2_{\ddot{x}_G}$ = obtained from Eq. 6.25.

The results are shown in Table 7.3.

Table 7.3 Hysteretic System Parameters

Case	1	2	3	4
n	0.9	1.8	1.8	4.5
β	$.944 \times 10$	$.125 \times 10^3$	$.111 \times 10^3$	$.120 \times 10^6$
K (p/f)	$.363 \times 10^7$	$.298 \times 10^7$	$.279 \times 10^7$	$.218 \times 10^7$
$E[\dot{Z}u]$	$.438 \times 10^{-4}$	$.232 \times 10^{-3}$	$.579 \times 10^{-3}$	$.143 \times 10^{-2}$
σ_u	$.632 \times 10^{-2}$	$.153 \times 10^{-1}$	$.231 \times 10^{-1}$	$.373 \times 10^{-1}$

Through the random vibration analysis with the system parameters of Table 7.3, the statistics of the time to failure, T_f, for several stationary loadings with different peak base acceleration $a_{\max}$ are given in Table 7.4.

Table 7.4 Statistics of T_f (seconds)

$E[a_{\max}]$ at the Toe Level		0.1 g	0.2 g	0.3 g	0.4 g
T_f Time to Failure	μ_{T_f}	535.78	14.43	6.46	3.08
	σ_{T_f}	51.43	4.50	2.49	1.65

The values of μ_{T_f} were calculated by

$$\mu_{T_f} = \frac{D_f}{X \cdot E[\dot{E}_T]} \tag{7.4}$$

where all the quantities in Eq. 7.4 are defined in Chapters 4 and 5, X being the equivalent amplitude for random loading defined by Eq. 5.12. The standard deviation of T_f is calculated by $\sigma_{T_f} = \mu_{T_f} \cdot \delta_{T_f}$ where δ_{T_f} is the same as δ_{E_T} at time $t = \mu_{T_f}$. The validity of this technique for calculating σ_{T_f} was verified with Monte-Carlo simulations.

The variation of μ_{T_f} with the intensity of the earthquake loading is shown in Fig. 7.4. The mean plus and minus one standard deviation of T_f are also shown in Fig. 7.4.

The coefficient of variation of the duration of strong motion necessary for

failure decreases as the mean duration increases. A similar behavior was found with the coefficient of variation of the total hysteretic energy dissipated, i.e. the COV of the hysteretic energy decreases as the duration of the load increases.

Figures such as Fig. 7.4 are used to calculate the factors of safety against sliding failure for a specific seismic loading, as well as the associated reliability levels. Suppose that the intensity of the loading is given as $a_{\max} = 0.30$ g, and the strong-phase duration $T_E = 5.0$ seconds. According to Fig. 7.4, the cut slope can withstand an intensity of 0.33 g for a mean duration of 5.0 seconds prior to sliding failure. The factor of safety, therefore, is $F_a = 0.33/0.30 = 1.10$, with a coefficient of variation of 0.182. The associated reliability is $\mathrm{P}[F_a > 1.0] = 0.67$.

7.2.3 Alternate Approach

The seismic safety of a cut slope is also evaluated with the alternate method. Two basic assumptions are made as follows:

(i) The variation of the horizontal acceleration with depth at any instant during an earthquake is the same as the variation of A_f with depth Z.

(ii) Vibration can be considered approximately to be a narrow-band process.

Based on the above assumptions, the earthquake-induced total shear force along a potential failure surface can be regarded as a sequence of repeated dynamic loadings, the amplitude of which is Rayleigh-distributed with an average period of $T_1 = 2\pi/\omega_1$.

The damage, D, induced by one cycle of loading of F(N) is 1.0/N. Failure is then defined to occur when the accumulated damage reaches unity. A typical $D-F$ curve is shown in Fig. 7.5 which can be constructed from the

corresponding F(N)-N relation.

The amplitudes of the cyclic dynamic loadings are correlated depending on the autocorrelation properties of the peaks or the envelope function of dynamic loadings. By assuming the envelope of the accelerations to be as shown in Fig. 7.6, simulation is performed to obtain the autocorrelation of the envelope of horizontal accelerations at the top of the layers for Case 3 of Table 7.2. The results are shown in Fig. 7.7; the correlation coefficient $\rho(\tau)$ may be expressed approximately as an exponential function.

The generation of the amplitudes of dynamic loadings with the above correlation property as well as the evaluation of the time to failure, T_f, can be done through the following simulation procedure:

(i) Generate the sequences of correlated normal random numbers satisfying the equation indicated in Fig. 7.7; procedures described in Sect. 3.3.1 can be applied.

(ii) Transform the correlated normal random numbers into Rayleigh-distributed random variables, which are the generated amplitudes of the dynamic loadings; for this purpose the inverse transform method (Ang and Tang, 1984) can be used.

(iii) Through the $D-F$ relation such as Fig. 7.5, the damage corresponding to each amplitude of loadings is evaluated.

(iv) The total damage, D_T, through n cycles of loadings are evaluated as the sum of the individual damages.

(v) If D_T exceeds unity, failure is considered to take place and T_f is evaluated as

$$T_f = n \cdot T_1 \tag{7.5}$$

Otherwise, increase n by 1 and return to step (iv).

Repeating the simulation process, the mean and COV of T_f are obtained to be 5.75 sec and 0.929, respectively. Corresponding values obtained with the proposed method of Chapter 6 are 6.46 sec and 0.385, respectively. It is to be noted that the mean time to failure obtained with the alternate approach is slightly on the safe side compared to that of the proposed method i.e. the method based on random vibration analysis; both results, however, are still in fairly good agreement in spite of the difference of a failure criterion. This implies that both methods may be adequate for evaluating the mean time to failure. Regarding the COV of T_f, on the other hand, the alternate approach gives much larger COV of time to failure than that of the random vibration method. The large COV of T_f with the alternate approach implies that this approach is less reliable than the random vibration method. Supposing that the strong-phase duration $T_E = 4.0$ seconds, P_F obtained with the alternate approach is 0.473 as opposed to 0.135 with the random vibration method. Therefore, in the evaluation of failure probability, the alternate approach may be too conservative.

7.2.4 Reliability Evaluation

This section investigates the influence of the various sources of uncertainty on the strong-phase duration necessary for failure, μ_{T_f}. Also, the reliability evaluation over a specific life is performed taking into account the above-mentioned uncertainties.

Suppose the case where the $\tau - \gamma$ curve of a soil is of hyperbolic form

with a reference strain, γ_r, which is assumed to be a random variable as shown in Table 7.5. The corresponding $G/G_0 - \gamma$ relation of the soil is, therefore, a random variable, and the COV of μ_{T_f} associated with the uncertainty of $G/G_0 - \gamma$ relation, Δ_1, is evaluated as 0.215 for expected $a_{\max}$ at the toe of 0.3 g.

Table 7.5 Uncertainty due to Variation of $G/G_0 - \gamma$ and $h - \gamma$ Relation

γ_r	Probability	μ_{T_f} (sec)	
			$E[\mu_{T_f}] = 6.10$ sec
0.0008	0.2	7.52	
0.0010	0.6	6.46	$\Delta_1 = COV[\mu_{T_f}] = 0.215$
0.0012	0.2	3.61	

The influence of the variation of F(N) on μ_{T_f} is then examined. For this purpose, the $\tau_d(N)/\tau_f - \tau_s/\tau_f$ relation for N = 10, obtained from experimental results (Seed and Chen, 1966) shown in Fig. 7.8, is used. Based on this data, the COV of F(N = 10), δ_F, is evaluated to be 0.025 through the simulation described in Sect. 6.3. Assuming that δ_F is constant for any N and that F(N) for different values of N are perfectly correlated, log-normal random variables, μ_{T_f}, are evaluated for several values of F(N) discretized as shown in Table 7.6. The COV of μ_T due to the variability of F(N), Δ_2, is 0.104. Fig. 7.8 shows the experimental results for two different clays plotted together. In spite of this, Δ_2 is still less than half of Δ_1, implying that Δ_2 may be neglected rela-

tive to Δ_1 in practice.

Table 7.6 Uncertainty due to Variation of F(N)

F(N = 1) (p)	Probability	μ_{T_f} (*sec*)	
130810	0.083	5.19	$E[\mu_{T_f}] = 6.47$ (sec)
134110	0.167	5.76	
137490	0.500	6.45	$\Delta_2 = COV[\mu_{T_f}]$
140960	0.167	7.29	$= 0.104$
144510	0.083	7.66	

Finally, the effect of the randomness in the frequency content of a ground excitation on μ_{T_f} of a specific sliding mass is examined. μ_{T_f} is evaluated for $a_{\max} = 0.3$ g and $\zeta_B = 0.94$, but with five different values of ω_B. With the statistics of ω_B for "rock" site conditions suggested by Lai (1980), the expected time to failure, μ_{T_f}, is calculated assuming both normal and gamma distributions for ω_B. The results are summarized in Tables 7.7a and 7.7b. μ_{T_f} for a load with the same expected maximum ground acceleration but with a different frequency content i.e. $\omega_B = 16.9$ rad/sec and $\zeta_B = 0.94$ are also shown in Table 7.7b. μ_{T_f} in the latter analysis is similar to the average of μ_{T_f} obtained with the earlier analysis. The COV of μ_{T_f} due to the randomness in the frequency content of a ground excitation, Δ_3, is of the order of 0.2, which will have an influence on the overall uncertainty of μ_{T_f}.

Table 7.7a μ_{T_f} for several ω_B

ω_B	PDF		S_0 (ft^2/sec^3)	μ_{T_f} (sec)
	Gamma	Normal		
5.0	0.0323	0.0664	0.2929	12.63
15.0	0.3141	0.2404	0.0976	6.88
25.0	0.3895	0.3833	0.0586	6.10
35.0	0.1999	0.2465	0.0418	8.82
45.0	0.0642	0.0634	0.0325	9.65

Table 7.7b Average μ_{T_f} with Normal and Gamma PDFs for ω_B

PDF	$E[\mu_{T_f}]$ (sec)	$COV[\mu_{T_f}]$
Gamma	7.33	0.209
Normal	7.62	0.238
$\omega_B = 16.9$ $\zeta_B = 0.94$	6.46	

With the above-mentioned sources of uncertainties, the probability of failure conditional on the intensity and duration of an earthquake, $P_F(a,t)$, is calculated for several levels of earthquake intensities with a wide range of strong-phase durations of the ground motions. The results are summarized in Fig.7.9. The statistics and probabilities of the duration of strong-phase motion given in Sect. 6.4.2 (the gamma-distributed random variable with its mean

given by Eq. 6.27 and its COV being 0.804) are combined with the results in Fig. 7.9 to obtain the unconditional probability of failure, $P_F(a)$ which is represented by the dashed line in Fig. 7.9.

The lifetime reliability is illustrated for Tokyo, Japan. The corresponding seismic hazard curves are obtained with the method of Der Kiureghian and Ang (1977) using the data reported by Hattori (1977). Because the epicenters of past earthquakes around Tokyo scatters without any particular trend, the type-3 source model is used in the hazard analysis. The results are shown in Fig. 7.10. Both Figs. 7.9 and 7.10 can then be used to calculate the lifetime reliability against sliding failure of cut slopes in Tokyo. The calculated reliabilities are summarized in Table 7.8 for the cut slope discussed earlier.

Table 7.8 Lifetime Reliability for Tokyo

Life Time (years)	1	20	50
Probability of No Sliding-Failure	0.994	0.898	0.784

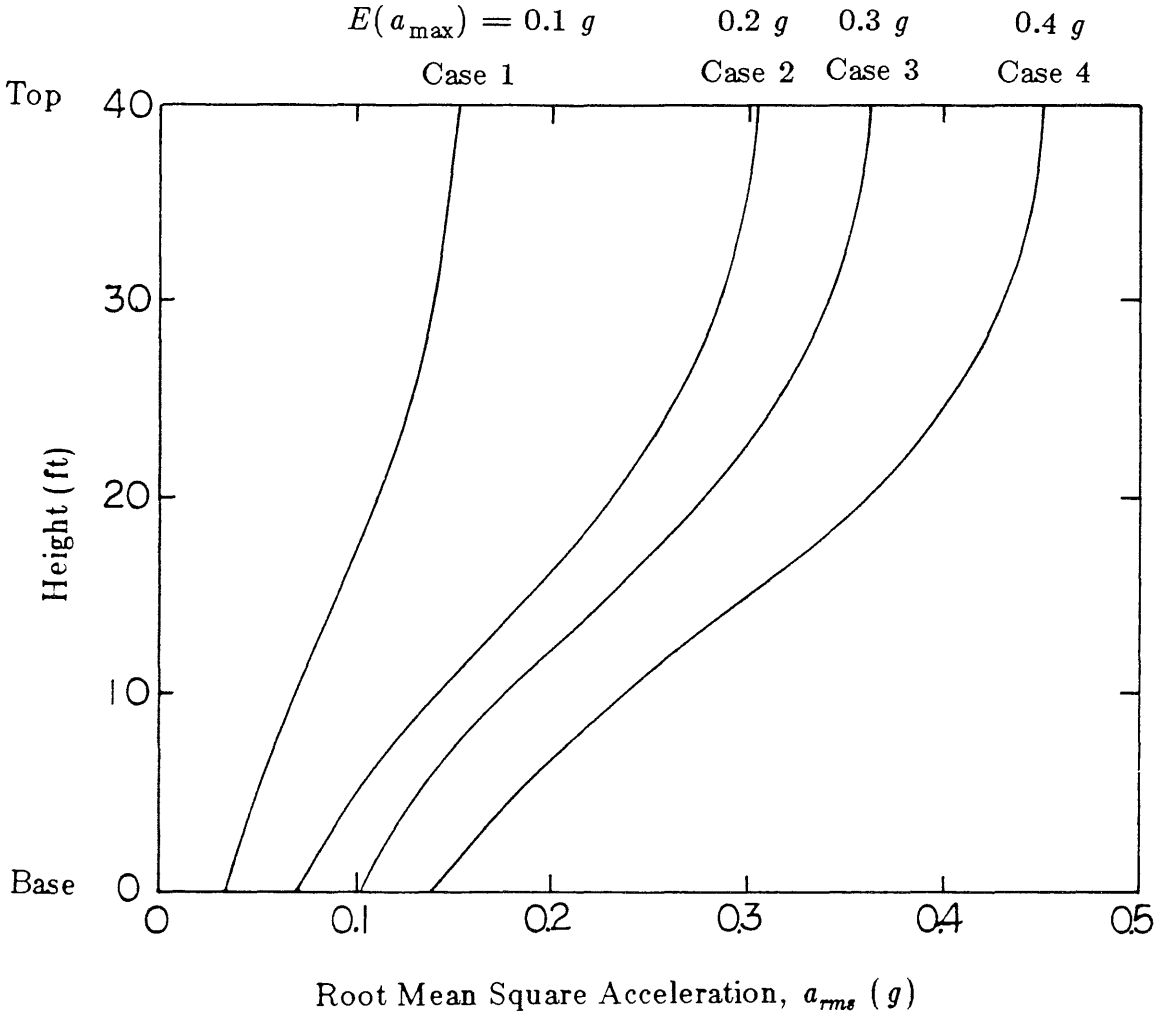

Fig. 7.1 Profile of RMS Absolute Accelerations

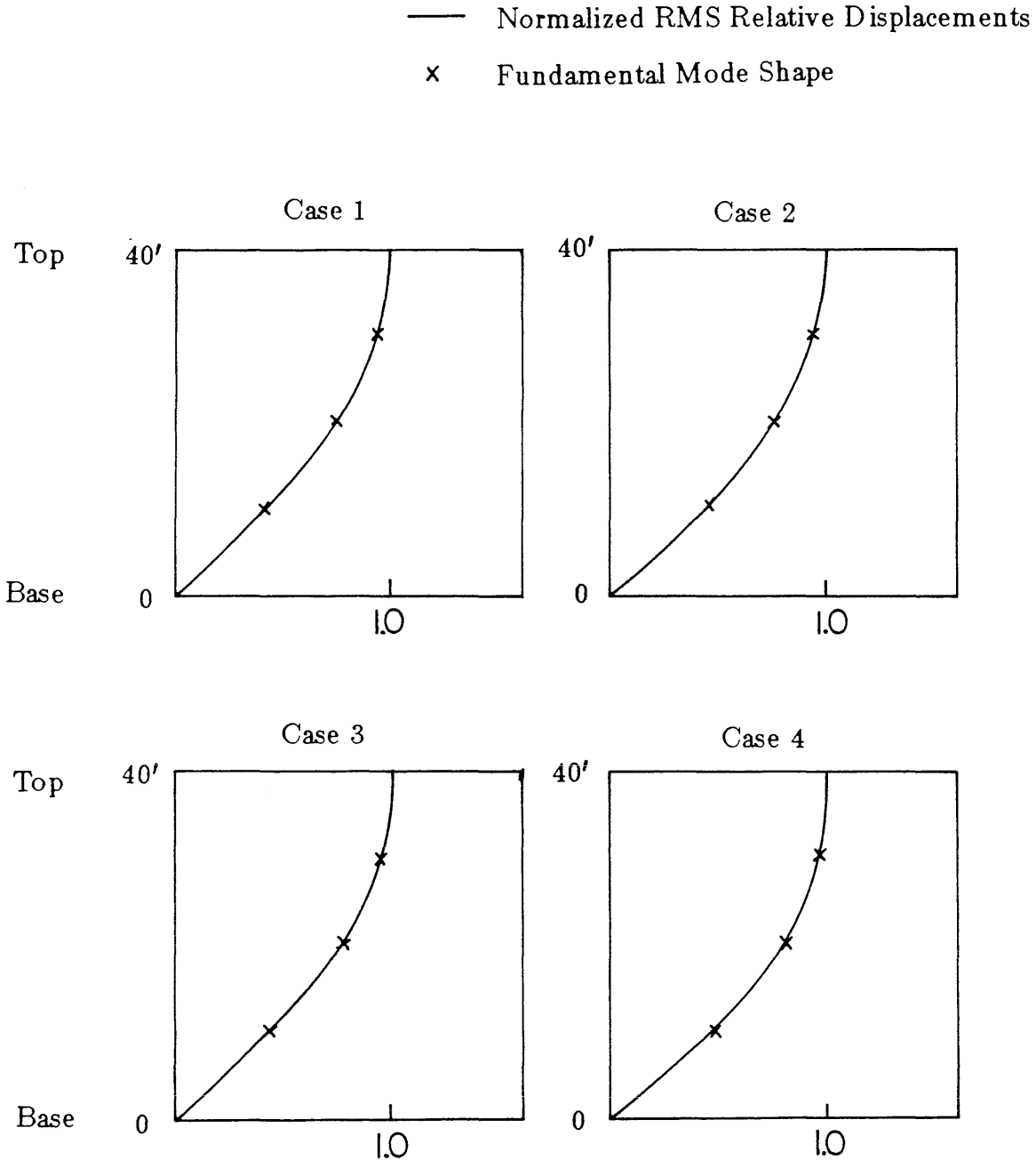

Fig. 7.2 Comparison of Normalized RMS Relative Displacement and the Fundamental Mode Shape

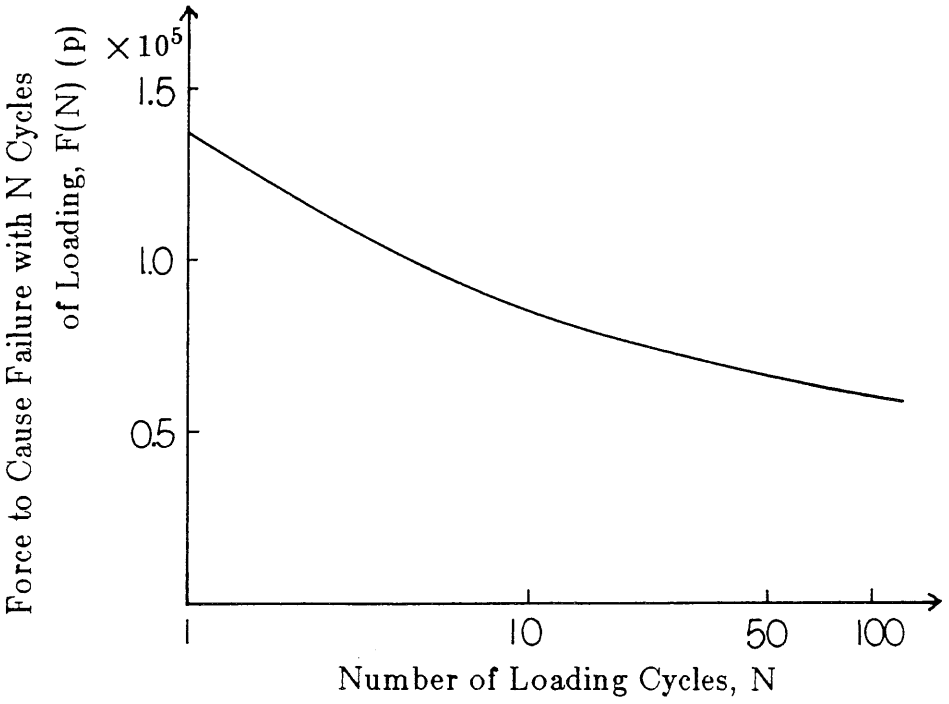

Fig. 7.3 F(N) versus N

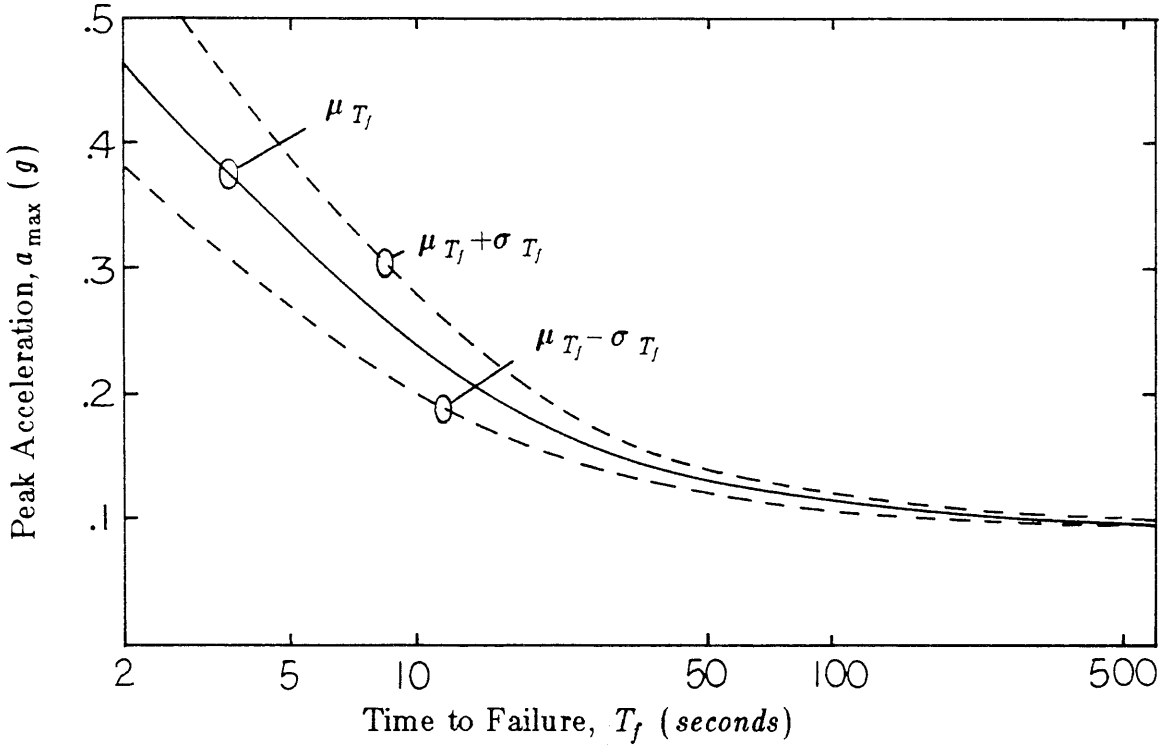

Fig. 7.4 Statistics of Time to Failure

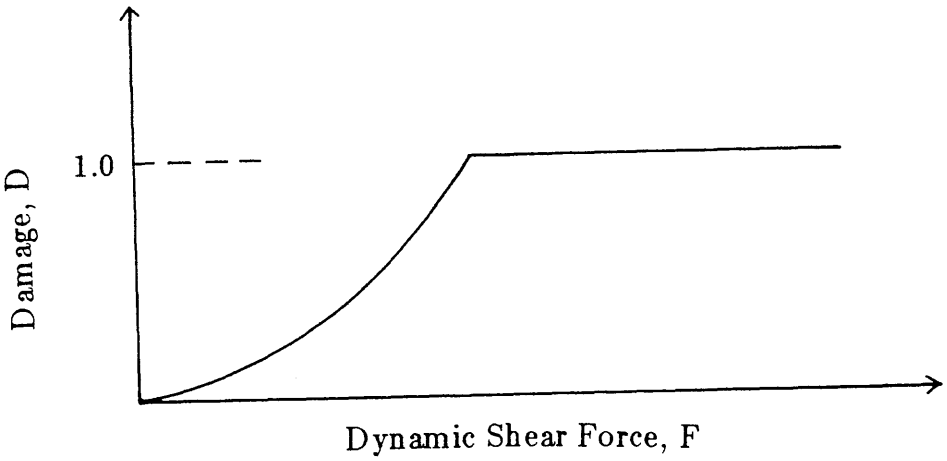

Fig. 7.5 D versus F

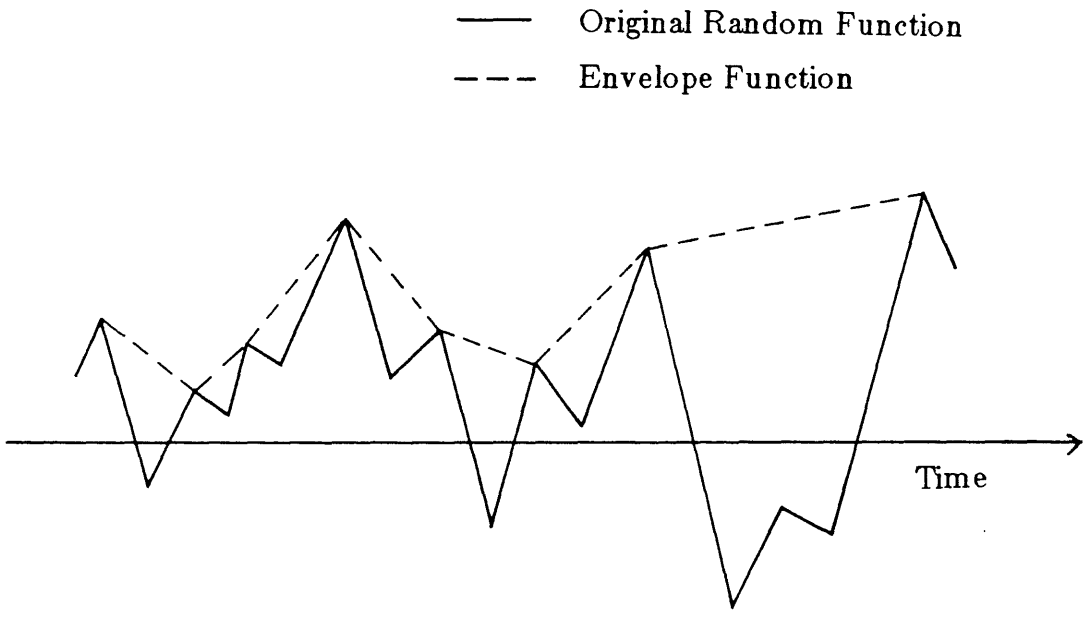

Fig. 7.6 Definition of Envelope Function

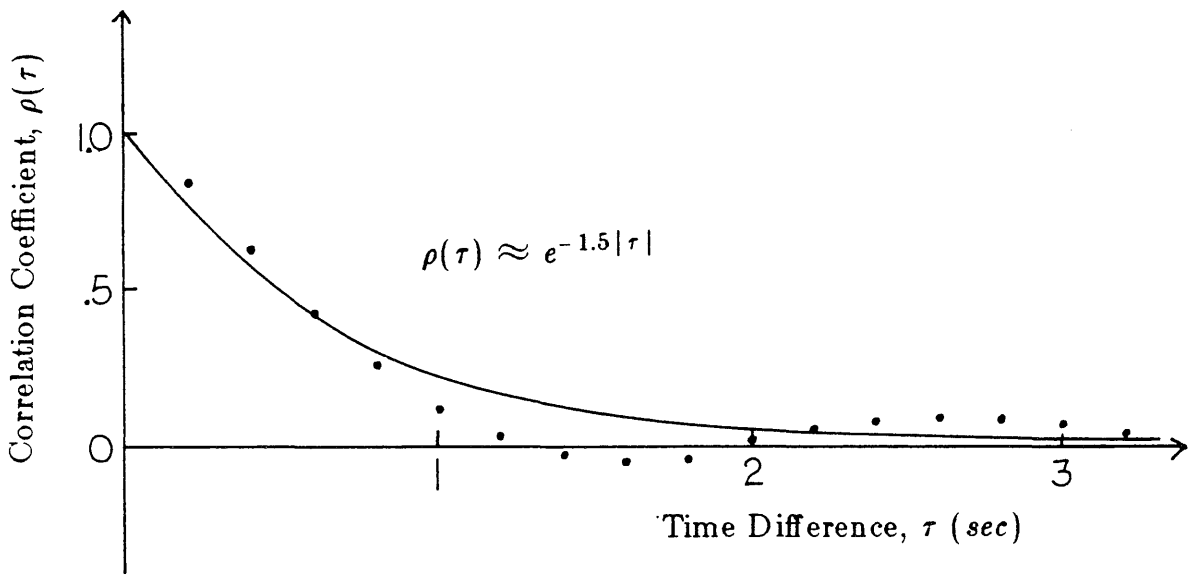

Fig. 7.7 Autocorrelation Coefficient of an Envelope Function

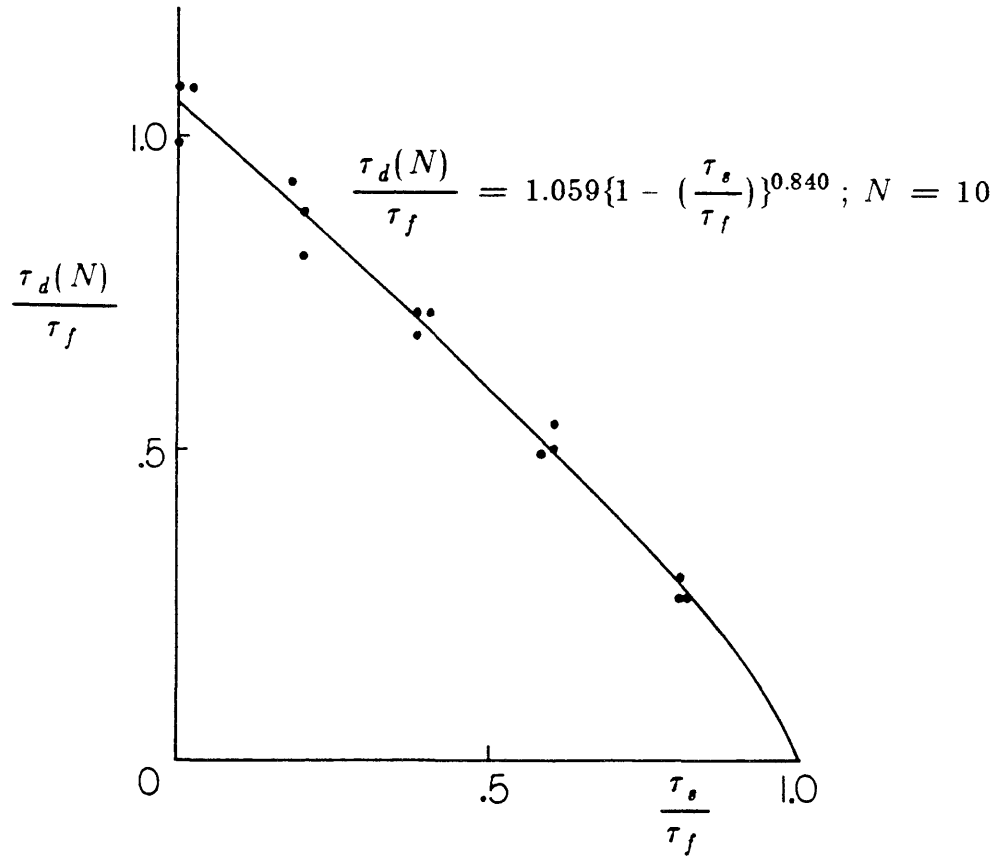

Fig. 7.8 Relation between $\tau_d(N)/\tau_f$ and τ_s/τ_f

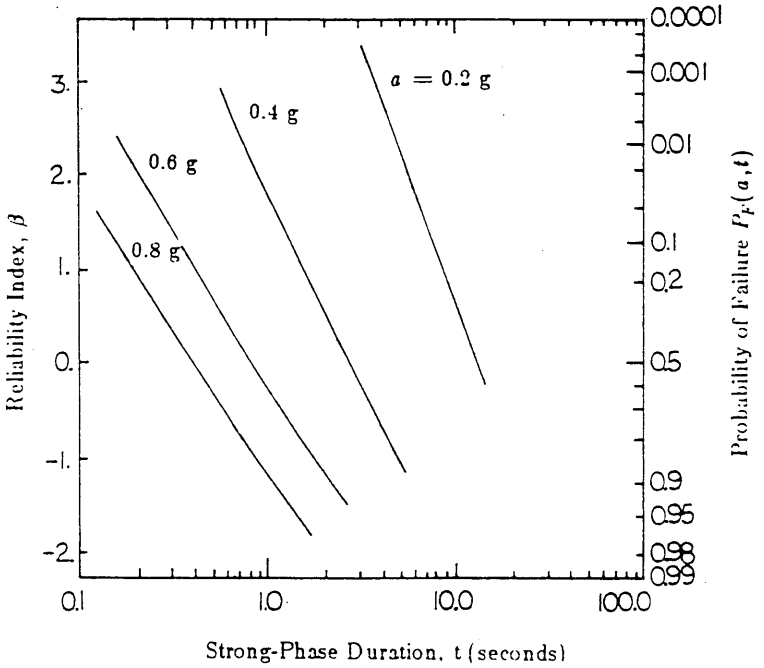

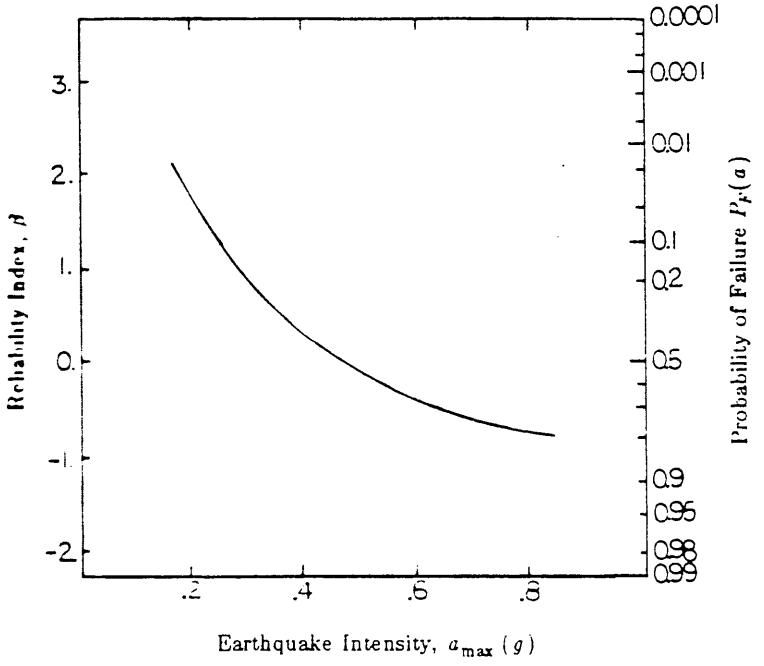

Fig. 7.9 Reliability Against Sliding Failure

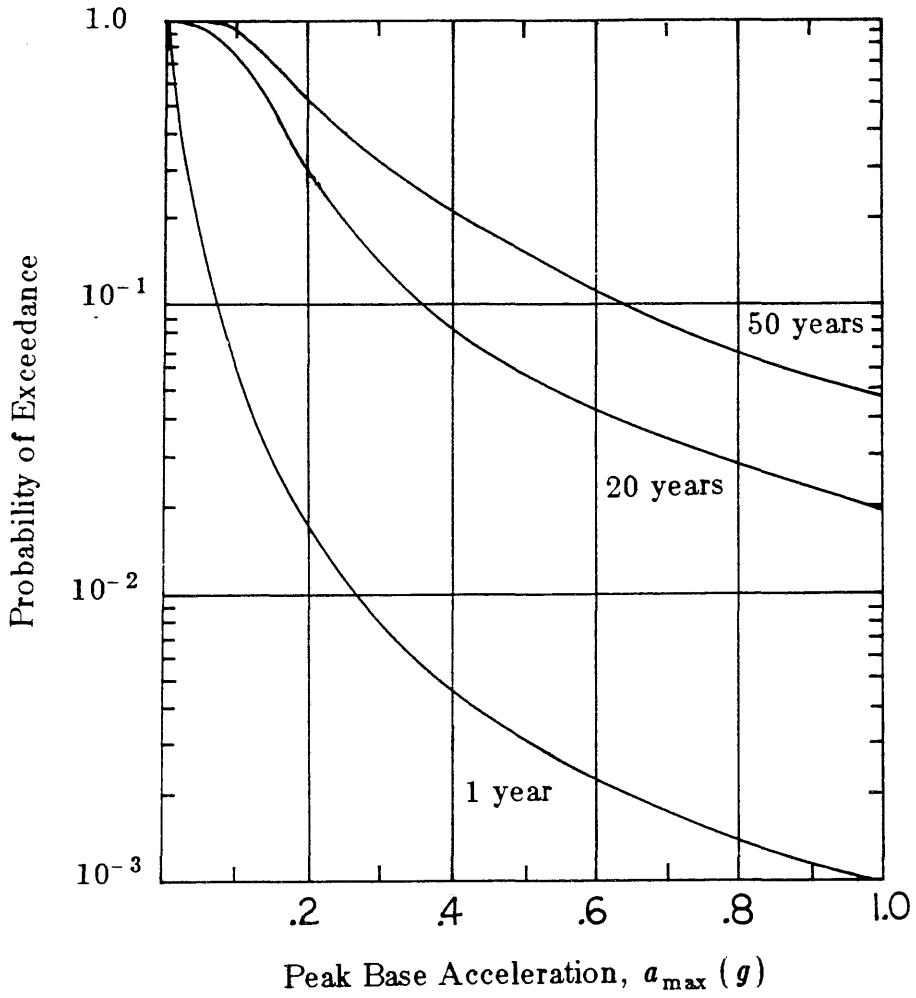

Fig. 7.10 Seismic Hazard for Tokyo

CHAPTER 8

SUMMARY AND CONCLUSIONS

8.1 Summary

8.1.1 Static Stability of Cut Slopes

In the static stability evaluation of a cut slope formed by strain-softening soil such as highly overconsolidated clay, progressive failure should be considered as the critical failure mode.

The stress condition along a potential failure surface both prior to and after an excavation is investigated by finite-element elasto-plastic analysis; in this process, a potential failure surface is modeled as joint elements. Through the investigation, the redistribution of an unbalanced force caused by a local failure is determined. This stress redistribution is combined with the inherent variability of the shear strength of a soil, which is the main contributor to the uncertainties in the static stability evaluation of a cut slope, to determine the failure probability and the expected length of local failure along an assumed potential failure surface.

8.1.2 Seismic Stability of Cut Slopes

A method is developed for evaluating the seismic stability of a cut slope consisting of the following: (1) the horizontal vibration of a sliding mass subjected to an earthquake loading is converted into an equivalent SDF system with a smooth hysteretic restoring force; (2) a failure criterion and a damage index for the converted SDF system is established; and (3) the safety based on

the response statistics obtained through random vibration analysis is evaluated.

The mean and variance of a strong-motion duration necessary for sliding failure of a cut slope were calculated through random vibration analysis. These statistics can be used to define the seismic resistance curves against sliding failure of a cut slope. On this basis, the factors of safety and the associated reliability levels can be obtained for a given seismic loading.

Alternatively, the results of the random vibration analysis can be used to calculate the reliability against sliding failure of a cut slope under a random seismic load with a prescribed duration and intensity.

The reliability against sliding failure conditional on the intensity and duration of a loading was obtained using the results from the random vibration analysis; the uncertainties associated with several parameters including the dynamic soil properties and the randomness in the frequency content of an earthquake loading are considered.

8.2 Conclusions

8.2.1 Static Stability of Cut Slopes

The proposed method has advantages over the conventional reliability-based method in that it can evaluate the expected toe-failure length as well as the failure probability (P_F) with acceptable accuracy; the conventional method gives only the lower and upper bounds of P_F.

Among some factors affecting P_F, the COV of shear strengths (δ) is the most dominant. β_V becomes equally influential on P_F if δ is small. Also, the difference of the expected water level has marked effect on P_F, whereas the uncertainty associated with the expected water level is less important.

8.2.2 Seismic Stability of Cut Slopes

The main conclusions of the dynamic part of this study can be summarized as follows:

(i) The proposed methodology, that evaluates the seismic reliability of a cut slope conditional on the intensity and duration of an earthquake loading, is important and useful for a risk-based design against sliding failure. The comparison of the results obtained from the proposed random vibration method with those from the simplified alternate approach, which is straightforward but less sophisticated from a probabilistic standpoint, shows that the proposed method is a more reliable tool for determining the seismic reliability of a cut slope against sliding failure, and for assessing the relative risks between design alternatives.

(ii) The reliability against sliding failure conditional on the intensity and duration of a given earthquake is equally sensitive to the uncertainties in the $G/G_0 - \gamma$ relation of a soil and in the Kanai-Tajimi filter parameters. The COV of the time to sliding failure associated with the uncertainties in the Kanai-Tajimi filter parameters is of the order of 0.2.

(iii) The conditional reliability against sliding failure is sensitive to the strong-motion duration as well as the intensity of a seismic excitation. This implies that the probabilities of occurrence of all significant loads at the site have to be considered in the design process, as opposed to a deterministic method that postulates the lifetime earthquake load.

APPENDIX

EQUIVALENT LINEAR COEFFICIENTS

For real n > 0 the coefficients in Eq. 4.17 are:

$$C_e = A - (\beta F_1 + \delta F_2) \tag{A.1}$$

$$K_e = -(\beta F_3 + \delta F_4) \tag{A.2}$$

where

$$F_1 = \frac{\sigma_Z^n}{\pi}\Gamma\left(\frac{n+2}{2}\right)2^{n/2} \times 2\int_{\theta}^{\pi/2} \sin^n(\theta)\, d\theta \tag{A.3a}$$

$$F_2 = \frac{\sigma_Z^n}{\sqrt{\pi}}\Gamma\left(\frac{n+1}{2}\right)2^{n/2} \tag{A.3b}$$

$$F_3 = \frac{n\sigma_{\dot{u}}\sigma_Z^{n-1}}{\pi}\Gamma\left(\frac{n+2}{2}\right)2^{n/2} \times 2\left\{(1-\rho_{\dot{u}Z}^2)^{(n+1)/2} + \rho_{\dot{u}Z}\int_{\theta}^{\pi/2} \sin^n(\theta)\, d\theta\right\} \tag{A.3c}$$

$$F_4 = \frac{n}{\sqrt{\pi}}\rho_{\dot{u}Z}\sigma_{\dot{u}}\sigma_Z^{n-1} \times \Gamma\left(\frac{n+1}{2}\right)2^{n/2} \tag{A.3d}$$

$$\theta = \arctan\left(\frac{\sqrt{1-\rho_{\dot{u}Z}^2}}{\rho_{\dot{u}Z}}\right) \tag{A.3e}$$

LIST OF REFERENCES

1. Amin, M. and Ang, A. H-S., *A Nonstationary Stochastic Model for Strong Motion Earthquakes,* Structural Research Series No. 306, University of Illinois, Urbana, Ill., 1966.

2. Amin, M. and Ang, A. H-S., *Nonstationary Stochastic Model for Earthquake Motions,* Journal of the Engineering Mechanics Division, ASCE, Vol. 94, No. EM2, April 1968, pp. 559-583.

3. Ang, A. H-S. and Amin, M., *Studies of Probabilistic Safety Analysis of Structures and Sructural Systems,* Structural Research Series No. 320, University of Illinois, Urbana, Ill., 1967.

4. Ang, A. H-S. and Tang, W. H., *Probability Concepts in Engineering Planning and Design - Vol. 1,* John Wiley and Sons, 1975.

5. Ang, A. H-S. and Tang, W. H., *Probability Concepts in Engineering Planning and Design - Vol. 2,* John Wiley and Sons, 1984.

6. Atalik, T. S. and Utku, S., *Stochastic Linearization of Multidegree of Freedom Nonlinear System,* Int. J. of Earthquake Engineering and Structural Dynamics, Vol. 4, 1976, pp. 411-420.

7. Baber, T. T. and Wen, Y. K., *Stochastic Equivalent Linearization for Hysteretic, Degrading, Multistory Structures,* Structural Research Series No. 471, University of Illinois, Urbana, Ill., 1979.

8. Baber, T. T. and Wen, Y. K., *Random Vibration of Hysteretic, Degrading Systems,* Journal of the Engineering Mechanics Division, Vol. 107, No. EM6, Proc. Paper 16712, December 1981, pp. 1069-1087.

9. Bartels, R. H. and Stewart, G. W., *Solution of the Matrix Equation* $AX+XB=C$, Algorithm 432, Communications of the American Computing Machinery, Vol. 15, No. 9, September 1972, pp. 820-826.

10. Bjerrum, L., *Progressive Failure in Slopes of Overconsolidated Plastic Clay and Clay Shales,* Journal of the Soil Mechanics and Foundations Division, ASCE, Vol. 93, No. SM5, 1967, pp. 1-49.

11. Burland, J. B., Longworth, T. I. and Moore, J. F. A., *A Study of Ground Movement and Progressive Failure caused by a Deep Excavation in Oxford Clay,* Geotechnique, Vol. 27, No. 4, 1977, pp. 557-591.

12. Casagrande, A. and Shannon, W. L., *Research on Stress-Deformation and Strength Characteristics of Soils and Rocks under Transient Loading,* Harvard

University Soil Mechanics Series No. 31, 1948.

13. Chowdhury, R. N. and A-Grivas, D., *Probabilistic Model of Progressive Failure of Slopes,* Journal of the Geotechnical Engineering Division, ASCE, Vol. 108, No. GT6, June 1982, pp. 803-819.

14. Clough, R. W. and Penzien, J., *Dynamics of Structures,* McGraw-Hill, 1975.

15. Der Kiureghian, A. and Ang, A. H-S., *A Fault-Rupture Model for Seismic Risk Analysis,* Bulletin of the Seismological Society of America, Vol. 67, No. 4, August 1977, pp. 1173-1194.

16. Duncan, J. M. and Dunlop, P., *Slopes in Stiff-Fissured Clays and Shales,* Journal of the Soil Mechanics and Foundations Division, ASCE, Vol. 96, No. SM2, March 1969, pp. 467-493.

17. Ellis, W. and Hartman, V. B., *Dynamic Soil Strength and Slope Stability,* Journal of the Soil Mechanics and Foundations Division, ASCE, Vol. 93, No. SM4, 1967, pp. 355-373.

18. Faccioli, E. and Ramirez, J., *Earthquake Response of Nonlinear Hysteretic Soil Systems,* Earthquake Engineering and Structural Dynamics, Vol. 4, 1976, pp. 261-276.

19. Gazetas, G., Debchaudbury, A. and Gasparini, D. A., *Random Vibration Analysis for Seismic Response of Earth Dams,* Geotechnique, Vol. 31, No. 2, June 1981, pp. 261-277.

20. Goodman, R. E. and Taylor, R. L., *A Model for the Mechanics of Jointed Rock,* Journal of the Soil Mechanics and Foundations Division, ASCE, Vol. 94, No. SM3, May 1968, pp. 637-659.

21. Hanks, T. C. and McGuire, R. K., *The Character of High Frequency Strong Ground Motion,* Bullitin of the Seismological Society of America, Vol. 71, No. 71, December 1981, pp. 2071-2095.

22. Hardin, B. O. and Black, W. L., *Closure to Vibration Modulus of Normally Consolidated Clay,* Journal of the Soil Mechanics and Foundations Division, ASCE, Vol. 95, No. SM6, 1969, pp. 1531-1537.

23. Hardin, B. O. and Drnevich, V. P., *Shear Modulus and Damping in Soils : Measurement and Parameter Effects,* Journal of the Soil Mechanics and Foundations Division, ASCE, Vol. 98, No. SM6, 1972, pp. 603-624.

24. Hattori, S., *Earthquake Danger in the Whole Vicinity of Japan,* REport of the Building Research Institute, No. 81, June 1977.

25. Henley, E. J. and Williams, R. A., *Graph Theory in Modern Engineering,* Vol. 98, Mathematics in Science and Engineering Series, Academic Press, New York, NY, 1973.

26. Housner, G. W. and Jennings, P. C., *Generation of Artificial Earthquakes,* Journal of Engineering Mechanics Division, ASCE, Vol. 90, No. EM1, February 1964, pp. 113-150.

27. Idriss, I. M. and Seed, H. B., *The Response of Earth Banks During Earthquakes,* Report, Soil Mechanics and Bituminous Material Laboratory, University of California, Berkeley, Calif., April 1966.

28. Jaky, J., *The Coefficient of Earth Pressure at Rest,* Journal for Society of Hangarian Architects and Engineers, Budapest, Hungary, October 1944, pp. 355-358.

29. Kobori, T. and Minai, R., *Linearization Techniques for Evaluating the Elastoplastic Response of Structural Systems to Nonstationary Random Excitations,* Annual Report of the Disaster Prevention Research Institute, Kyoto University, No. 10A, 1967, pp. 235-260 (in Japanese).

30. Kondner, R. L. and Zelasko, J. S., *A Hyperbolic Stress-Strain Formulation of Sands,* Proc. 2nd Pan American Conference on Soil Mechanics and Foundations Engineering, 1963, pp. 289-324.

31. Lai, S-S. P., *Overall Safety Assessment of Multistory Steel Buildings Subjected to Earthquake Loads,* Department of Civil Engineering, Publication No. R80-26, Massachusetts Institute of Technology, Cambridge, Massachusetts, June 1980.

32. Lin, Y. K., *Probabilistic Theory of Structural Dynamics,* McGraw-Hill, 1967.

33. Liu, S. C., *Evolutionary Power Spectral Density of Strong-Earthquakes,* Bullitin of the Seismological Society of America, Vol. 60, No. 3, June 1970, pp. 891-900.

34. Lo, K. Y. and Lee, C. F., *Analysis of Progressive Failure in Clay Slopes,* Proceedings of ICSMFE, 8, Vol. 1, Moscow, 1973.

35. Lumb, P. and Holt, J. K., *The Undrained Shear Strength of a Soft Marine Clay from Hong Kong,* Geothchnique, Vol. 18, 1970, pp. 25-36.

36. Martin, P. P., *Non-Linear Methods for Dynamic Analysis of Ground Response,* thesis presented to the University of California at Berkeley, California, 1975.

37. Matsuo, M., Asaoka, A. and Kawamura, K., *Reliability-Based Design of Geotechnical Engineering Problems,* Memoirs of Faculty of Engineering,

Nagoya University, Vol. 32, No. 1, 1980, pp. 86-142.

38. Mayne, P. W. and Kulhawy, F. H., K_0 - *OCR Relationships in Soil,* Journal of the Geotechnical Engineering Division, ASCE, Vol. 108, No. GT6, June 1982, pp. 851-872.

39. Miner, M. A., *Cumulative Damage in Fatigue,* Journal of the Applied Mechanics, Vol. 12, 1945.

40. Moayyad, P. and Mohraz, B., *A Study of Power Spectral Density of Earthquake Accelerograms,* Civil and Mechanical Engineering Department, Southern Methodist University, Dallas, Texas, June 1982.

41. Newmark, N. M., *Effects of Earthquakes on Dams and Embankments,* Geotechnique, Vol. 15, No. 2, 1965, pp. 139-160.

42. Nishi, K., Esashi, Y. and Okamoto, T., *Mechanical Properties of Mudstone (part 3),* No. 382013, Electronic Power Central Institute, Abiko, Chiba, Japan, 1982 (in Japanese).

43. Olson, R. E. and Kane, K., *Dynamic Shearing Properties of Compacted Clay at High Pressures,* Proc. of the 6th ICSMFE, Montoreal, Vol. 1, 1965, pp. 328-332.

44. Pender, M. J., *Modeling Soil Behavior Under Cyclic Loading,* Proc. of the 9th ICSMFE, Tokyo, Vol. 2, 1977, pp. 325-331.

45. Pires, J. E. A., Wen, Y-K. and Ang, A. H-S., *Stochastic Analysis of Liquefaction under Earthquake Loading,* Structural Research Series, No. 504, Civil Engineering Department, University of Illinois, Urbana, Ill., April 1983.

46. Ramberg, W. and Osgood, W. T., *Description of Stress Strain Curves by Three Parameters,* Technical Note 902, National Advisory Committee for Aeronautics, 1943.

47. Rice, S. O., *Mathematical Analysis of Random Noise,* Bell System Technical Journal, 23, 1941, pp. 282-332; 24, 1945, pp. 46-156; Reprinted in *Selected Papers on Noise and Stochastic Processes,* Ed. N. Wax, Dover Publication Inc., New York, 1954.

48. Richart, F. E., *Some Effects of Dynamic Soil Properties on Soil Structure Interaction,* The 10th Terzaghi Lecture, Journal of Geotechnical Engineering Division, ASCE, Vol. 101, No. GT12, 1975, pp. 1197-1240.

49. Schmidt, B., *Discussion of Earth Pressure at Rest Related to Stress History,* Canadian Geotechnical Journal, National Research Council, Ottawa, Ontario, Canada, Vol. 3, No. 4, 1966, pp. 239-242.

50. Seed, H. B., *Considerations in the Earthquake-Resistant Design of Earth and Rockfill Dams,* Geotechnique, Vol. 29, No. 3, 1979, pp. 215-263.

51. Seed, H. B. and Chan, C. K., *Clay Strength under Earthquake Loading Conditions,* Journal of the Soil Mechanics and Foundations Division, ASCE, Vol. 92, No. SM2, 1966, pp. 53-78.

52. Shinozuka, M. and Sato, Y., *Simulation of Nonstationary Random Processes,* Journal of the Engineering Mechanics Division, ASCE, Vol. 93, No. EM1, February 1967, pp. 11-40.

53. Skempton, A. W., *Long-Term Stability of Clay Slopes,* Geotechnique, Vol. 14, No. 2, 1964, pp. 77-102.

54. Streeter, V. L., Wylie, B. and Richart, F. E., *Soil Motion Computations by Characteristic Method,* Journal of the Geotechnical Engineering Division, ASCE, Vol. 100, No. GT3, March 1974, pp. 247-263.

55. Sues, R. H., *Stochastic Seismic Performance Evaluation of Structures,* ph.D. Thesis, Department of Civil Engineering, University of Illinois, Urbana, Ill., 1983.

56. Tajimi, H., *Dynamics for Building Structures,* Korona-sha, Tokyo, Japan, 1965.

57. Tang, W. H., Chowdhury, R. and Sidi, I., *Progressive Failure Probability of Slopes,* Proc. of the 4th ICOSSAR, Kobe, Japan, May 1985.

58. Terzaghi, K., *Mechanisms of Landslides,* The Geological Survey of America, Engineering Geology (Berkey) Volume, 1950.

59. Vanmarke, E. H. and Lai, S-S. P., *Strong-Motion Duration and RMS Amplitude of Earthquake Records,* Bulletin of the Seismological Society of America, Vol. 70, No. 4, August 1980, pp. 1293-1307.

60. Wen, Y. K., *Method for Random Vibration of Hysteretic Systems,* Journal of the Engineering Mechanics Division, ASCE, Vol. 102, No. EM2, April 1976, pp. 249-263.

61. Wen, Y. K., *Equivalent Linearization for Hysteretic Systems Under Random Excitation,* Journal of Applied Mechanics, Transaction of the ASME, Vol. 47,March 1980.

62. Wu, T. H., *Uncertainty, Safety and Decision in Soil Engineering,* Journal of the Geotechnical Engineering Division, ASCE, Vol. 100, No. GT3, 1974, pp. 329-348.

63. Zienkiewicz, O. C., *The Finite Element Method in Engineering Science,* McGraw-Hill, 1971.